BRYAN ARTHUR SISSONS

THE HORIZONTAL KINEMATICS OF THE NORTH ISLAND OF NEW ZEALAND

Submitted for the degree of
Doctor of Philosophy
Department of Geology
Victoria University of Wellington

August 1979

CONTENTS

LIST OF FIGURES

LIST OF TABLES

ACKNOWLEDGEMENTS

I thank first my supervisor, Professor Harold Wellman, for the energy and good humour with which he attacked my elliptical writings and I am indebted for many useful discussions and criticisms to Drs. Hugh Bibby and Dick Walcott of Geophysics Division, D.S.I.R. and Dr. Martin Reyners of Victoria University.

I am indebted also to the staff of the Department of Lands and Survey at the Hamilton and Wellington district offices and particularly at the Computing Branch, Head Office for assistance in obtaining the data I have used.

My thanks to Professor R. H. Clark for the opportunity to work in the Department of Geology at Victoria University.

The thesis was typed most efficiently from a rough manuscript by Jane Dudley and I thank Jill Goodwin for reading the typescript.

ABSTRACT

The advantages and disadvantages of the 'displacement' approach and the 'strain' approach to the analysis of repeated geodetic surveys for crustal deformation are discussed and two methods of geodetic strain analysis are described in detail.

Repeated geodetic surveys in the central North Island show

i) secular widening of the Taupo Volcanic Zone (TVZ) at 7 mm y^{-1} without significant transcurrent motion

ii) north-south dextral motion at 14 mm y^{-1} and east-west narrowing at 4 mm y^{-1} across the northern end of the North Island Shear Belt

iii) 3.1 m extension at 135° across a 15 km-wide region north of Lake Taupo, and adjacent zones of compressive rebound all associated with the 1922 Taupo Earthquakes.

From the epicentral distribution and horizontal strain pattern a 15 km-square fault dipping 40° and striking parallel to the TVZ is inferred for the 1922 earthquakes. The seismic moment, 1.3×10^{26} dyne cm, and the stress drop, 134 bars, are abnormally high for the TVZ.

Widening of the TVZ is considered to be back-arc spreading. The spreading axis is postulated to extend northeast into the Havre Trough via a north-south dextral transform; and southwest into the Waverley Fault Zone and Waimea Depression via the sinistral reverse Raetihi Transform.

Deformation of the North Island is not homogeneous. Fault zones are idealized as line plate boundaries and four plates - Indian, Central, Kermadec and Pacific - are postulated to account for the deformation. The Indian-Pacific macroplate pole is adopted and non-unique positions and rotation rates for the remaining poles are determined from geodetic strain data and the geometry of plate interactions. The Central Plate is moving away from the Indian Plate at the back-arc spreading axis; the Kermadec Plate is moving dextrally with respect to the Central Plate at the North Island Shear Belt which accommodates most of the transcurrent component of motion between the Indian and Pacific plates in the North Island and gives almost pure subduction of the Pacific Plate under the Kermadec Plate at the Hikurangi Margin.

CHAPTER 1 INTRODUCTION

In terms of plate tectonics the earth's crust is composed of a number of rigid plates. The boundaries between the plates are distinguished here as being divergent, transform or convergent. Divergent boundaries are sea-floor spreading centres, or continental rifts; transform boundaries are dextral or sinistral faults; and convergent boundaries are subduction or obduction zones. Where one side of a convergent boundary is oceanic it is subducted and moves under the other side, which may be either continental or oceanic. Where both sides of a convergent boundary are continental, the buoyancy of continental crust prevents subduction and obduction occurs.

Subducted plates plunge into the mantle causing regions of intermediate and deep earthquakes termed Benioff Zones. In many parts of the world spreading occurs behind the subduction zones, i.e. overlying the Benioff Zones and is therefore termed "back-arc spreading".

1.1 Tectonic Setting

New Zealand lies on the Indian-Pacific plate boundary for which the present shift pole as determined by Chase (1978) from worldwide data is at $62^{\circ}S$, $174^{\circ}E$. The rotation rate is 1.27°/My and relative motion across the boundary in the New Zealand region is dextral-convergent. In the North Island and to the north, the Pacific Plate is subducted under the Indian Plate with a westward dipping Benioff Zone (Sykes, 1966; Adams and Ware, 1977) and consequent back-arc spreading. In the South Island there is oblique obduction. The approximate position of the boundary and relative plate velocities are shown in figure 1.1.

The Indian-Pacific plate boundary is in reality a complex zone which, in New Zealand, is manifest as a 300 km-wide, northeast striking belt of crustal seismicity (figure 1.2). For the purposes of this thesis the boundary zone is assumed

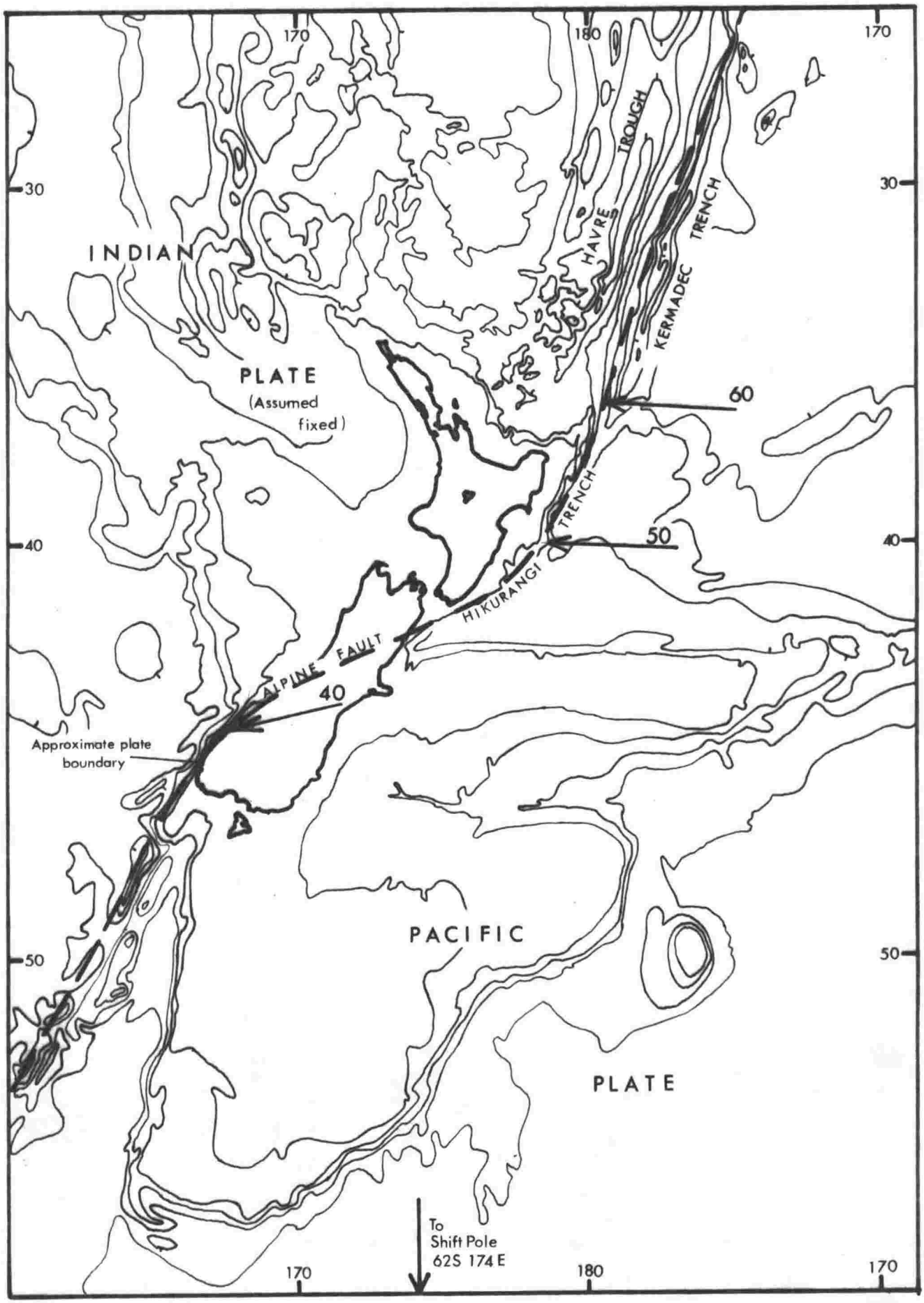

Figure 1.1 A Mercator projection of the New Zealand region showing the velocity of the Pacific Plate relative to the Indian Plate in mm per year as inferred from Walcott (1978a) Bathymetry after Lawrence (1967).

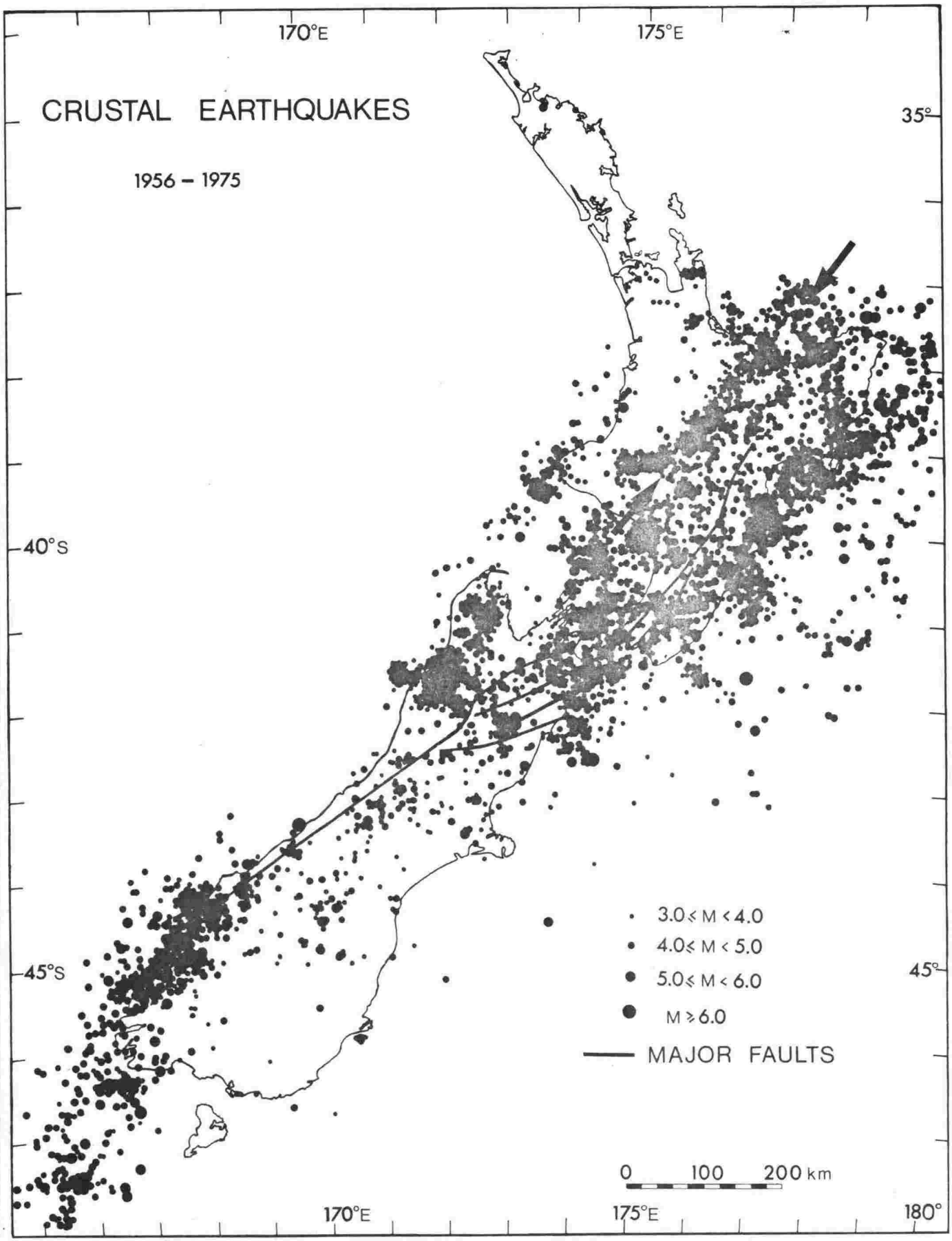

Figure 1.2 New Zealand crustal earthquakes compiled by T. Hatherton. Arrows indicate the Taupo Volcanic Zone.

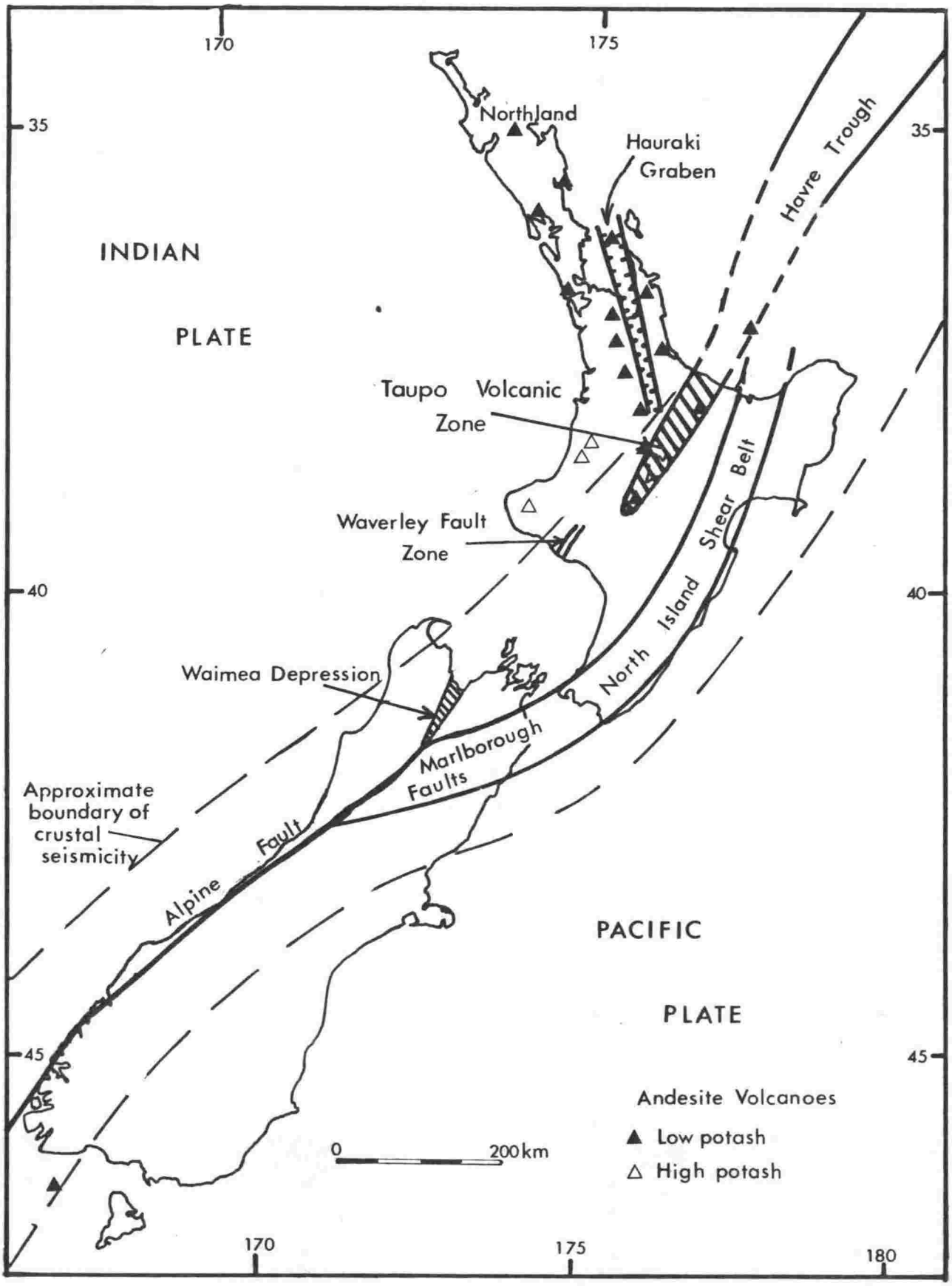

Figure 1.3 Components of the Indian-Pacific boundary zone in New Zealand.

to include both the dextral-convergent and the associated back-arc spreading zones. The following components are defined.

1. Hikurangi Margin: A subduction zone consisting of the Kermadec and Hikurangi trenches (figure 1.1) and their associated Benioff Zones. The axis of the Hikurangi Trench is considerably further to the east, i.e. oceanward, of the intermediate depth earthquake activity in the Benioff Zone than is the Kermadec Trench. The top of the Benioff Zone dips at a shallow angle here and the point of bending of the subducting plate may be moving further oceanward due to loading of the plate by sediment derived from the North Island land mass. The Hikurangi Trench is very different from the Kermadec Trench (figure 1.1) and there is argument as to its nature. Walcott (1978b) inferred that 'stickslip' subduction is occurring under the North Island west of the Hikurangi Trench; the plates being locked for most of the time at the shallow dipping part of the Benioff Zone. Compressive stresses therefore arise due to plate convergence and are transmitted into the overlying Indian Plate to be released from time to time in large thrusting earthquakes following which the locked zone unlocks and subduction occurs. Katz (1974) however preferred to interpret the Hikurangi Trench as a purely depositional basin not having any affinities with subduction.

2. North Island Shear Belt: A 50 km-wide belt of active faults striking north to northeast and extending from the south coast of the North Island to the Bay of Plenty (figure 1.3). Cotton (1951) first showed that there was dextral movement in the belt on the Wellington Fault and subsequent measurements have shown that many of the faults in the belt are dextral reverse (e.g. faults 7 to 10 in table 1.1). Lensen (1975) gave a postglacial average rate of dextral displacement for the zone of 14-18 mm y^{-1}.

3. Marlborough Faults (figure 1.3): Five major dextral faults and a number of smaller faults all striking about 060 form a 100 km-wide belt in the northeast of the South Island. Detailed fault (Lensen, 1968), microearthquake (Arabasz and Robinson, 1976) and geodetic (Bibby, 1975, 1976) studies

make this one of the best understood parts of the Indian-Pacific boundary zone. The average slip direction of the southeast side of the belt relative to the northwest side is about 250° and the displacement rate for the belt is about 45 mm y^{-1}.

4. Alpine Fault: A single major northeast striking reverse dextral fault with a remarkably straight trace for over 450 km along the western side of the South Island (figure 1.3). Wellman (e.g. 1964) has demonstrated a total dextral offset of 450 km across the Alpine Fault which has been regarded as being the actual Indian-Pacific plate boundary in the South Island. Displaced river terraces (Wellman, 1953) at a number of sites indicate that postglacial movement has occurred on the fault. Geodetic analyses (Walcott, 1978a) show that crustal strain in the same sense as the reverse dextral movement is occurring in a zone greater than 20 km wide straddling the fault but small scale repeated surveys (Lensen, pers.comm., 1979) show that creep is not occurring at present. Argument exists as to whether the strain is currently taking place plastically or accumulating elastically to be released in a large earthquake. A magnitude 6.9 earthquake occurred near the fault at Arthurs Pass in 1929 but crustal seismicity along the fault has been low at least since 1956 as will be seen in figure 1.2.

5. New Zealand Spreading Axis: Here defined to consist of the Taupo Volcanic Zone, Waverley Fault Zone and Waimea Depression - a set of almost co-linear features parallel to the Kermadec Margin all of which show evidence of spreading normal to the Margin. The Taupo Volcanic Zone (figure 1.3) is a belt of active normal faults striking northeast from the centre of the North Island to the Bay of Plenty. It is discussed in detail below. The Waverley Faults (figure 1.3) are north-northeast striking normal faults at the Wanganui coast (Fleming, 1953). The Waimea Depression (figure 1.3) is a northeast striking basin in the northwest of the South Island. It is filled with Quaternary gravels and has no active faults but geodetic analyses (Bibby, pers.comm., 1979) indicate a shear strain

rate of 0.3 μrad y^{-1} with the principal axis of extension at 150°.

6. Havre Trough (figure 1.1): A marine back-arc basin shown by Karig (1970, 1971) to be underlain by ridges and troughs of oceanic crust striking parallel to the main trough axis and covered by a thin sedimentary layer from which an extensional origin for the trough is inferred. Diffuse magnetic anomalies in the Lau Basin - the northern extension of the Havre Trough - are interpreted by Lawver et al (1976) and Weissel (1977) as indicating spreading.

The Havre Trough and the Taupo Volcanic Zone are extensional features similarly placed with regard to the Hikurangi Margin. The Taupo Volcanic Zone is therefore regarded as a continuation of the Havre Trough though it is considerably narrower and is offset to the east. Karig (1970a) considered the difference in widths to be due to the difference in mechanical response of oceanic and continental crust to back-arc spreading forces.

Also in the North Island, situated to the north of the TVZ, is the Hauraki Graben (figure 1.3) which strikes north-northwest and is bounded by active faults (Healy et al, 1964). It may represent a current or former line of spreading but retriangulations reported below show that current strain rates across it are very low.

On land there are three main sources of information concerning current earth deformation: active faults, earthquake mechanisms, and repeated geodetic surveys. Table 1.1 summarizes measurements of displacements on active faults throughout New Zealand; figure 1.4 is a compilation of crustal earthquake mechanisms and figure 1.5 is a compilation of strain rates determined from resurvey data. The average slip rate (where known) and average slip direction determined from the compilations above are set out for each of the component parts of the Indian-Pacific boundary zone in table 1.2. The slip direction is for the south or east side of a zone relative to the north or west side. Equations

Fault	Latitude (degrees)	Longitude (degrees)	Strike (degrees)	S (m)	V (m)	Dip (degrees)	Nature	Slip Direction (degrees)
1 Alpine	43.93	168.98	059	8.0	0.9	c90	D	239
2 Alpine	42.72	171.48	056	7.0	1.0	c60	Dr	241
3 Alpine	42.35	172.22	046	9.0	2.4	c60	Dr	235
4 Clarence	42.08	172.80	069	8.5	0.3	c90	D	249
5 Awatere	42.08	173.17	065	6.1	0.2	c60	Dr	246
6 Wairau	41.67	173.20	063	37.5	1.5	c60	Dr	244
7 Wellington	40.67	175.53	040	18.0	1.8	c60	Dr	223
8 West Wairarapa	40.95	175.52	040	76.0	3.0	c60	Dr	221
9 Mohaka	39.30	176.62	020	6.0	1.0	c90	D	200
10 Whakatane	38.60	176.97	015	6.0	1.0	c60	Dr	200
11 Raetihi	39.43	175.30	095	6.0	1.0	c60	Sr	85
12 Waverley i)	39.77	174.68	026	25.0	7.5	c60	Dn	190
ii)	39.77	174.68	082	22.0	2.6	c60	Sr	78

Table 1.1: S = strike slip displacement, V = vertical displacement, D = dextral, Dr = dextral reverse, Dn = dextral normal, Sr = sinistral reverse. S, V after Berryman (pers.comm., 1979).

Component Zone	Faulting or Magnetics	Earthquake Mechanisms	Geodetic
Marlborough	246[a]	260-265[b]	247[c]
Alpine Fault	238[a]		266[d]
NISB i) south end	221[a]	257[e]	276[d]
ii) north end	200[a]		202[f]
NZSA i) TVZ	112-135[g]		106[f]
ii) Waverley i)	196[a]		
ii)	78[a]		
iii) Waimea			165[h]
Havre Trough	130[i]		

(a) from table 1.1
(b) Arabasz and Robinson (1976)
(c) Bibby (1976)
(d) Walcott (1978a, b)
(e) Robinson (in press)
(f) this thesis
(g) assumes normal faulting in TVZ
(h) from strike of 150° for extension axis (Bibby, pers.comm., 1979)
(i) Lawver et al (1977)

Table 1.2 Average slip directions for the component zones of the Indian-Pacific boundary zone.

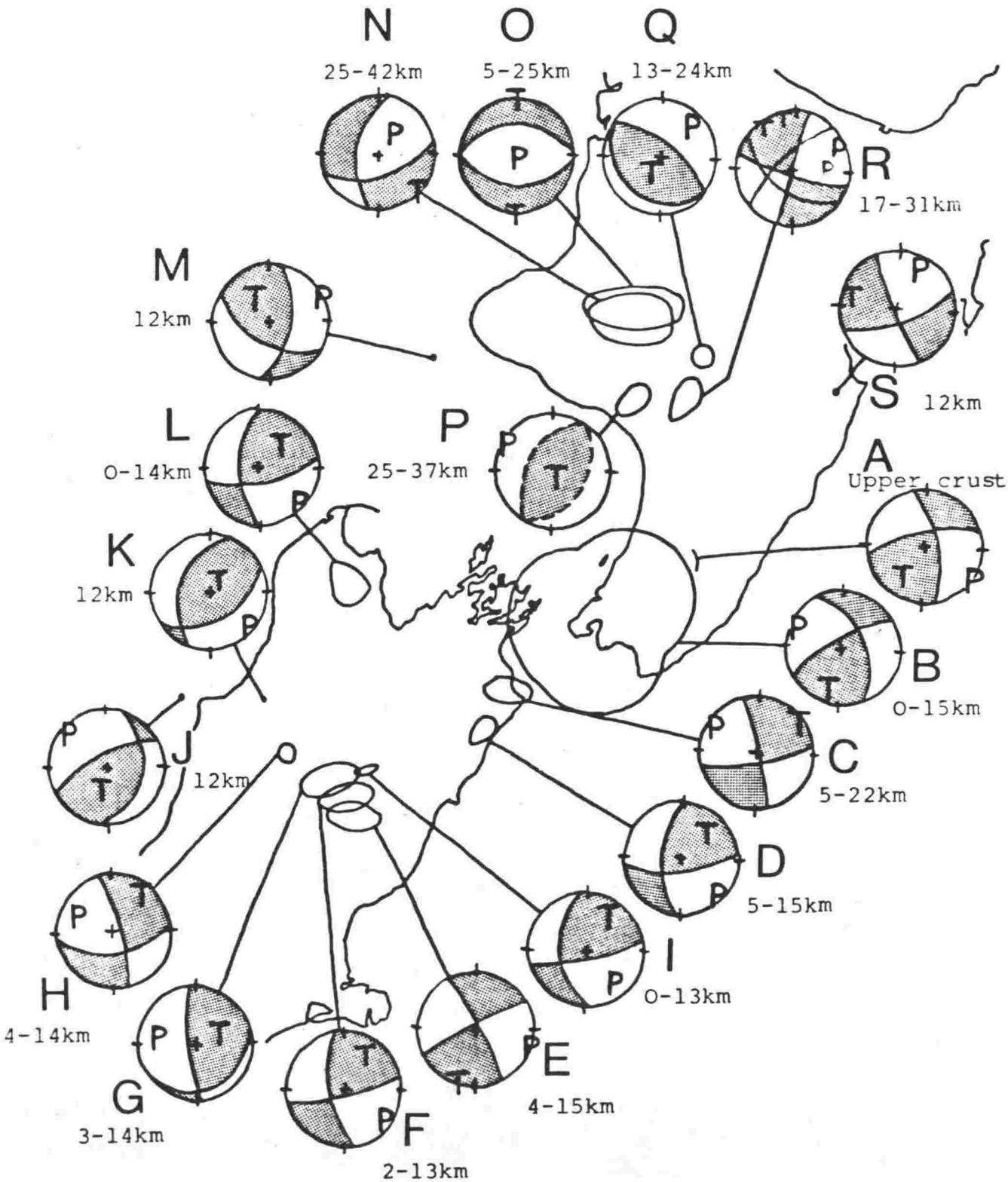

Figure 1.4 Focal mechanisms for shallow earthquakes in the Indian Plate, after Reyners (1978). Upper hemisphere projections.

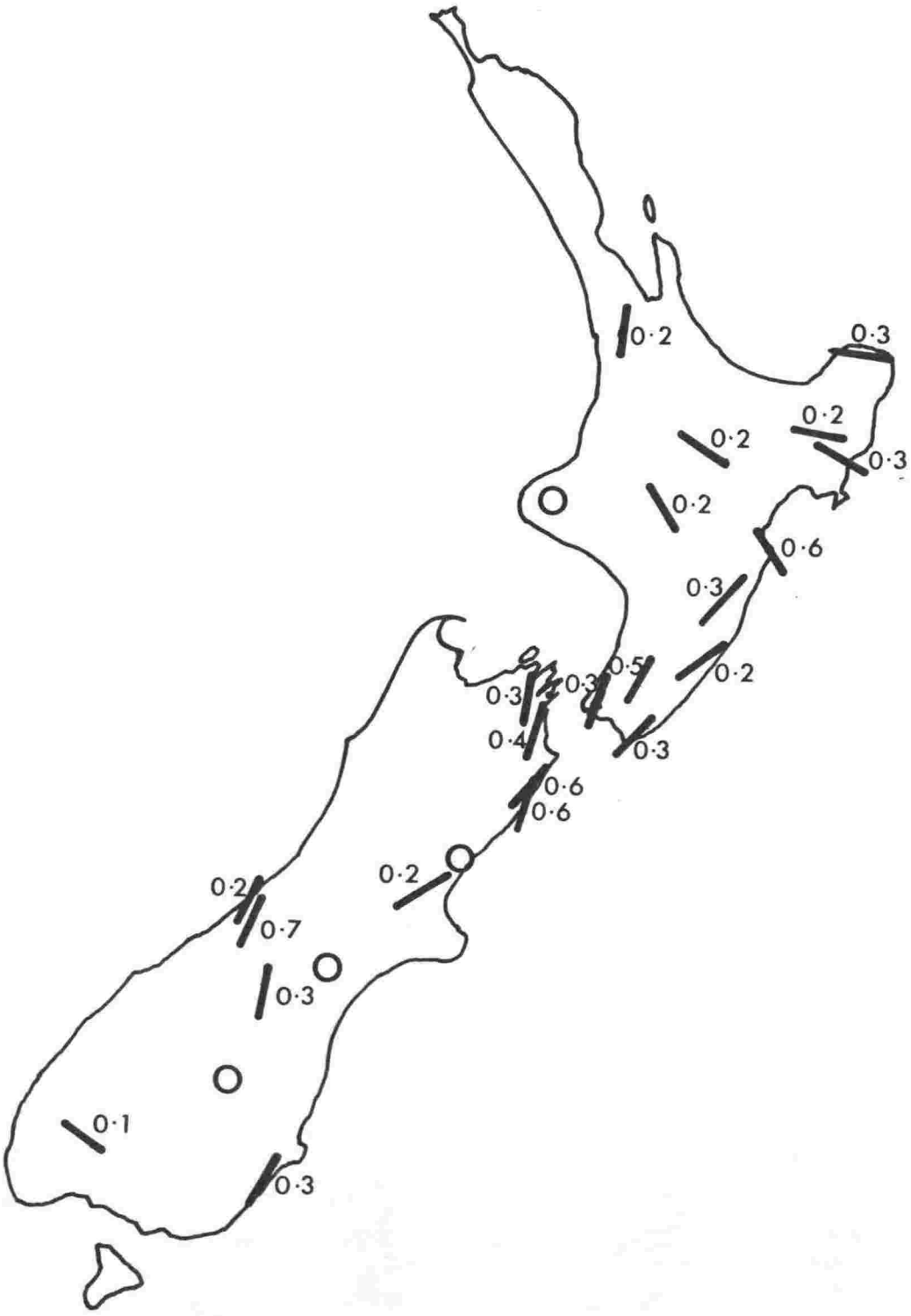

Figure 1.5 Horizontal shear strain rates in New Zealand compiled from Bibby (1976), Walcott (1978a, b), and this thesis. Bars indicate the direction of the principal axis of extension, units $\mu rad\ y^{-1}$, circles indicate zero strain rate.

used for deriving the slip direction from fault, earthquake and resurvey data are as follows.

For faults, the angle, α between the slip direction and the fault strike is given by

$$\alpha = \text{Tan}^{-1} \left(\frac{V}{S \text{ Tan } d}\right)$$

where V is the vertical and S the strike slip component of fault motion, and d is the fault dip.

For earthquake mechanisms the strike and dip of two orthogonal planes either of which could be the fault plane are determined. The plane most consistent with geology is chosen as the fault and α is given by

$$\text{Sin}\,\alpha = \text{Cot } d_1 \text{ Cot } d_2$$

where d_1 is the dip of the fault plane and d_2 the dip of the auxiliary plane.

For resurvey data if the change in length and azimuth parallel to faults are assumed zero it follows from equations 25 in Chapter 2 that

$$\alpha = \text{Tan}^{-1} \frac{\gamma_1}{\gamma_2}$$

where γ_1 and γ_2 are the components of shear strain relative to the fault direction.

1.2 Major Historical Earth Movements in the North Island

There have been four historically recorded occasions in the North Island when sudden earth movements of a metre or more took place; these are briefly described below.

The Wairarapa Earthquake of 1855 is the largest historical earthquake in New Zealand. Felt over almost the entire country, it caused severe damage in Wellington and Wanganui and was considered by Eiby

(1968) to be of magnitude 8. It was accompanied by fresh breaks for more than 40 km along the north-northeast striking Wairarapa Fault, one of the major faults at the southern end of the North Island Shear Belt (Ongley, 1943). The vertical component of motion was in the same sense as previous movements on the fault, i.e. upthrow to the west. On the south coast of the North Island, 10 km west of the fault, at the crest of an anticline formed during the earthquake uplift was 2.5 m (Wellman, 1969). The amount of displacement on the fault was not recorded at the time of the earthquake but at Waiohine River where movements on the fault are well shown in displaced river terraces the latest displacement, presumed to be that due to the earthquake, has a vertical component of 0.9 m and a strike slip component of 13 m (Lensen and Vella, 1971). The slip direction assuming a fault dip of 60° is 225°.

Tarawera Eruption: In June 1886 a basalt dyke was intruded into the rhyolite dome of Tarawera Volcano and a line of coalescing craters, referred to as the Tarawera Rift, 5 km long and 200 m deep striking at 050° was formed (Cole, 1970). New and intense hydrothermal activity began at the south end of the rift and has continued to the present day. Minor earthquakes accompanied the eruption but no surface faulting was reported.

The dyke crops out at two sites only, and is 1 m thick at one site and 10 m at the other. The bridge overlying the dyke between the outcrops is undisturbed (Cole, 1970) implying that there was no spreading above the dyke during emplacement. Land-based magnetic measurements (Cole and Hunt, 1968) show that the dyke is 7 km long and underlies the floor of the rift and that there is a totally concealed parallel dyke, which may be older, 200 m to the southeast. Neither dyke has an aeromagnetic expression. It is assumed that the exposed dyke is continuous and at least 1 m thick and that corresponding widening took place during emplacement. Therefore since it was inferred above that widening did not occur in the

volcano above the dyke it appears necessary to postulate subhorizontal faults isolating the volcanic edifice from the subjacent country rock which widened.

Taupo Earthquake Swarm: From April to December 1922 there was a swarm of several hundred earthquakes centred near the north shore of Lake Taupo. For almost all the earthquakes the maximum intensity was less than VI on the Rossi-Forel scale. The largest shock was probably that at 8.16 a.m. on June 10 with an intensity of VIII (Morgan, 1923). It was felt at distances of 70 km but is not listed from any seismograph then operating, the nearest being a Milne seismograph in Wellington. From the distribution of felt intensities it was considered by Eiby (1968) to have a magnitude of 6.5 to 7. The earthquake swarm continued and Morgan et al (1922) state that the locus of earthquakes moved to and fro on a fault plane striking parallel to local surface faults and situated some kilometres west of Taupo township. An attempt was made to locate epicentres using two portable seismographs and by comparing the arrival times at Taupo, Wairakei, Oruanui and Mokai (figure 1.6) by telephone. Earthquake waves were found to reach the first three stations simultaneously and Mokai two seconds later (Morgan et al, 1922). By swinging arcs from the first three stations an epicentre is found to lie 9 km northwest of Taupo township and 16 km southeast of Mokai (figure 1.6). For trial focal depths of 10 and 20 km the wave velocity over the additional distance to Mokai is found to be 2.76 km s^{-1} and 1.84 km s^{-1} respectively. 2.76 km s^{-1} is perhaps a reasonable velocity for S waves in the heterogeneous volcanics which underlie the area but any lower velocity is unlikely, and therefore a focal depth of 10 km or less is inferred.

Large fault displacements occurred progressively during the swarm and although the epicentral region was sparsely populated they were recorded (Ward, 1922a, b). The displacements occurred on existing faults of the Central Fault Belt of the Taupo Volcanic Zone and formed a graben 9 km wide bounded by the Whangamata and Kaipo Faults (figure 1.6). Grange (1932) records that fresh traces on the Whangamata Fault

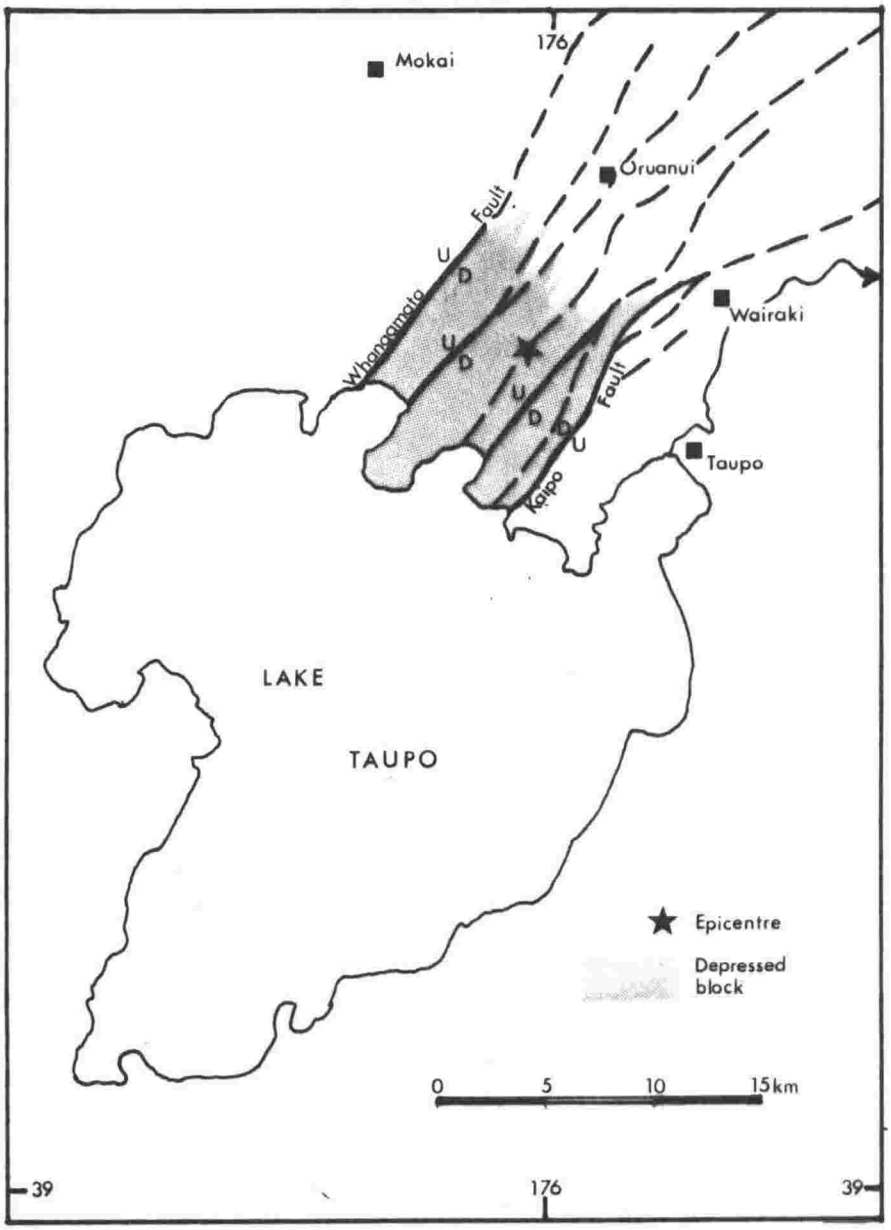

Figure 1.6 Vicinity of the 1922 Taupo Earthquakes. Faults active in the Quaternary shown dashed, faults which moved in 1922 shown as full lines.

extended 10 km north from the shore of Lake Taupo and that the fault was downthrown on the eastern side by 2 m. Fresh traces on the Kaipo Fault extended 11 km north from the lake shore and the fault was downthrown on the western side by 1 m. No transcurrent displacements were reported. Other, smaller, faults that were noticed are shown in figure 1.6. In addition to the faults, Ward (1922a) reported open fissures up to 300 mm wide, 1 m deep and tens of metres long. The fissures were parallel to the faults and the faulting is therefore inferred to be normal. Fissuring extended as far north as Oruanui where re-levelling of a railway indicated a 0.3 m vertical movement over an unstated distance, downthrown east. Re-levelling also showed that westward tilting of the graben block had occurred. By December 1922, when the swarm ended, total subsidence in the centre of the graben amounted to 4 m relative to the level of the outlet of Lake Taupo (Grange, 1932).

Hawkes Bay Earthquake: On February 2, 1931 a magnitude $7\frac{3}{4}$ earthquake occurred in Hawkes Bay causing severe damage in Napier City. Bullen (1938) put the epicentre 25 km north-west of Napier with a focal depth of 15-20 km. An elongated dome 100 km long by 20 km wide centred 50 km north of Napier and striking north-northeast was formed. The maximum uplift was 3 m. There was also a narrow belt of subsidence to the east of the uplifted zone; the line of no change in level being near the coast of Hawkes Bay (figure 1.7). Very little surface faulting took place, the largest faults being reverse dextral with a strike of 045° (Henderson, 1933). The slip direction was 300°, consistent with shortening approximately normal to the dome.

The earthquake is interpreted as thrusting on a fault dipping northwest at a shallow angle and reaching the surface near the line of no change in elevation. Walcott (1978b) has estimated the horizontal strain associated with the earthquake from first order surveys made in 1925 and 1931 (figure 1.7). In the zone nearest the Taupo Volcanic Zone, the only zone of direct relevance to this thesis, the earthquake strain was 10 μrad and the azimuth of the principal axis

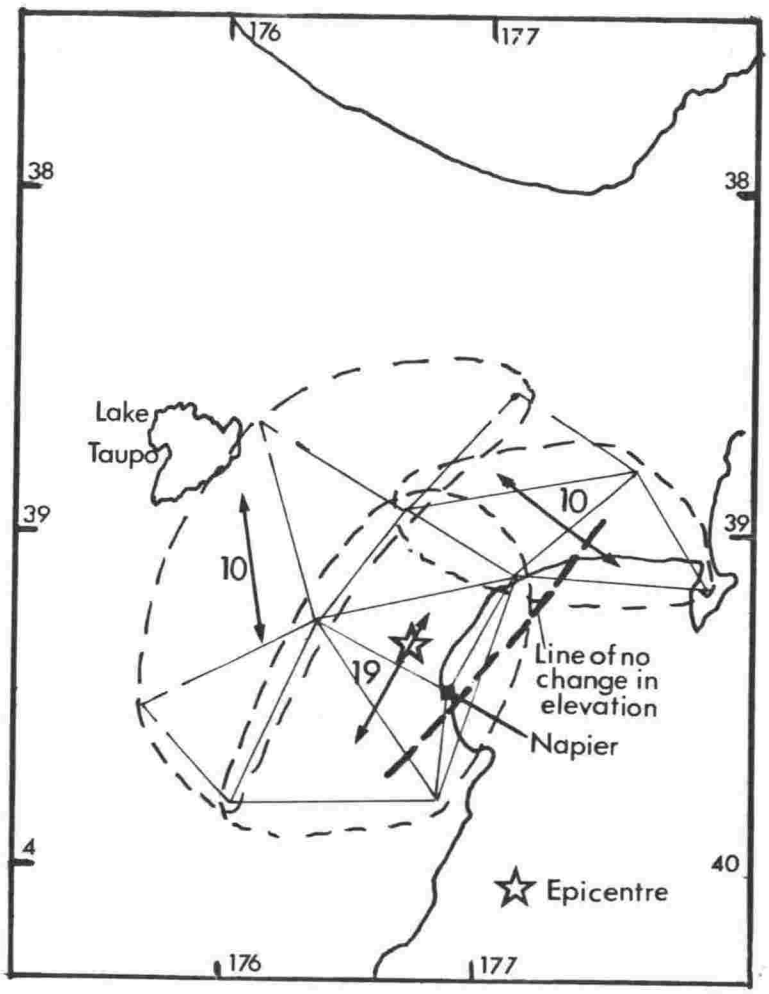

Figure 1.7 Vicinity of the 1931 Hawkes Bay Earthquake. Figures of 1st order surveys made in 1925 and 1931 are shown. Earthquake strain as determined by Walcott (1978b) is given in μrad, the arrows indicate the direction of the principal axis of extension.

of extension 171°.

1.3 Taupo Volcanic Zone

The Taupo Volcanic Zone (TVZ), referred to above as the belt of active faults striking northwest from the centre of the North Island, was defined by Healy (1962) as the belt of active volcanoes parallel to the fault belt and extending from Ruapehu to White Island. The zone contains a number of hydrothermal systems and has an average heatflow 10 to 15 times greater than the normal continental heatflow.

Active faults in the TVZ are confined to a belt about 15 km wide termed here the Central Fault Belt (figure 1.8). South of Lake Taupo the belt strikes at 022° and north of Lake Taupo at 040°-045°. The faults are inferred to be normal. Extensive drilling for hydrothermal exploration shows that dips are generally greater than 70° and that throw increases with depth indicating long-continued cumulative movements (Grindley, 1965, 1970). The Central Fault Belt has been mapped in detail by Grindley (1960, 1965) and by Nairn (1976) and no evidence for either dextral or sinistral motion has been found.

The boundaries of the TVZ are partly formed by a pair of sub-parallel faults - Hauhangaroa and Kaingaroa - 40 km apart and downthrown towards each other. The bounding faults are non-active over most of their lengths but become active south of Ruapehu Volcano where the Central Fault Belt is absent. Near Raetihi they curve round and meet thus terminating the TVZ. Outside the bounding faults the smooth Mamaku and Kaingaroa ignimbrite plateaux dip outwards at about 1°. South of Lake Taupo the plateaux are absent and instead there are disected greywacke mountains.

Associated with the TVZ are over 15,000 km^3 of, mainly rhyolitic, ignimbrite, lava, tephra and redeposited volcanic sediment. Most has accumulated as interbedded ignimbrites and sediment in the graben of the TVZ, with lesser amounts mantling the flanking ignimbrite plateaux. The oldest dated rocks are basal ignimbrites 1.1 My old (Murphy, 1977).

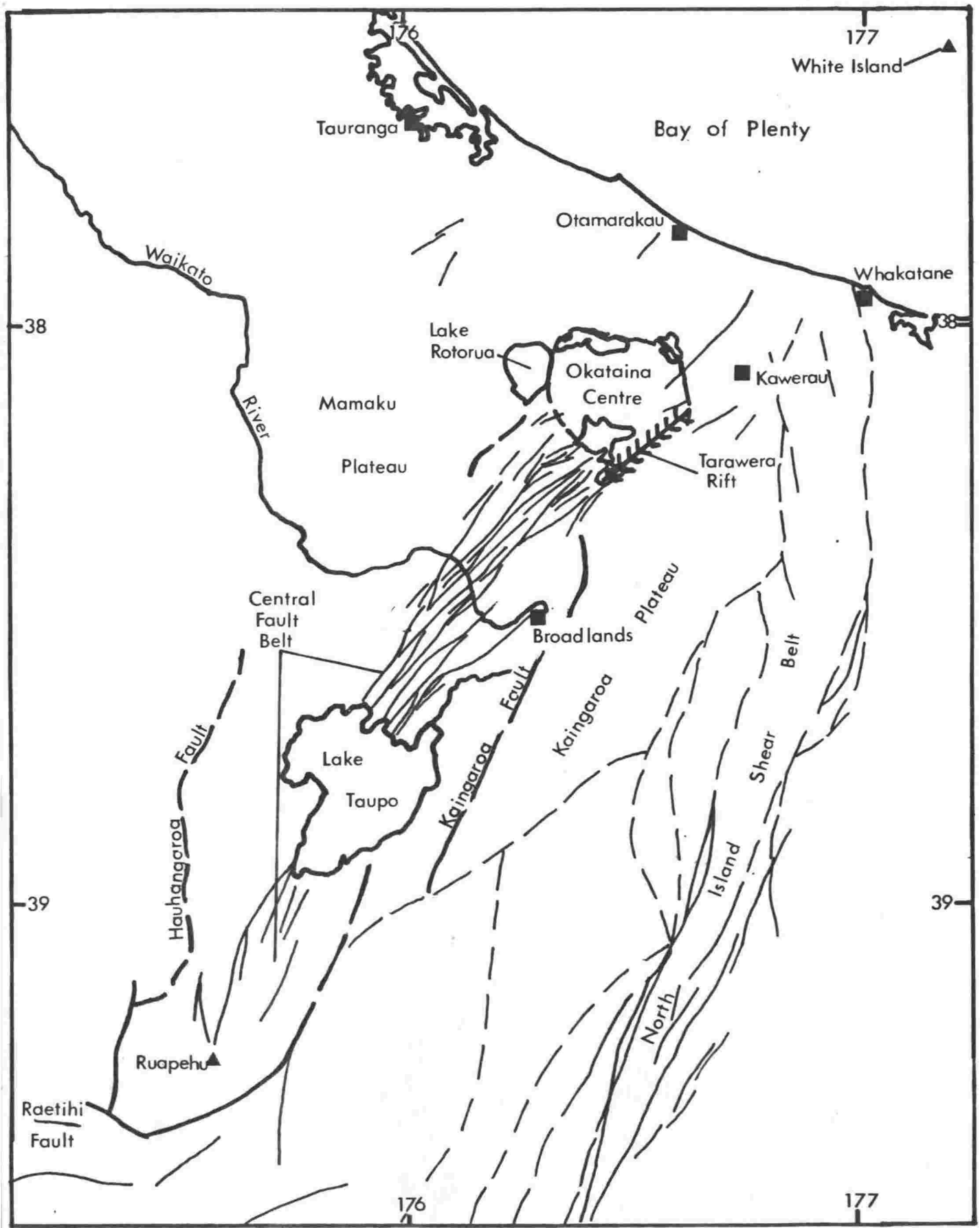

Figure 1.8 Locality map of the central North Island. Quaternary faults shown dashed, faults displacing features younger than 10,000 years shown full.

Recent rhyolitic eruptive vents are concentrated in 'centres' of which Okataina and Lake Taupo are the most prominent. Both centres are surrounded by arcuate faults downthrown inwards (M. Rogan and D. Northey, pers.comm., 1978) and neither is traversed at the surface by the faults of the Central Fault Belt.

Basalts are minor in volume (5 km^3), occur at 9 sites, and are everywhere associated with rhyolite domes (Cole, 1973). The latest basalt eruption was the fissure eruption at Tarawera in 1886 described above.

Andesites are also minor in volume (250 km^3). It is noteworthy that all recently active andesite volcanoes in the TVZ are less than 5 km from the straight line between Ruapehu and White Island. The line is situated near the southeastern boundary of the TVZ and over most of its length is about 15 km southeast of the Central Fault Belt. It is thought to represent the southward continuation of the Tonga-Kermadec Island Arc into New Zealand. Depending on their potash content the andesites were inferred by Hatherton (1969) to be derived from particular depths in the Benioff Zone. However, Hamilton and Gale (1968) have pointed out that the Ruapehu-White Island line strikes 10° more northerly than the North Island Benioff Zone, and therefore the lavas would appear to come from deeper levels in the north than in the south, even though there is little difference in potash content.

Structure: Topographically the Taupo Volcanic Zone is an elongate depression partially obscured by rholite domes, andesite volcanoes and a number of lake-filled calderas (figure 1.9). The cross-section, neglecting the volcanic landforms is given in figure 1.10. The typical rift valley according to Tapponier and Francheteau (1978) is a 30-35 km-wide set of nested grabens 1-2 km deep with steep inward-facing walls formed by normal faults; active faulting being confined to a central 10-15 km-wide belt. It will be seen that the topographic cross-section (figure 1.10) along line AB in figure 1.9 corresponds closely with this

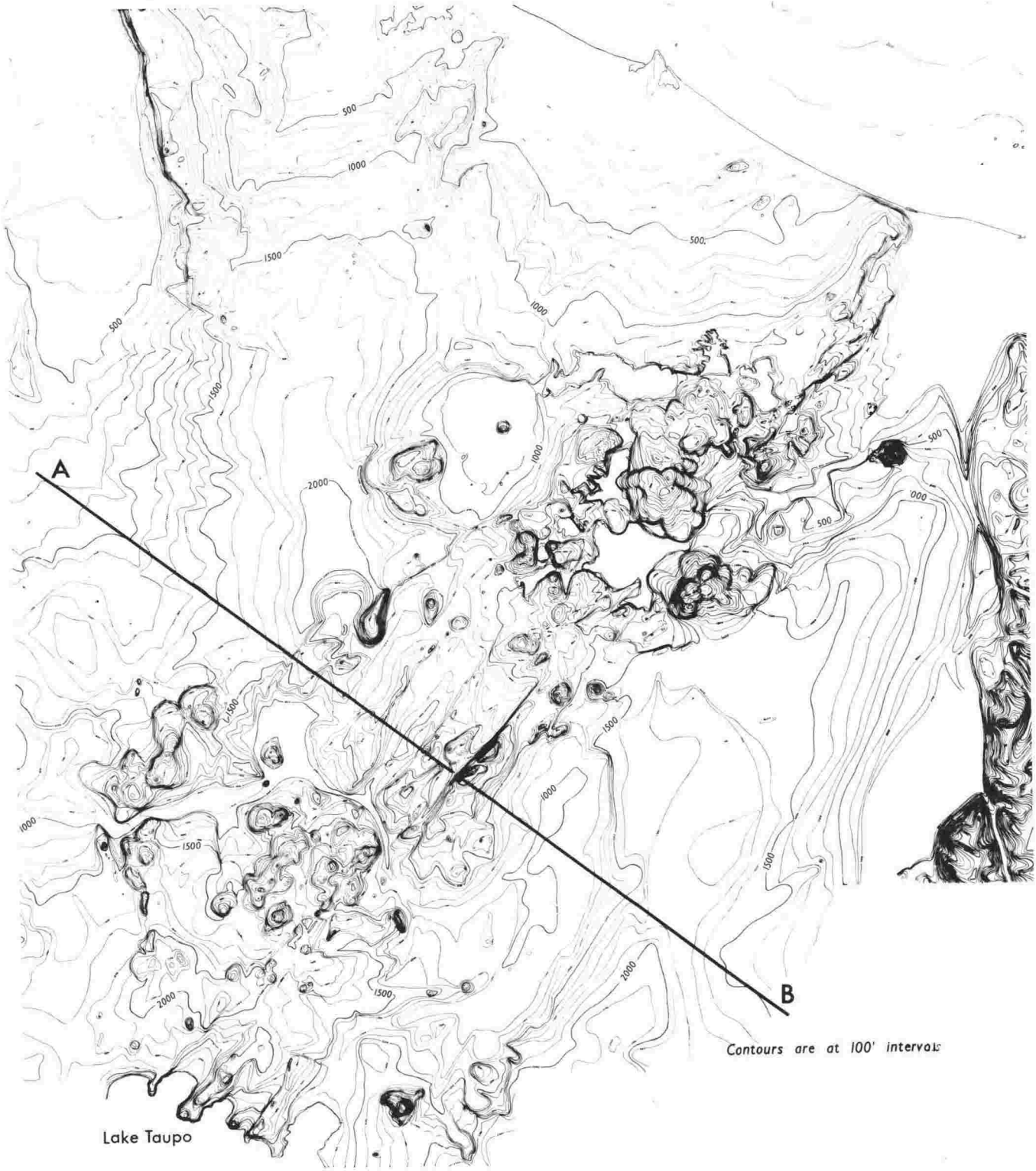

Figure 1.9 Topographic map of part of the central North Island, after Healy (1964). The Taupo Volcanic Zone is the belt of coalescing domes striking northeast from Lake Taupo in the southwest corner. Major faults of the Central Fault Belt appear as northeast-striking lineations between Lake Taupo and Okataina.

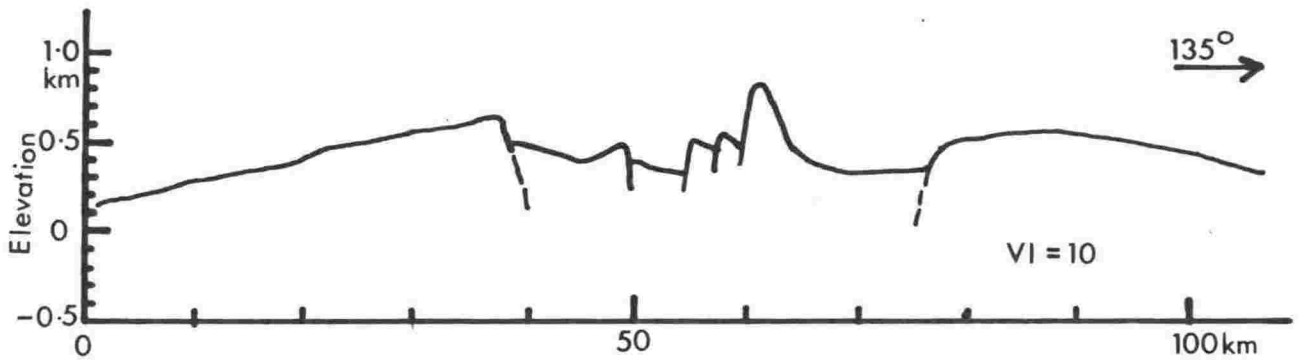

Figure 1.10 Topographic cross-section at 135° across the central North Island (along line AB in figure 1.9).

description, except that the TVZ is only 0.3 km deep. In addition it should be noted that the TVZ is not flanked by rift mountains which, according to the model of Tapponier and Francheteau, will be the product of mature spreading. Thus the Taupo Volcanic Zone is perhaps in the early stages of rifting.

The TVZ is clearly delineated by magnetic anomalies. Figure 1.11 is a residual total force magnetic anomaly map of the central Nórth Island from aeromagnetic observations at an altitude of 1,525 m. Within the TVZ there are numerous mainly positive dipoles with amplitudes up to 750 nT and typical wavelengths of 15 km, while outside the zone magnetic variation is slight. The region of anomalies almost coincides with the topographic depression but terminates at Okataina. Marine observations (Roberts, 1967) show that the Bay of Plenty is magnetically undisturbed and that there is an isolated closed anomaly around White Island.

There is a close correlation between the rhyolite domes (figure 1.9) and the positive dipoles (figure 1.11). Simple quantitative interpretations made by Malahoff (1968) assuming a magnetization contrast of 2 A/m show that most magnetic sources in the TVZ are less than 2 km deep. Statistical analysis of the wavelength of anomalies (Stern, pers.comm., 1979) indicates a maximum source depth of 8 km which may correspond to the depth of the Curie point isotherm below the TVZ.

The isostatic gravity anomaly map of the central North Island (figure 1.12) shows a broad low extending northeast from Ruapehu which, like the magnetic anomalies, coincides with the TVZ and terminates at Okataina but in addition has two northwesterly striking lobes one of which appears to connect with the Hauraki Graben. When the regional field (determined by fitting a surface to those anomalies measured on greywacke basement) is removed, residual anomalies are up to -350 μN/kg (Stern, 1979). The residual anomaly pattern is consistent with there being, underlying the surface depression, a basement depression 2-3 km deep filled with volcanics 0.5 Mg/m^3 lighter than basement. From detailed two-dimensional interpretations,

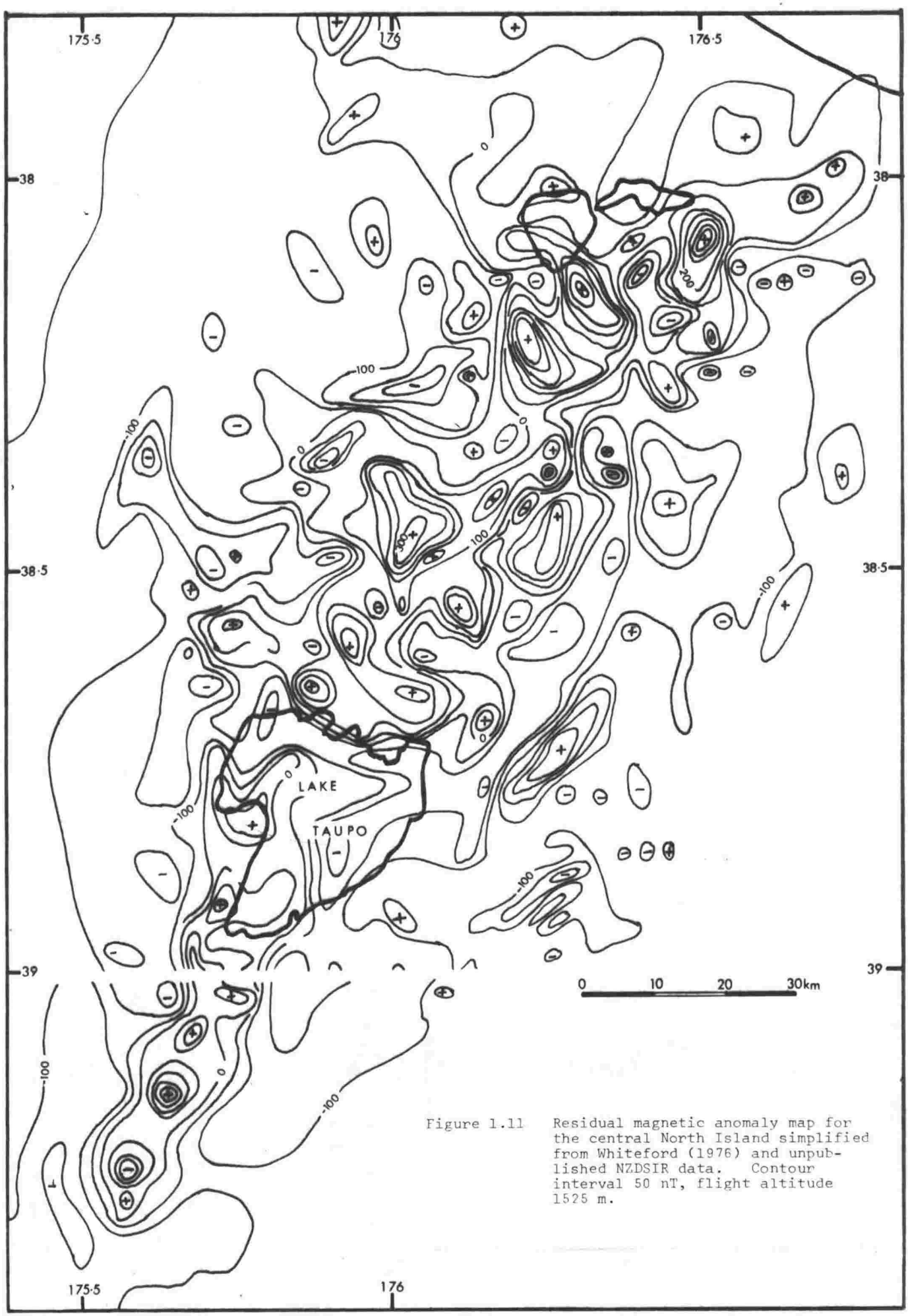

Figure 1.11 Residual magnetic anomaly map for the central North Island simplified from Whiteford (1976) and unpublished NZDSIR data. Contour interval 50 nT, flight altitude 1525 m.

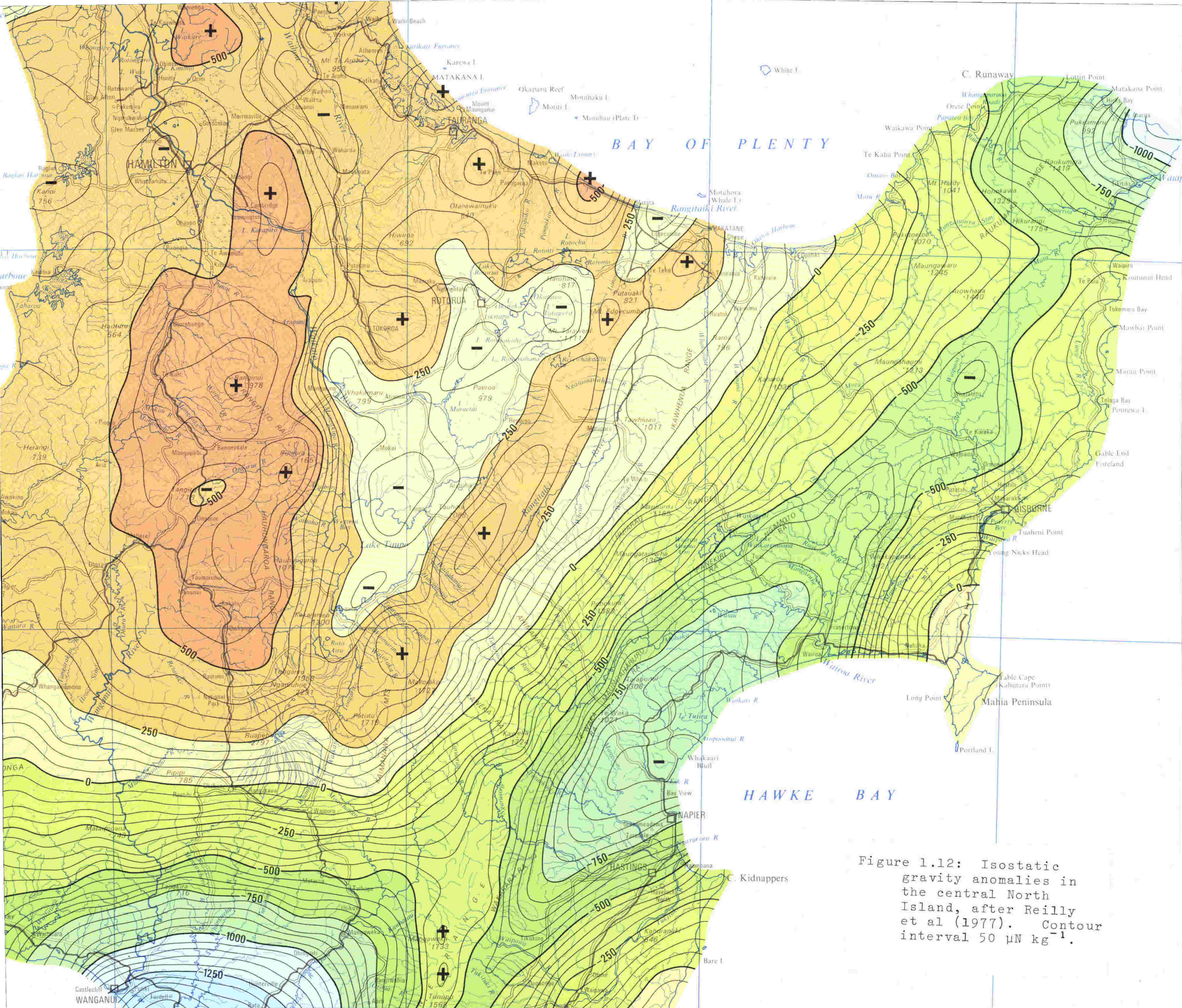

Figure 1.12: Isostatic gravity anomalies in the central North Island, after Reilly et al (1977). Contour interval 50 μN kg^{-1}.

Modriniak and Studt (1959) found close correlation between the basement relief inferred from the gravity variation and the major topographic relief due to faulting. Hence the basement graben is inferred to have grown by long continued normal faulting in the Central Fault Belt.

Basement in the central North Island is the Mesozoic greywacke found throughout eastern New Zealand. In the south it crops out on both sides of the TVZ. In the north it crops out at Otamarakau on the west and near Whakatane in the east. Within the TVZ greywacke has been reached by drillholes at Broadlands and Kawerau (Browne, 1978; Grindley, 1970; locations on figure 1.8) and a refractor with a velocity of 5.4 km s^{-1} typical of greywacke was found at a depth of 2 km on a line extending 20 km north-northwest from Taupo township (R. Robinson, pers.comm., 1978).

Deep structure: Molten magma has been suggested as the source of the high hydrothermal heatflow of the TVZ (e.g. Banwell, 1964; Hochstein, 1976) but the attenuation of S waves and the velocity of P waves rising subvertically through central North Island crust were shown by Robinson (pers.comm., 1978) to be much the same within the TVZ and without, and therefore widespread molten magma is unlikely. Midha (1979) has found, by magnetic sounding methods, a conductivity anomaly of 10 Ωm in the depth range 0 to 7 km under the TVZ which he associates with hot hydrothermal waters. Below 7 km the conductivity is 1,000 Ωm, a value which may be associated with hot rock but at temperatures below the solidus.

It is suggested (e.g. Andrews and Sleep, 1974; Toksöz and Hsui, 1978) that back-arc spreading and high back-arc heatflows are a result of rotational asthenosphere flow caused by the motion of the subducting plate. As the rotational flow evolves, temperatures in the lithosphere overlying the rising limb increase, and the asthenosphere-lithosphere boundary, which depends on viscosity and therefore temperature, rises. Shear stress from the top horizontal limb of the asthenosphere causes horizontal tensile stresses in the back-arc spreading zone.

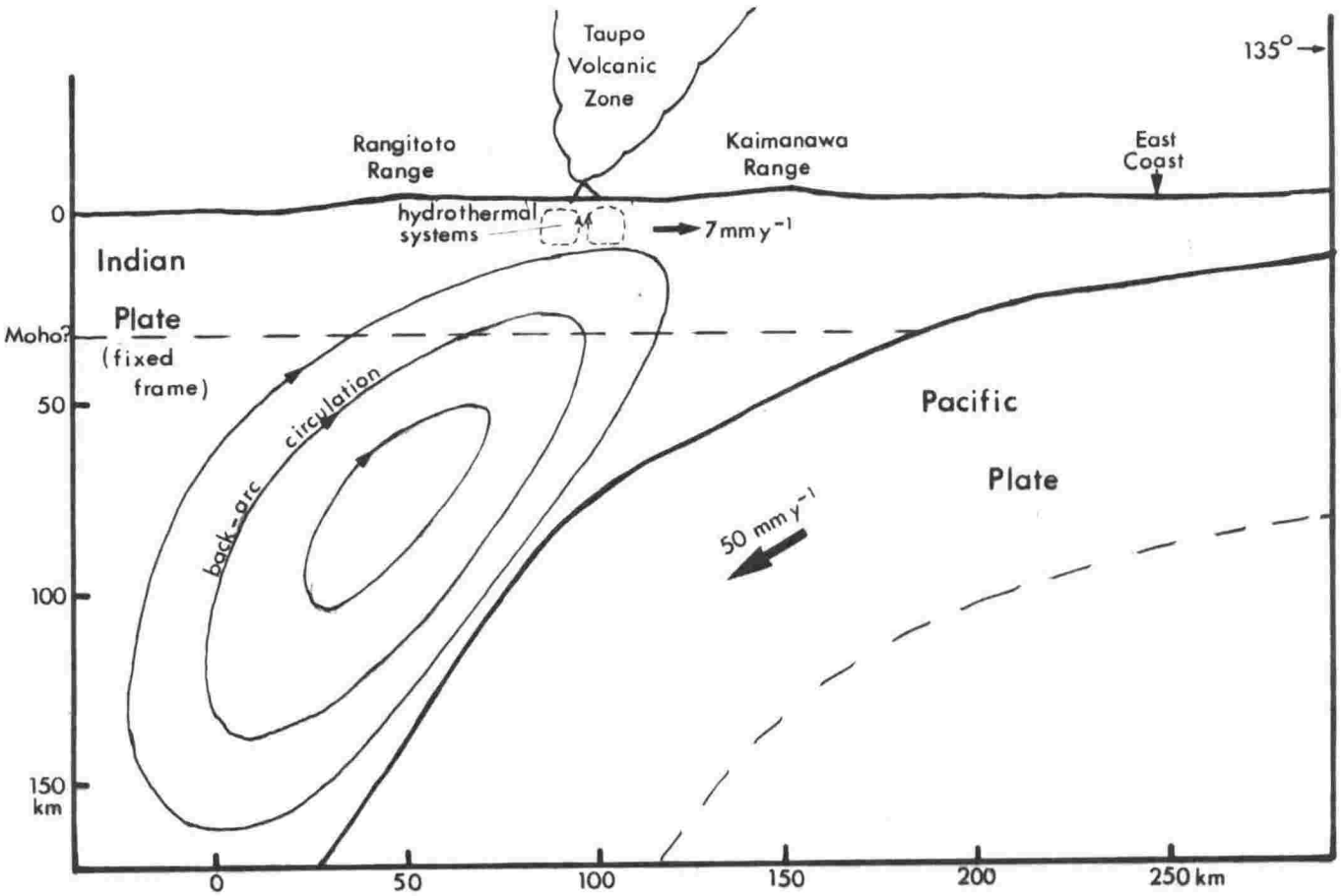

Figure 1.13 Schematic structural cross-section of the North Island, normal to the Benioff Zone and showing back-arc asthenosphere circulation as postulated by Andrews and Sleep (1974). Pacific Plate profile after Reyners (1978).

Under the TVZ it is suggested that the lithosphere-asthenosphere boundary is at a depth of 10-15 km and that hydrothermal circulation penetrates the entire lithosphere and is essentially in contact with the asthenosphere flow.

Crustal seismicity: As will be seen in figure 1.2, the TVZ is a region of high crustal seismicity on the northwest side of the main New Zealand seismic belt. Within the TVZ the maximum size of earthquakes is smaller than elsewhere in the main belt. Historically the largest was that in 1922 with a magnitude of 6.5 to 7 discussed above. Since continuous records began (about 1956), the largest shocks have been of magnitude 5.4.

In figure 1.14 central North Island earthquakes have been separated into two groups, B and A, depending on whether or not they occurred in swarms. For the purposes of separation, swarms were defined as any group of five or more earthquakes in a region not larger than 35 km square with not more than 24 hours between consecutive events. Swarms are confined to a region slightly wider than the Taupo Volcanic Zone. The total seismicity has a northwestern limit which corresponds to the northwestern boundary of the TVZ but has no southeastern limit.

Swarms with a main event such as that in 1922 are regarded as tectonic (related to the main regional stress field) whereas swarms without a main event such as the 1964 Taupo Swarm (Gibowicz, 1973) are not necessarily tectonic (as defined above) and according to Gibowicz are characteristic of the fracture of heterogeneous materials under concentrated external stress. Much of the activity in the TVZ is of the latter kind and is thought to be very shallow. The only study in the TVZ in which unrestricted focal depths have been determined showed that microearthquakes occur in the depth range 6 to 15 km under the Central Fault Belt (Evison et al, 1976). Stress drops in the TVZ as inferred from dislocations estimated spectrally by the AR parameter (Gibowicz and Hatherton, 1975) are low.

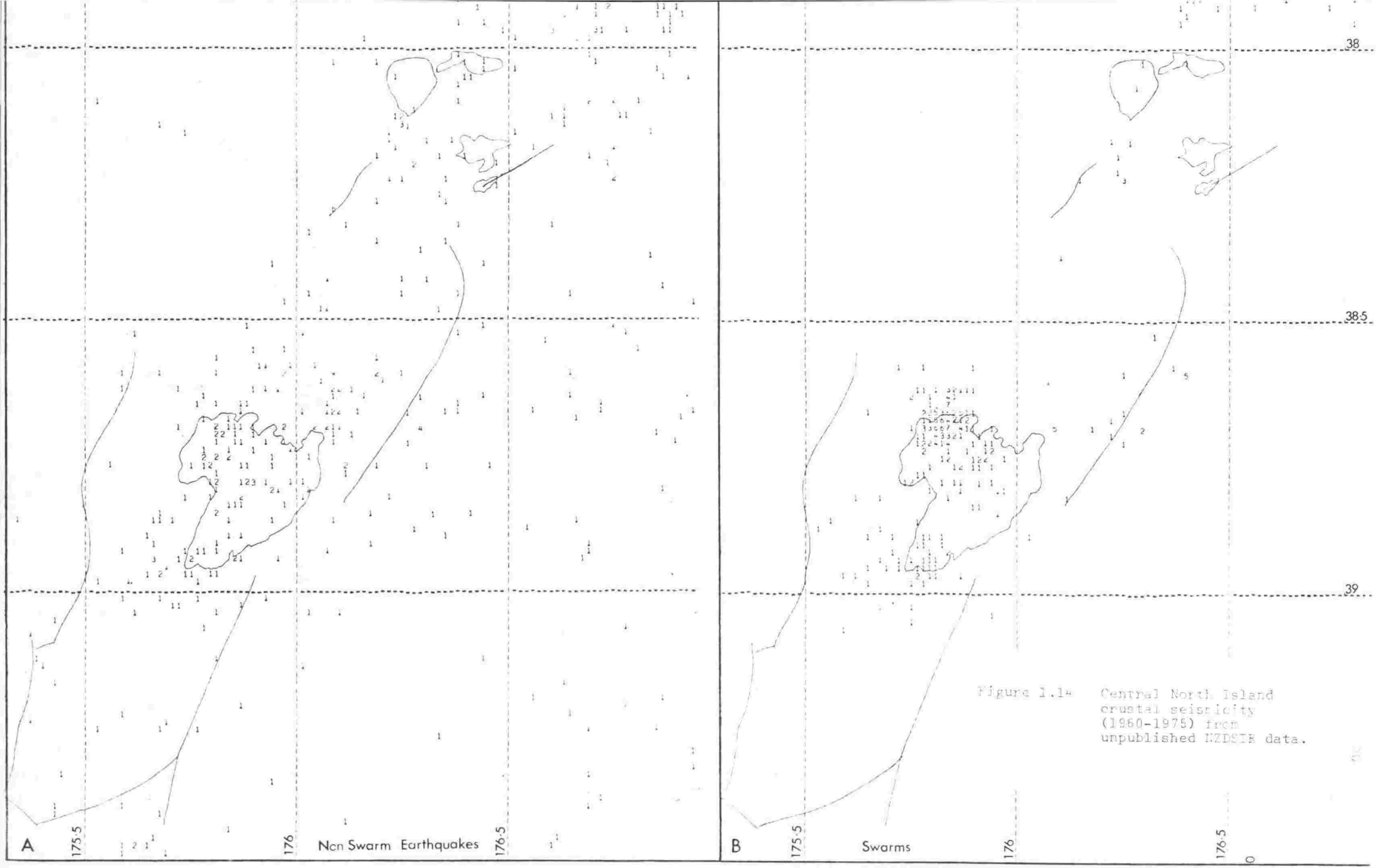

Figure 1.14 Central North Island crustal seismicity (1960-1975) from unpublished NZDSIR data.

CHAPTER 2 THE MEASUREMENT OF HORIZONTAL EARTH DEFORMATION USING REPEATED GEODETIC SURVEYS

2.1 Introduction

On many parts of the earth permanent survey marks have been established in nets which are surveyed from time to time and the data from the surveys constitute a large source of information regarding earth deformation. The earliest surveys suitable for earth deformation studies were made in the nineteenth century. They were triangulations, that is they consist of observations of the angles between rays connecting points. Very few distance measurements were made until the mid-1960s when electronic methods of distance measurement accurate to a few parts per million over distances of up to 50 km became available. Although distances are now commonly measured, the bulk of suitable data is still that from triangulations.

Broadly speaking there are two approaches to the analysis of resurvey data for crustal deformation; these are referred to here as the 'displacement' approach and the 'strain' approach. In the displacement approach the co-ordinates of points are obtained separately for each of two surveys and co-ordinate differences computed, thus giving displacement vectors for individual points. It was pointed out by Frank (1966) that the components of shear strain can be obtained directly from changes in angles without assuming any fixed points. A generalization of Frank's method, together with another more general strain method developed by Bibby (1973) are described in detail below.

With the displacement approach it is necessary, when distances have not been measured in both surveys, to assume that at least two points have remained fixed in the interval between the surveys. If only a portion of a surveyed net has been deformed, as for instance may be the case where a landslide or earthquake is the cause of the deformation, it may be possible to select two or more points remote from

the centre of deformation which can reasonably be assumed to have remained fixed, but for the analysis of secular tectonic deformation which may not have a focus, it is preferable to avoid a priori assumptions that certain regions have not deformed.

The accuracy of angular observations in modern surveys is about 5 seconds of arc and the accumulated errors in co-ordinates determined by triangulation across a net say 30 km wide with rays 10 km long are of the order of a metre. Typical secular crustal strain rates are about 0.5 μrad y^{-1} (e.g. Walcott, 1978a) and over, say 50 years, the relative displacement of two points 30 km apart will be up to 0.75 m depending on the orientation of the line. Hence individual displacement vectors due to secular strain will in general be smaller than errors of estimate and therefore not significant. Whitten and Claire (1960) noted that the 'displacement' analysis of resurvey data in California gave apparent displacements which exceeded any conceivable ground movement and lead to erroneous interpretations.

Strain methods are easily formulated in terms of over-determined systems which can be solved by least squares thus greatly facilitating the separation of earth strain from random observational error. Strain methods are therefore preferred and have been used exclusively in the deformation analyses presented below. It is usual to assume homogeneous strain in zones typically containing between 5 and 20 re-observed points. In each zone four components of strain can be determined and therefore there are four unknowns. By contrast in the displacement approach there are two unknowns per re-observed point.

To facilitate the derivation of the strain methods the standard formulae of two dimensional strain analysis are derived in the following section. An approach similar to that of Ramsey (1967) or Jaeger and Cook (1971) is used.

2.2 Two-dimensional Strain Analysis

In two dimensions, strain is the change in shape or

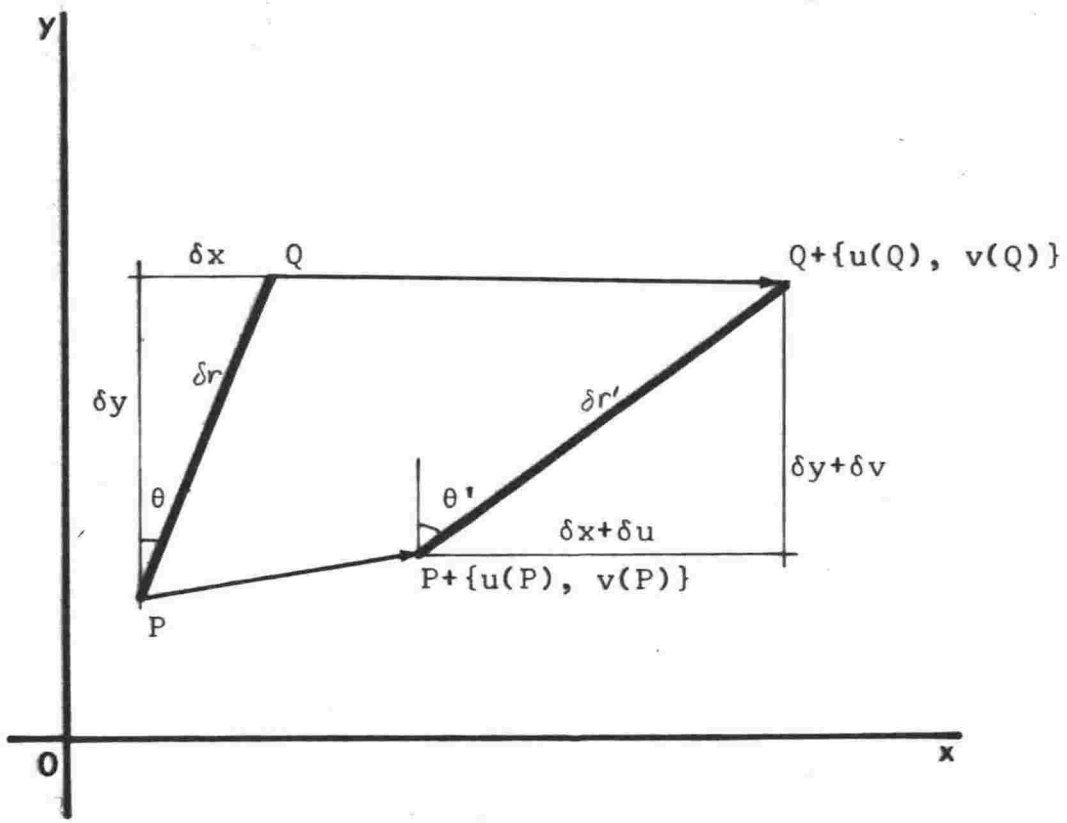

Figure 2.1

area of a surface. Suppose that a surface in plane Oxy is strained and that a point located with respect to the origin by the position vector $\underline{P}$ moves to $\underline{P}$ + {u(P), v(P)} and a nearby point $\underline{Q}$ moves to $\underline{Q}$ + {u(Q), v(Q)} where u and v are differentiable functions of displacement in the directions x and y respectively (figure 2.1). Then, by Taylor's theorem

$$u(Q) = u(P) + \frac{\partial u}{\partial x}\delta x + \frac{\partial u}{\partial y}\delta y + \text{higher derivatives of } u$$

$$v(Q) = v(P) + \frac{\partial v}{\partial x}\delta x + \frac{\partial v}{\partial y}\delta y + \text{higher derivatives of } v \qquad - 1$$

where δx and δy are the co-ordinates of Q with respect to P.

We will restrict consideration to homogeneous strain, that is where displacements vary linearly in the plane. In this case differentials $\frac{\partial u}{\partial x}$ etc. are constants and higher derivatives zero; hence equations (1) reduce to

$$\delta u = u(Q) - u(P) = \frac{\partial u}{\partial x}\delta x + \frac{\partial u}{\partial y}\delta y$$

$$\delta v = v(Q) - v(P) = \frac{\partial v}{\partial x}\delta x + \frac{\partial v}{\partial y}\delta y \qquad - 2$$

where δu and δv are the components of the displacement of Q relative to P.

We introduce and define the components of strain at a point as:

$$\sigma = \tfrac{1}{2}\left(\frac{\partial u}{\partial x} + \frac{\partial v}{\partial y}\right)$$

$$\omega = \tfrac{1}{2}\left(\frac{\partial u}{\partial y} - \frac{\partial v}{\partial x}\right)$$

$$\gamma_1 = \tfrac{1}{2}\left(\frac{\partial u}{\partial x} - \frac{\partial v}{\partial y}\right) \qquad - 3$$

$$\gamma_2 = \tfrac{1}{2}\left(\frac{\partial v}{\partial x} + \frac{\partial u}{\partial y}\right)$$

where σ is the dilatation, γ_1 and γ_2 are the components of 'tensor' shear strain and ω is not a deformation but a rigid body rotation which does however enter into considerations.

Substituting (3) in (2) gives:

$$\delta u = (\sigma + \gamma_1)\delta x + (\gamma_2 + \omega)\delta y$$

$$\delta v = (\gamma_2 - \omega)\delta x + (\sigma - \gamma_1)\delta y \qquad - 4$$

Let the length of PQ be δr and of P'Q' be $\delta r'$, then from figure 2.1:

$$\delta r'^2 = (\delta x + \delta u)^2 + (\delta y + \delta v)^2$$
$$= [\delta x(1+\sigma+\gamma_1)+\delta y(\gamma_2+\omega)]^2+[\delta y(1+\sigma-\gamma_1)+\delta x(\gamma_2-\omega)]^2$$

Now, and in all that follows, we assume that σ, γ_1, γ_2 and ω are small quantities, i.e. that their squares and higher terms are much less than one. Then, applying the binomial expansion gives:

$$\delta r'^2 = \delta x^2(1+2\sigma+2\gamma_1) + 4\delta x\delta y\gamma_2 + \delta y^2(1+2\sigma-2\gamma_1) + O(\gamma^2)$$

Putting $\delta x = \delta r\mathrm{Sin}\theta$ and $\delta y = \delta r\mathrm{Cos}\theta$ where θ is the angle between PQ and the direction Oy, i.e. transforming to polar co-ordinates we have, using the binomial expansion:

$$\delta r'^2 = \delta r^2(1 + 2\sigma - 2\gamma_1\mathrm{Cos}2\theta + 2\gamma_2\mathrm{Sin}2\theta) + O(\gamma^2)$$

$$\text{i.e. } \delta r' = \delta r(1 + \sigma - \gamma_1\mathrm{Cos}2\theta + \gamma_2\mathrm{Sin}2\theta) + O(\gamma^2) \qquad - 5$$

We define the elongation ε of PQ by $\varepsilon = (\delta r' - \delta r)/\delta r$, then from (5):

$$\varepsilon = \sigma - \gamma_1\mathrm{Cos}2\theta + \gamma_2\mathrm{Sin}2\theta \qquad - 6$$

Now consider the rotation of line PQ. From figure 2.1:

$$\mathrm{Tan}\theta' = \frac{\delta x + \delta u}{\delta y + \delta v} \qquad - 7$$

$$= \frac{\delta x(1 + \sigma + \gamma_1) + \delta y(\gamma_2 + \omega)}{\delta y(1 + \sigma - \gamma_1) + \delta x(\gamma_2 - \omega)}$$

which, noting that $\text{Tan}\theta = \frac{\delta x}{\delta y}$

$$= \frac{(1 + \sigma + \gamma_1) + (\gamma_2 + \omega)\text{Cot}\theta}{(1 + \sigma - \gamma_1) + (\gamma_2 - \omega)\text{Tan}\theta} \text{Tan}\theta$$

Therefore, using the binomial expansion:

$$\text{Tan}\theta' = \{1+2\gamma_1+(\gamma_2+\omega)\text{Cot}\theta-(\gamma_2-\omega)\text{Tan}\theta\}\text{Tan}\theta+0(\gamma^2) \qquad - 8$$

Putting $\alpha_1 = \theta' - \theta$ and noting that the change in azimuth of PQ is small we can write:

$$\text{Tan}\theta' = \text{Tan}(\theta+\alpha_1) \simeq \frac{\text{Tan}\theta+\alpha_1}{1-\alpha_1\text{Tan}\theta} \simeq \text{Tan}\theta+\frac{\alpha_1}{\text{Cos}^2\theta} \qquad - 9$$

Hence, eliminating $\text{Tan}\theta'$ from (8) and (9) we have:

$$\alpha_1 = \gamma_1\text{Sin}2\theta + \gamma_2\text{Cos}2\theta + \omega \qquad - 10$$

Positive α_1 is the clockwise rotation of PQ; it is independent of σ. Let PR be normal to PQ and α_2 the rotation of PR. Replacing θ by $\theta + \frac{\pi}{2}$ in (10) gives:

$$\alpha_2 = -\gamma_1\text{Sin}2\theta - \gamma_2\text{Cos}2\theta + \omega \qquad - 11$$

Putting $P_2 = \frac{1}{2}(\alpha_1 - \alpha_2)$ we have:

$$P_2 = \gamma_1\text{Sin}2\theta + \gamma_2\text{Cos}2\theta \qquad - 12$$

Consider the change in the angle between a pair of originally orthogonal lines oriented $\frac{\pi}{4}$ clockwise from PQ and PR. Denote this change P_1, it is obtained by substituting $\theta + \frac{\pi}{4}$ for θ in (12).

$$P_1 = \gamma_1\text{Cos}2\theta - \gamma_2\text{Sin}2\theta \qquad - 13$$

P_1 and P_2 are the components of tensor shear strain relative to a set of axes oriented θ clockwise from those to which γ_1 and γ_2 refer. It will be noted that they represent half the change in the right angles between pairs of orthogonal lines. The full angular changes are referred to

as 'engineering' shear strains. Therefore the numerical values of engineering shear strains are twice those of tensor shear strains. In the strain analyses reported below engineering shear strains have been computed; the symbols used for them are γ_1 and γ_2 as have been used for tensor shear strain in this chapter.

Differentiating (6) with respect to θ shows that ε has stationary values where

i) $\quad \mathrm{Sin}2\theta = \frac{\gamma_2}{\gamma}$ and $\mathrm{Cos}2\theta = \frac{-\gamma_1}{\gamma}$

and ii) $\quad \mathrm{Sin}2\theta = \frac{-\gamma_2}{\gamma}$ and $\mathrm{Cos}2\theta = \frac{\gamma_1}{\gamma}$ - 14

Where $\gamma^2 = \gamma_1^2 + \gamma_2^2$. i) and ii) define an orthogonal pair of lines termed the principal axes of strain; ε is a maximum on i) which is the principal axis of extension and a minimum on ii) which is the principal axis of compression.

Differentiating (11) with respect to θ shows that P_2 has stationary values where $\mathrm{Tan}2\theta = \frac{\gamma_1}{\gamma_2}$, i.e. on an orthogonal pair of lines oriented at $\frac{\pi}{4}$ to the principal axes of strain. The maximum of P_2 is γ and the minimum is $-\gamma$ where $\gamma^2 = \gamma_1^2 + \gamma_2^2$ as above; γ is referred to as the total shear strain. From (12) and (13) we have

$$P_1^2 + P_2^2 = \gamma_1^2 + \gamma_2^2 = \gamma^2$$

i.e. the total shear strain is an invariant.

2.3 Least Squares Shear Strain Estimates from Angular Changes (Frank's Method)

In a region which has been homogeneously strained the change $\delta\theta_{ij}$ in the azimuth of a line ij with original azimuth θ_{ij} is given by equation (10). Rewriting this for the change $\delta\phi_{jk}$ in the angle ϕ_{jk} between two lines ij and ik (figure 2.2) we have

$$(\mathrm{Sin}2\theta_{ik} - \mathrm{Sin}2\theta_{ij})\gamma_1 + (\mathrm{Cos}2\theta_{ik} - \mathrm{Cos}2\theta_{ij})\gamma_2 = \delta\theta_{ik} - \delta\theta_{ij}$$

i.e. $2\mathrm{Cos}(\theta_{ik} + \theta_{ij})\mathrm{Sin}\phi_{jk}\gamma_1 - 2\mathrm{Sin}(\theta_{ik} + \theta_{ij})\mathrm{Sin}\phi_{jk}\gamma_2 = \delta\phi_{jk}$

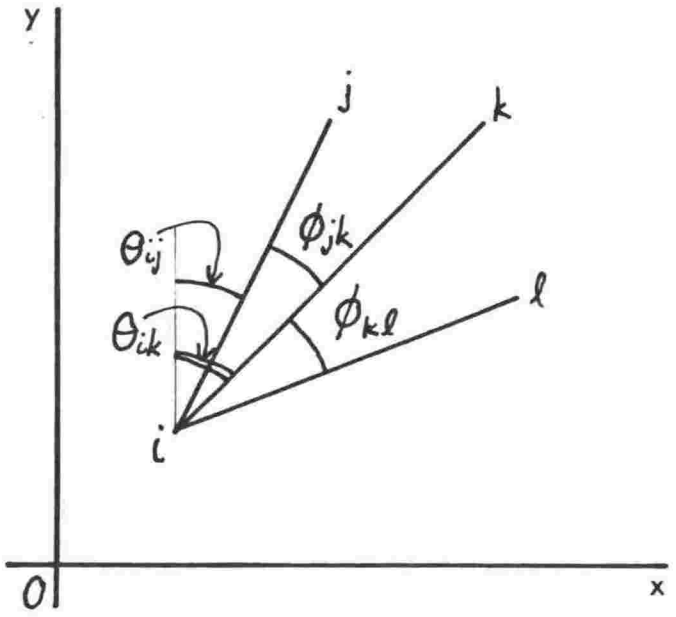

Figure 2.2 Lines ij, ik, il showing azimuths θij and θik and angles φjk, φkl.

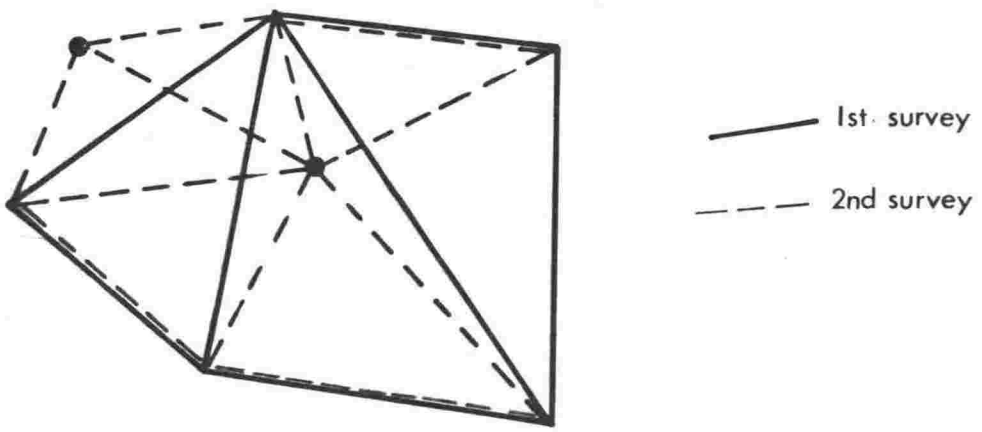

Figure 2.3 Hypothetical triangulation nets showing that with the addition of a few new points old points may be resurveyed without repeating observations of the angles observed in the first survey.

which may be rewritten with obvious substitution as:

$$a_{i1}\gamma_1 + a_{i2}\gamma_2 = b_i \qquad - 15$$

defining a_{i1}, a_{i2} and b_i.

If a number of angles are observed in a region at time t_0 and re-observed at a later time t_a, in general, the angles recorded at t_a will be slightly different from those recorded at t_0; the difference being partly due to observational error and partly due to deformation of the survey net in the interval. If it is postulated that the net has been homogeneously strained then the angular changes b_i constitute a set of observations from which least squares estimates of the components of shear strain can be made. Assuming that the strain rate is constant, observation equations have the form (following equation (15)):

$$(t_a - t_0)(a_{i1}\dot{\gamma}_1 + a_{i2}\dot{\gamma}_2) = b_i + \upsilon_i \qquad - 16$$

where $\dot{\gamma}_1$ and $\dot{\gamma}_2$ are estimates of shear strain rates and υ_i are residuals the sum of squares of which is to be minimized. In matrix notation (15) is written

$$t\ A\ \Gamma = b + \upsilon \qquad - 17$$

where t $(= t_a - t_0)$ is a scalar, Γ is the vector $\{\dot{\gamma}_1, \dot{\gamma}_2\}$ and, if there are n observations, A is a nx2 matrix composed of a_{i1} and a_{i2}; b and υ are vectors. It is usual to multiply each observation equation by a weight according to the reliability ascribed to it, whence (17) becomes

$$t\ W^{\frac{1}{2}}\ A\ \Gamma = W^{\frac{1}{2}}b + W^{\frac{1}{2}}\upsilon$$

where W is the weighting matrix. If all observations are independent the leading diagonal of W is composed of the inverses of variances of observations and all other components are zero. If observations are correlated, off-diagonal components of W will be non-zero. In the case considered

here some observations are correlated. For instance, for adjacent angles (e.g. ϕ_{jk} and ϕ_{kl} in figure 2.2) a positive error in one correlates with a negative error in the other. Prescott (1976) gives formulae for the generation of the weighting matrix for this problem and shows that disregarding correlations may lead to underestimation of standard errors of $\dot{\gamma}_1$ and $\dot{\gamma}_2$ by the order of 25%; strain estimates are not biased however.

The Normal Equations (see for instance Bomford, 1971) are

$$A^T W A \Gamma = \frac{1}{t} A^T W b$$

A^TWA is a 2 x 2 matrix hence solution of (17) is rapid. Neglecting correlation considerations the problem is programmable for pocket calculators (Bibby and Walcott, 1977), and with a small computer subsets of data can quickly be analysed interactively to test the stability of results. Poor data resulting from observational blunders or mislocation of stations can easily be located and corrected or excluded, a facility which is particularly useful with old data. The main limitation is that the method only makes use of repeated observations of angles when it is frequently the case that while many points are common to old and new surveys the networks connecting them are quite different and the number of re-observed angles small (e.g. figure 2.3). This problem is overcome by the method of Bibby (1973) in which the components of strain are estimated by the simultaneous least squares adjustment of as many surveys with common points as exist in a particular area. The exposition of Bibby's method requires first a description of the 'adjustment' of a single survey.

2.4 Bibby's method of estimating crustal strain from survey data

In the course of a survey of a net of points more observations will generally be made than are necessary to determine the co-ordinates of the points. A least squares 'adjustment' is therefore made to produce a unique and most likely set

of co-ordinates (see for instance Bomford, 1971). For the least squares procedure equations are constructed relating observations to the co-ordinates of points. The set of equations is non-linear and therefore requires an iterative solution. By some prior means first estimates are made of the co-ordinates (x_i, y_i) of points relative to an arbitrary origin. Small corrections δx_i and δy_i are then sought which will minimize the sum of the squares of residuals. Generally, observations are either of distances between points or angles between rays connecting points. Observation equations have the form

i) for distance observations

$$\frac{\partial \overline{s_{ij}}}{\partial x_i}\delta x_i + \frac{\partial \overline{s_{ij}}}{\partial y_i}\delta y_i + \frac{\partial \overline{s_{ij}}}{\partial x_j}\delta x_j + \frac{\partial \overline{s_{ij}}}{\partial y_j}\delta y_j = (s_{ij} - \overline{s_{ij}}) + \upsilon_s \qquad - 18a$$

where $\overline{s_{ij}}$ is the distance between points i and j, computed from the trial co-ordinates, s_{ij} is the measured distance and υ_s is the residual.

ii) for angular observations

$$\left(\frac{\partial \overline{\theta_{ik}}}{\partial x_i}\delta x_i + \frac{\partial \overline{\theta_{ik}}}{\partial y_i}\delta y_i + \frac{\partial \overline{\theta_{ik}}}{\partial x_k}\delta x_k + \frac{\partial \overline{\theta_{ik}}}{\partial y_k}\delta y_k\right) - \left(\frac{\partial \overline{\theta_{ij}}}{\partial x_i}\delta x_i + \frac{\partial \overline{\theta_{ij}}}{\partial y_i}\delta y_i + \frac{\partial \overline{\theta_{ij}}}{\partial x_j}\delta x_j + \frac{\partial \overline{\theta_{ij}}}{\partial y_j}\delta y_j\right)$$

$$= (\phi_{jk} - \overline{\phi_{jk}}) + \upsilon_a \qquad - 18b$$

where $\overline{\theta_{ij}}$ and $\overline{\theta_{ik}}$ are the azimuths of the lines ij and ik computed from trial co-ordinates, $\overline{\phi_{jk}}$ is the trial value of the angle between ij and ik, ϕ_{jk} is the measured angle and υ_a is the residual (figure 2.2).

Least squares estimates of δx_i etc. are obtained by solving the normal equations derived from these observation equations. Differentials $\frac{\partial \overline{s_{ij}}}{\partial x_i}$, $\frac{\partial \overline{\theta_{ik}}}{\partial y_k}$ etc. have been computed using trial values of $x_i y_i$ and therefore are only approximate. Estimates δx_i are correspondingly approximate but if the original trial values of x_i etc. were sufficiently near

true values the corrections δx_i so obtained will improve the estimates of x_i from which more accurate values of $\frac{\partial s_{ij}}{\partial x_i}$ etc. can be computed etc. In practice when applied to reasonably well conditioned survey data the system converges in three or four iterations.

Now consider a situation where a survey of a net is made at time t_0 and at a later time t_a a second survey is made of some or all of the points in the first survey. If the net has deformed in the interval the positions of stations relative to the chosen origin will be different in the second survey than in the first and different δx_i etc. will be required. In the very simple net shown in figure 2.4 the true configuration at time t_0 is OPQ and at t_a, OP'Q'. P_s and Q_s are trial positions for the points. $\overline{P_sP}$ and $\overline{Q_sQ}$ are the corrections sought by least squares to give the co-ordinates of P and Q at time t_0. $\overline{PP'}$ and $\overline{QQ'}$ are the additional corrections required for the later survey. If the net has been homogeneously strained the components of $\overline{PP'}$ and $\overline{QQ'}$ will be given by the integrals of equations (4). Assuming a constant strain rate we write $\gamma_1 = A_1 t$, $\gamma_2 = A_2 t$, $\sigma = A_3 t$ and $\omega = A_4 t$ where $t = t_a - t_0$. If the co-ordinates of P are, for instance, (x, y), then following equations (4) the components Δu, Δv of $\overline{PP'}$ will be

$$\Delta u = t\{(A_3 + A_1)x + (A_2 + A_4)y\} \qquad - 19a$$

$$\Delta v = t\{(A_2 - A_4)x + (A_3 - A_1)y\} \qquad - 19b$$

Observation equations for the second survey will have exactly the same form as those for the first (i.e. equations (18)) but with δx_i, δy_i replaced by $\delta x_i'$, $\delta y_i'$ where

$$\delta x_i' = \delta x_i + \Delta u + \delta(\Delta u) \qquad - 20$$

where $\delta(\Delta u)$ are the corrections to be made to Δu etc.

Substituting (19a) in (20) gives

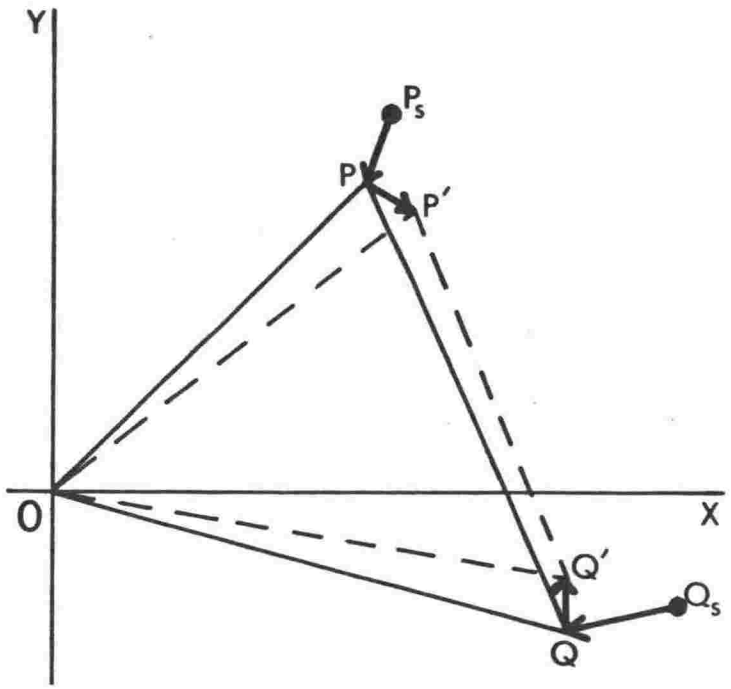

Figure 2.4 Hypothetical net with true configurations OPQ at time t_0 and OP'Q' at time t_a. P_s and Q_s are trial points.

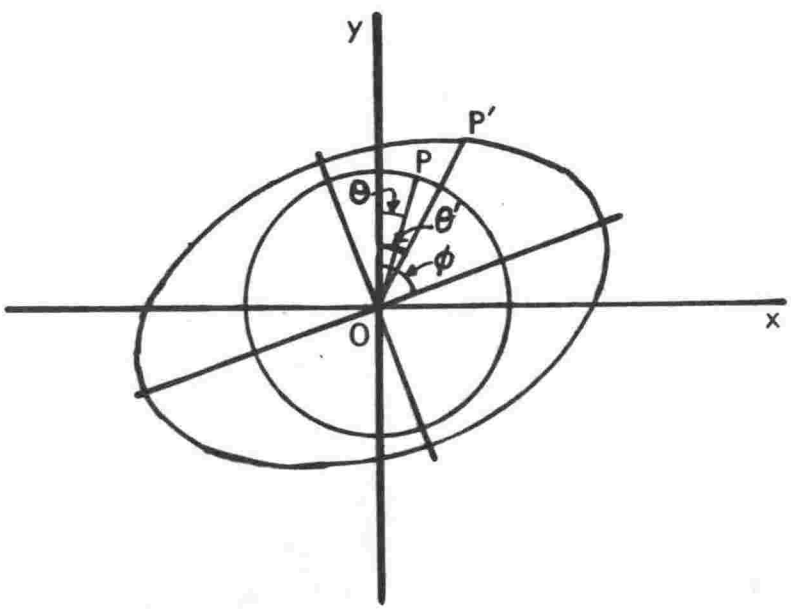

Figure 2.5 A circle when homogeneously strained becomes an ellipse.

$$\delta x_i' = \delta x_i + t\{(A_3 + A_1)x + (A_2 + A_4)y\} + t\{(\delta A_3 + \delta A_1)x + (A_3 + A_1)\delta x + (\delta A_2 + \delta A_4)y + (A_2 + A_4)\delta y\} \qquad - 21$$

$\delta y_i'$ can be similarly derived from equation (19b).

Using equations (18) and (21) a single set of linear observation equations including observations from both surveys can be set up and solved iteratively to give least squares estimates of both the co-ordinates of points at time t_0 and the components of strain rate. Prior estimates of the strain rate components $A_j (j=1,4)$ are required in the same way as are prior estimates of point co-ordinates. It is sufficient however to begin assuming zero strain rates. δA_j are unknown small corrections sought to improve the estimates of A_j. In the least squares procedure δA_j are analogous to δx_i.

Since both angular and distance measurements can be included it is necessary to multiply observation equations by appropriate weights to make them dimensionally equivalent. Ideally, weights should equal the reciprocal of the standard errors of observation. These are not known precisely in advance but can be estimated. When an iteration is completed standard errors are known, new weights are computed using the standard errors from the previous iteration and another iteration made etc. until no further refinement ensues (Bosman and Kubik, 1971). In the weighting procedure adopted group standard errors σ_s and σ_a are estimated for distance and angular measurements separately for each survey, viz.

$$\sigma_s^2 = \frac{1}{N_s} \sum_1^{N_s} \upsilon_s^2 \qquad \sigma_a^2 = \frac{1}{N_a} \sum_1^{N_a} \upsilon_a^2$$

where N is the number of observations in a group and υ_s and υ_a are distance and angular residuals respectively. Thus more accurate surveys are weighted more heavily.

Bibby's method is not restricted to the use of two surveys. An observation made at any time t can be entered

with an equation including the appropriate value for time, i.e. $(t - t_0)$. And the method is easily extended to estimate strain as a function of time or position. For instance, if displacements Δu, Δv were assumed to vary as polynomials on plane Oxy equations (19) and (21) would have more terms and there would accordingly be additional unknowns in the least squares adjustment. As long as the strain function is differentiable its form is not governed by the method, but in practice only homogeneous strain at a constant rate has been estimated.

Where distances and azimuths have been measured Bibby's method can be used to estimate dilatation and rotation as well as the components of shear strain. But where only angular measurements have been made the components A_3 and A_4 can be set to zero and the estimates thus restricted to the two components of shear strain without prejudicing the rest of the procedure.

The method requires that large sets of linear equations be solved and this limits the number of points which can be included in any one analysis. As set up at present the computer programme can deal with up to 28 points at a time.

2.5 Interpretation of Strain

The strain ellipse: Consider a point P on the circle $x^2 + y^2 = r^2$. Its co-ordinates are $(r\mathrm{Sin}\theta, r\mathrm{Cos}\theta)$ where θ is the azimuth of radius OP (figure 2.5). In general, when the circle is strained homogeneously the length and azimuth of OP will change. Let x' be the new x co-ordinate of P, then in the notation used in section 2.2

$$x' = (1 + \varepsilon)r\mathrm{Sin}(\theta + \alpha_1)$$

where ε is the elongation of OP and α_1 its change in azimuth. Since α_1 is small $\mathrm{Sin}(\theta + \alpha_1) \simeq \mathrm{Sin}\theta + \alpha_1\mathrm{Cos}\theta$, hence from equations (6) and (10)

$$\begin{aligned} x' &= r(1+\sigma-\gamma_1\mathrm{Cos}2\theta+\gamma_2\mathrm{Sin}2\theta)(\mathrm{Sin}\theta+\mathrm{Cos}\theta(\gamma_1\mathrm{Sin}2\theta+\gamma_2\mathrm{Cos}2\theta-\omega)) \\ &= r((1+\sigma)\mathrm{Sin}\theta+\gamma_1\mathrm{Sin}\theta+\gamma_2\mathrm{Cos}\theta-\omega\mathrm{Cos}\theta)+0(\gamma^2) \end{aligned} \qquad - 21$$

Similarly,

$$y' = r((1+\sigma)\cos\theta-\gamma_1\cos\theta+\gamma_2\sin\theta+\omega\sin\theta)+0(\gamma^2) \qquad - 23$$

Eliminating θ from (21) and (22) and neglecting squares and products of small quantities gives

$$(1 - 2\gamma_1)x'^2 + (1 + 2\gamma_1)y'^2 - 4\gamma_2 x'y' = (1 + 2\sigma)r^2 \qquad - 24$$

Thus, a circle when homogeneously strained becomes an ellipse. This is known as the strain ellipse.

By standard theory the azimuths of the axes of the ellipse are given by

$$\tan 2\lambda = -\frac{\gamma_2}{\gamma_1}$$

which is equivalent to equations (14), hence the axes of the strain ellipse are the principal axes of strain.

Related to its principal axes the equation of the ellipse is

$$(1 - 2\gamma)x^2 + (1 + 2\gamma)y^2 = (1 + 2\sigma)r^2$$

From this equation it can be seen that, for pure shear strain, i.e. zero dilatation and rotation $x = (1 + \gamma)r$ on the x axis and $y = (1 - \gamma)r$ on the y axis. Thus shear strain previously shown to be the change in azimuth between two orthogonal lines at $\frac{\pi}{4}$ to the principal axes is seen also to represent equal and opposite longitudinal strain on the principal axes.

The area A of the original circle was πr^2; the area A' of the ellipse is $\pi(1 + 2\sigma)r^2$. Hence $A' = (1 + 2\sigma)A$, i.e. the dilatation σ represents the change in area per unit area.

Additional interpretations of shear strain: From equations (6) and (10) it follows that for axes oriented such that Oy points north γ_1 represents east-west extension and north-south compression or southeast dextral motion or northeast sinistral motion; while γ_2 represents northeast-southwest

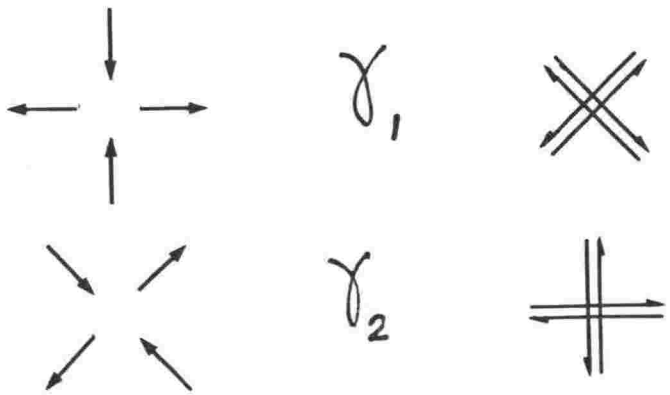

Figure 2.6 Interpretations of shear strain components.

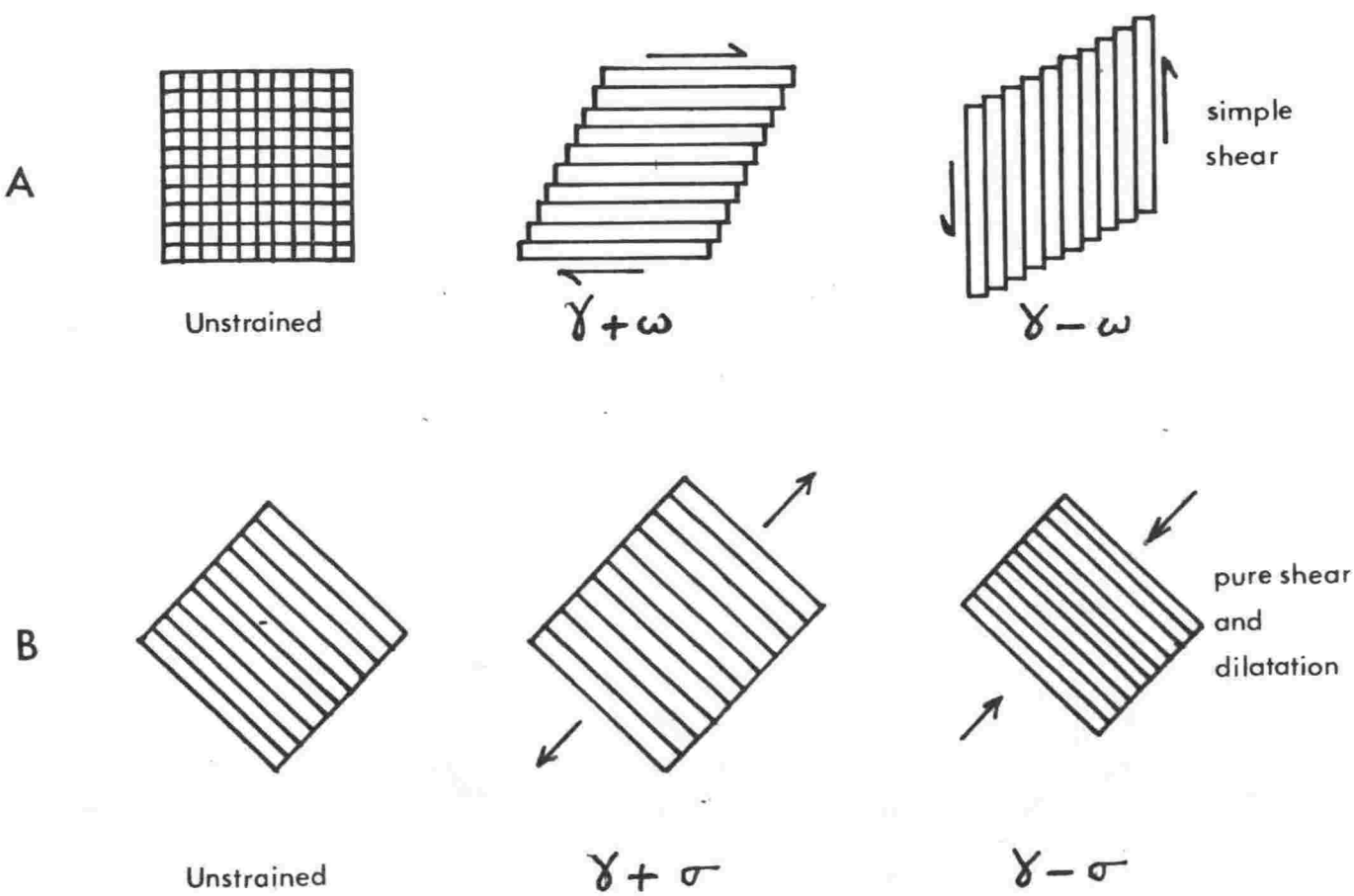

Figure 2.7 Homogeneous deformations by movements on parallel faults with zero length and azimuth change parallel to faults.

extension and northwest-southeast compression or east-west dextral motion or north-south sinistral motion. These alternatives are summarized in figure 2.6.

It follows also from (6) and (10) that shear strain transforms squares into rhombs. Strictly strain is a continuum concept so that the squares would be envisaged as deforming plastically or elastically into their new shapes, but if the deformation is thought of as occurring on closely spaced parallel faults it can be achieved in various ways as shown in figure 2.7. Figure 2.7A shows simple shear which includes a rotation of plus or minus ω and involves transcurrent faulting. Figure 2.7B shows irrotational shear with positive and negative dilatation σ, this mechanism involves normal or reverse faulting. Irrotational shear without dilatation is called pure shear.

The rotation ω is a small rotation relative to an external frame. Since azimuth is not often measured in geodetic surveys it is usually impossible to distinguish between pure and simple shear geodetically. It is possible however to infer the nature of shear from the orientation of faults relative to the principal axes of strain. It will be seen that in figure 2.7, for pure shear strain, faults are parallel to one principal axis and faulting is reverse or normal while for simple shear strain faults are at $\frac{\pi}{4}$ to the principal axes and faulting is transcurrent.

Displacements from strain: The relative displacements of points can be computed from strain using the integrals of equations (4). For a unique solution values of σ, γ_1, γ_2 and ω are required. Usually, however, only γ_1 and γ_2 are known and an infinite number of different displacements could be inferred depending on assumptions made concerning σ and ω. A particularly simple assumption which gives a unique solution is that changes of length and azimuth are zero in one direction. With this assumption if γ_1 and γ_2 are computed in a frame of reference such that Oy is parallel to the direction

of no change it follows from (6) and (10) that $\sigma = \gamma_1$ and $\omega = -\gamma_2$. In this case equations (4) reduce to

$$\Delta u = 2\gamma_1 \Delta x \qquad \Delta v = 2\gamma_2 \Delta x \qquad - 25$$

Where subparallel faulting is the dominant tectonic expression it may be argued that length and azimuth changes parallel to faults are negligible compared to changes in all other directions and therefore that equations (25) apply. In this case Δu is the normal or reverse component of fault motion and Δv is the transcurrent component. In the strain results presented in the following chapter, γ_1 and γ_2 are computed relative to fault directions.

2.6 Note on the Variation of Geodetic Strain with Time and Position

Geodetic analyses by Frank's or Bibby's method give average homogeneous strain rates for periods of 10 to 100 years in zones 10-30 km across depending on the survey data available. If 'secular' strain accumulates smoothly and homogeneously over a region containing several zones, a simple pattern of strain with principal axes oriented identically in all zones and with the same strain magnitude everywhere will obtain as is shown in rows 1 and 2 in figure 2.8. But if there is a large crustal earthquake in the period between surveys much larger apparent strain rate rates will be expected and the strain for the region as a whole will be non-homogeneous. Because strain is determined in zones of finite width a finite strain will be obtained for a zone straddling an earthquake fault even if the fault breaks the surface. The sense will be that of the secular strain and the magnitude will depend on the fault displacement and the width of the zone. Zones on either side of the fault will, due to elastic rebound, have strain in the opposite sense to the secular strain. In rows 3 and 4 of figure 2.8 patterns

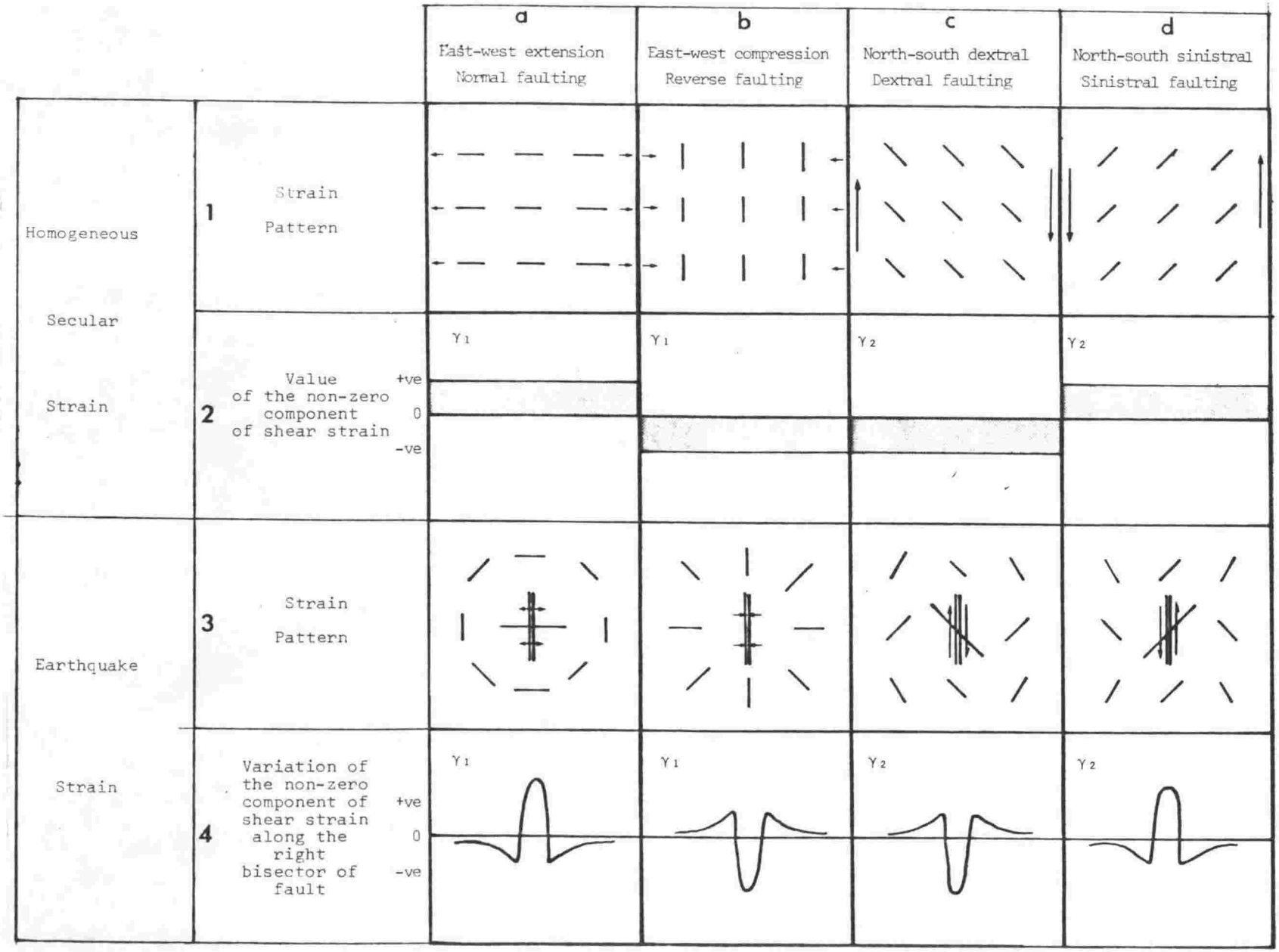
a
East-west extension
Normal faulting
b
East-west compression
Reverse faulting
c
North-south dextral
Dextral faulting
d
North-south sinistral
Sinistral faulting
Homogeneous
Secular
Strain
1
Strain
Pattern
2
Value
of the non-zero
component
of shear strain
+ve
0
-ve
γ1
γ1
γ2
γ2
Earthquake
Strain
3
Strain
Pattern
4
Variation of
the non-zero
component of
shear strain
along the
right
bisector of
fault
+ve
0
-ve
γ1
γ1
γ2
γ2

to be expected from normal, reverse, dextral, and sinistral faulting and elastic rebound are presented qualitatively. In Chapter 5 normal faulting associated with the 1922 Taupo Earthquakes is considered quantitatively.

CHAPTER 3 ANALYSIS OF CENTRAL NORTH ISLAND GEODETIC DATA FOR STRAIN

3.1 Data

Almost all data in New Zealand at present available for crustal strain analysis are from triangulations. The earliest triangulations in the central North Island were made in the 1870s with transit theodolites read by vernier to 10 seconds of arc for large instruments and to 20 seconds for small. From each point in a survey net eight or twelve sitings were made to each adjacent point and the averages adopted. Triangular closure errors are generally 5 to 15 seconds (25 to 75 μ). The figures were usually centred polygons with rays 5 to 10 km long and a few redundant rays.

Surveys made since about 1910 are graded as 1st, 2nd or 3rd order depending on the precision of the instrument used, the method of observation and the size of figure. Average triangular misclosures are required to be less than 1, 3 and 5 seconds (i.e. 5, 15 and 25 μ) respectively and the maximum triangular misclosures to be less than 3, 5 and 8 seconds (15, 25 and 40 μ) respectively. Rays are about 40 km long in 1st order surveys and 5 to 10 km long in 2nd and 3rd order surveys. Since the mid-1960s geodimeter distance measurements with accuracies of a few parts per million (about 5 μ) have been included in many surveys.

In the strain analyses reported below, raw field data from field books and summaries, and not adjusted data, were used. The data were collected in three groups covering the three areas, named here: 'Tongariro', 'North Taupo' and 'Bay of Plenty' (figure 3.1).

In the Tongariro and North Taupo areas the first surveys were made before 1890, and later surveys (all 2nd order) mainly between 1950 and 1976. In the Bay of Plenty area two 1st order surveys were used; the first was made between 1925 and 1929 and the second in 1976.

Field books and summaries containing all of the data are stored either at the Hamilton or at the Wellington district office of the Department of Lands and Survey. Summaries of 1st and 2nd order surveys are held at the Head Office, Wellington. The field books used are listed in Appendix 1.

3.2 Subdivision of Data Within Areas

Most of the data was analysed by Bibby's method and as mentioned above the computing time required by this method limits the number of points which can be included in a single adjustment. The computer programme was set up to take a maximum of 28 points and therefore the areas defined above were subdivided into zones with 28 or less points. Because not all points occur in more than one survey the number of re-observed points in any one zone is less than 28. A maximum of 14 was obtained. For statistical reasons discussed below a minimum of 5 re-observed points was required in each adjustment, and it was preferred also that zones be approximately equidimensional. For each adjustment strain is assumed to be homogeneous, thus the components of strain are constant within each zone but generally vary from zone to zone. The desirable size of zones depends on the wavelength of the variation in strain. The actual size used is found by trial and error where there are sufficiently detailed data. Most zones have 5 to 14 re-observed points and rays 5 to 10 km long and therefore are 10 to 30 km across. Generally it proved satisfactory to choose zones with 10 re-observed points, but in parts of the North Taupo area sharp variation in strain required smaller zones therefore with fewer points. In the Bay of Plenty area the surveys are first order and the rays are therefore much longer than elsewhere, hence for the same number of points zones are four to six times larger. Consequently the number of points in Bay of Plenty zones was kept small, even so, as will be seen in figure 3.1, they are larger than those in other areas.

Because of the unavoidably large size of Bay of Plenty zones care was taken to ensure that their boundaries coincide with structural boundaries. Specifically, zone BP2 spans the Taupo Volcanic Zone while zones BP1 and BP3 cover the relatively stable ignimbrite plateaux on each side, and BP4 spans the northern end of the North Island Shear Belt.

Although an even coverage of overlapping zones throughout the study areas would have been preferred available data did not permit this. Figures 3.1 and 3.2 show the zones finally adopted. Appendix 2 records the figures of surveys within the zones.

3.3 Computing

Raw data contain both normally distributed observational errors and 'blunders'. Blunders are where either numbers have been erroneously entered into or transferred from the field book (generally these are multiples of degrees, minutes or seconds) or, for instance, the theodolite has been pointed at a wrong marker. The old and the new surveys in each zone were first adjusted separately in order to locate blunders and to estimate the magnitude of observational errors. The data, minus blunders, were then combined in a single adjustment to determine strain. Because strain is not in practice homogeneous over entire zones residuals from strain adjustments are usually 25% to 50% larger than those for separate adjustments. If strain adjustment residuals are even larger this will generally be due to either

i) mislocation of old survey points (e.g. where a surface mark has been eroded out and incorrectly replaced)

or ii) nontectonic displacement of points (e.g. by hillside slumping or interference by stock).

The points causing large residuals are excluded and the data recomputed.

3.4 Results

The total shear strain rate, the components of shear strain rate, and the azimuth of the principal axis of

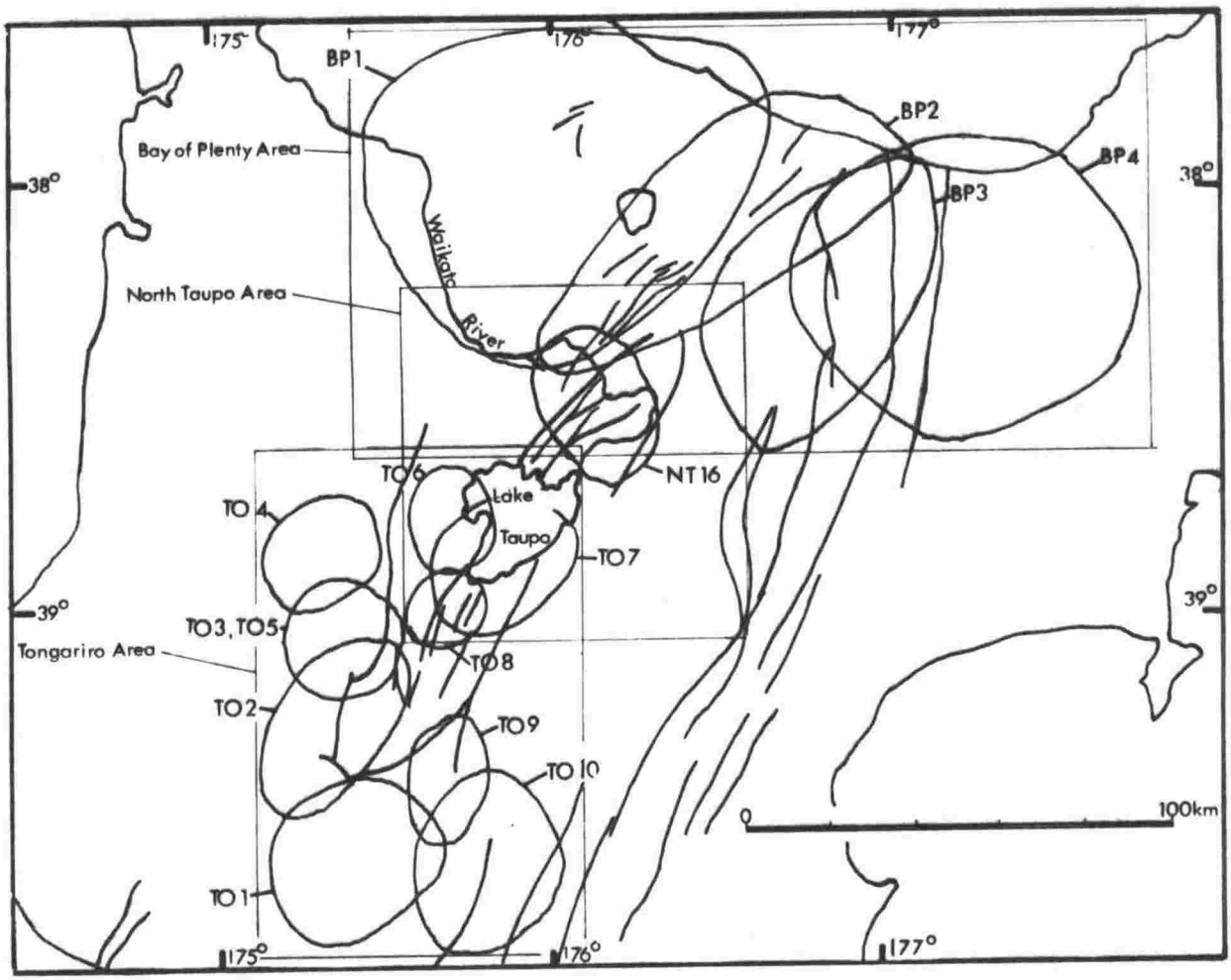

Figure 3.1 Central North Island showing the 'Areas' defined in the text and the 'Zones' for which the components' homogeneous strain have been estimated.

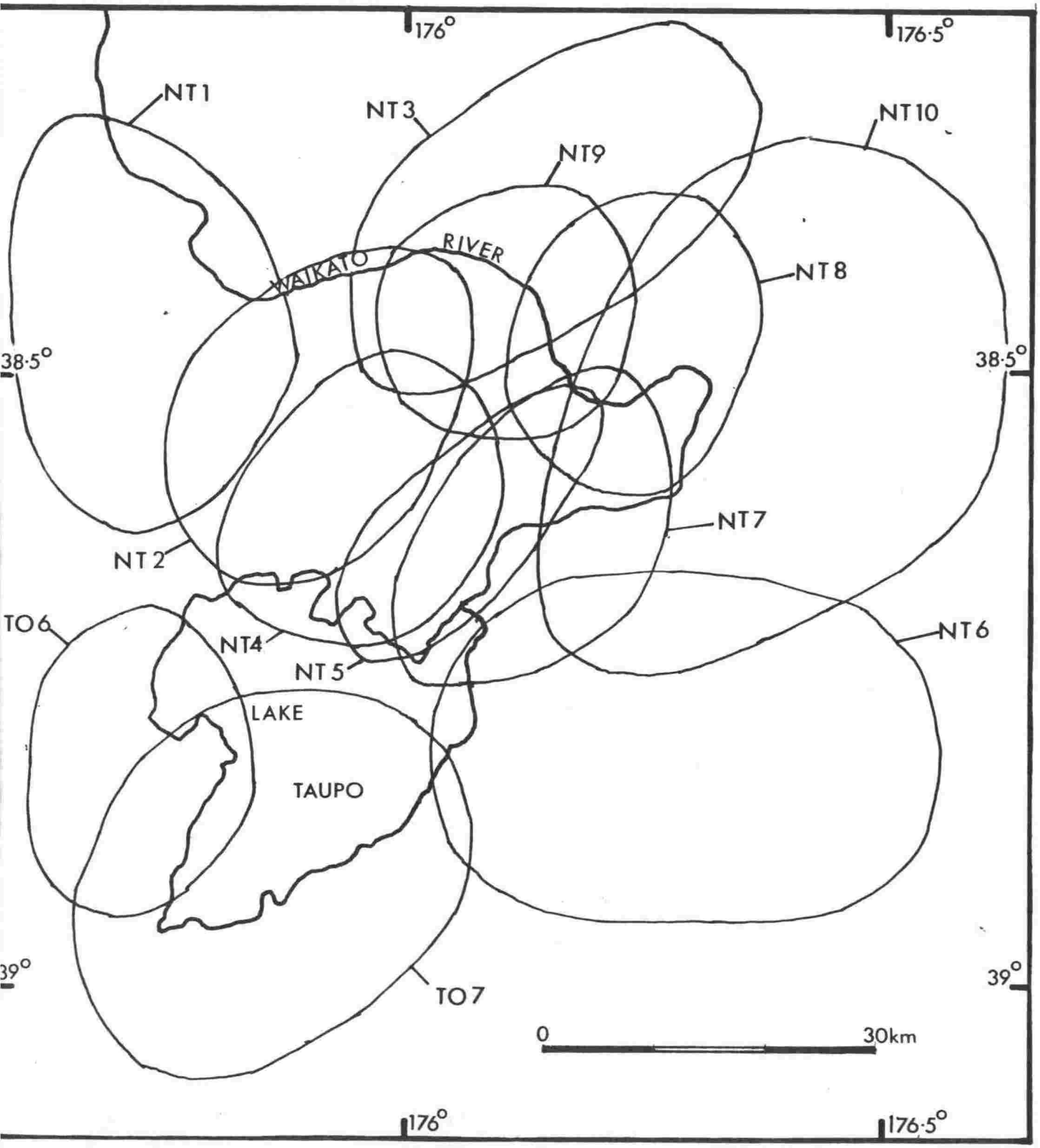

Figure 3.2 Zones near Lake Taupo for which homogeneous strain components have been estimated for the period c1880 to 1950.

extension for all zones for which adjustments converged, together with their standard errors, are given in tables 3.1, 3.2 and 3.3. The components of shear strain rate are computed, as discussed in section 2.5, according to the azimuth of local faults. The azimuths adopted are 022° in the Tongariro area, 040° in the North Taupo area and 045° in the Bay of Plenty area. Standard errors of estimates are derived from the least-squares adjustments. The quality gradings are discussed below. Adjustments for parts of zones and combinations of zones have been made, and in order to indicate the measure of stability in an area all results are recorded. The adopted results are underlined.

Tables 3.4, 3.5 and 3.6 set out the RMS errors for all separate adjustments and for all strain adjustments, and show that the degree of additional error in strain adjustments due to inhomogeneity of strain is about 25%-50%. In addition the tables show the maximum residuals for each strain adjustment and the number of re-observed points in each zone.

3.5 Statistical Significance of Results

For an estimate P of a parameter R, if the probability that the true value of R is in the range P±I is q% then I is the q% confidence interval. For a least-squares estimate, if residuals of the adjustment are normally distributed then $I = t \times \sigma$ where σ is the standard error of estimate and t is Students t which has a known distribution depending on the number of degrees of freedom in the system and on the probability q. In all cases considered here the number of degrees of freedom is greater than six and the t distribution indicates accordingly that I is approximately equal to σ for the 63% confidence interval and 2σ for the 95% confidence interval. For ordinary geodetic adjustments the residuals are usually normally distributed and therefore the above confidence intervals apply. For strain adjustments the residuals are normally distributed provided there are sufficient

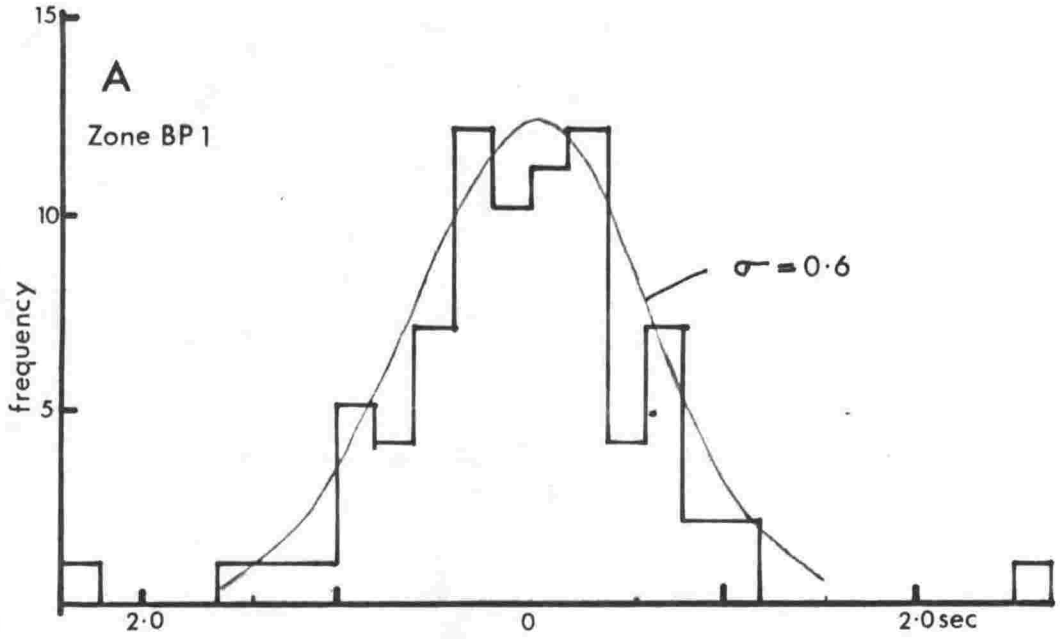

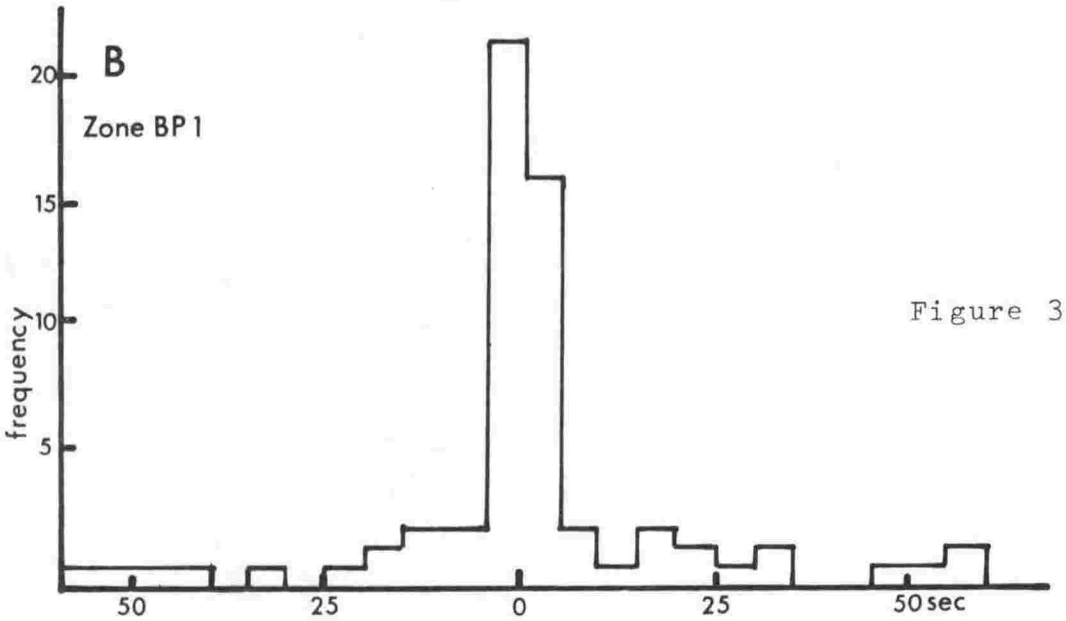

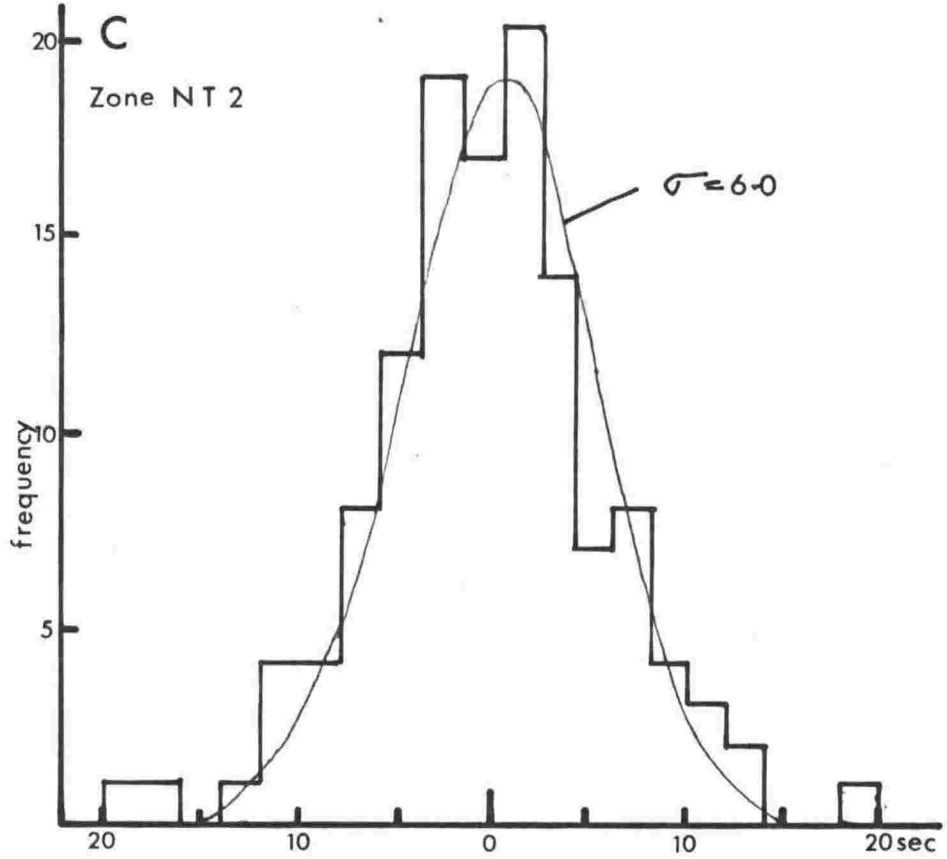

Figure 3.3 Residual distributions from least squares strain adjustments. A and B involve the same data but while in A there are 8 stations common to old and new surveys, in B only 4 have been held common.

re-observed points. For instance, the residuals from adjustments BP1 and NT2 which include 8 and 11 re-observed points respectively are approximately normally distributed (figures 3.3A, C). But when the data from zone BP1 are recomputed holding only four points common the residual distribution becomes non-normal (figure 3.3B) and the significance of standard errors is therefore unknown. It was found that residuals are almost invariably normally distributed for adjustments with seven or more re-observed points and non-normally distributed for adjustments with less than five. Accordingly results are graded A where there are seven or more re-observed points or where a residual plot has been made and is normal; B for adjustments with five or six re-observed points and no residual plot; and R where a residual plot is non-normal. For A graded results one standard error is the 63% confidence interval. B graded results all appear reasonable but the significance of their standard errors is unknown. R graded results are those which have a non-normal residual distribution. R graded results are not considered further.

3.6 Strain Estimates by Frank's Method

Frank's method was applied to those parts of the Bay of Plenty and North Taupo areas having relatively abundant data. The data used are a subset of those used with Bibby's method hence results from both methods should be similar. The results are set out in tables 3.7 and 3.8. In the Bay of Plenty area the only significant result is from zone BP4 where $\dot{\gamma}_1$ is 0.18±0.09 μrad y^{-1} and $\dot{\gamma}_2$ is +0.03±0.08 μrad y^{-1}. Values obtained by Bibby's method are 0.19±0.05 μrad y^{-1} and−0.05±0.05 μrad y^{-1}. In the North Taupo area zones for which Frank's method was applied are different from those for which Bibby's method was applied hence a direct comparison is not possible. However figure 3.4 summarizes results from both methods and there is seen to be good agreement.

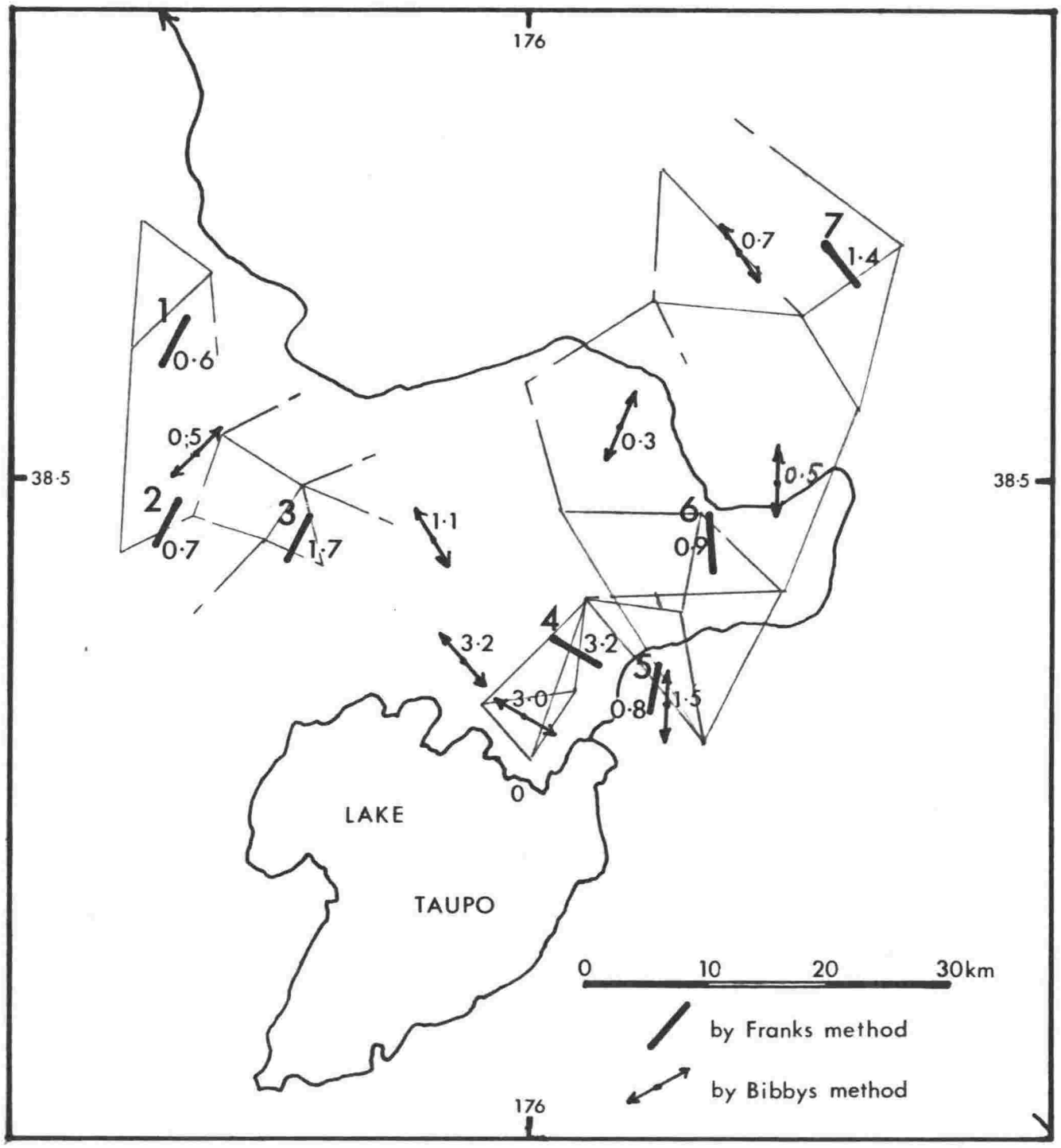

Figure 3.4 Summary of strain rates in the North Taupo Area as computed by Frank's Method and by Bibby's Method. Large numbers indicate zones as numbered in table 3.7, small numbers indicate total shear strain rate in μrad y^{-1}, bars indicate the direction of the principal axis of extension. Triangulation nets used for Frank's Method are shown.

Zone TO	$\dot{\gamma}_1$	$\dot{\gamma}_2$	$\dot{\gamma} = (\dot{\gamma}_1^2 + \dot{\gamma}_2^2)^{\frac{1}{2}}$	ψ^o	Quality Grading	Period
1	0.00±0.05	0.00±0.05	0.00±0.05	-	A	1911-1972
2	0.16±0.21	-0.09±0.21	0.18±0.21	127±40	A	1886-1972
3	0.18±0.16	0.17±0.16	0.25±0.18	090±15	B	1888-1972
4	0.01±0.12	-0.08±0.12	0.08±0.13	-	A	1888-1972
5	0.26±0.18	0.17±0.17	0.31±0.21	096±12	B	1890-1972
6	-0.23±0.13	-0.21±0.13	0.31±0.15	001±10	A	1870-1950
7	0.62±0.08	-0.28±0.08	0.68±0.08	124± 3	A	1899-1975
7M3, 9	0.80±0.27	0.15±0.26	0.82±0.28	107± 9	B	
7M4, 7	0.30±0.19	-0.47±0.19	0.56±0.21	141±10	B	
8	-0.14±0.13	0.65±0.13	0.66±0.13	061± 6	R	1899-1975
9	-0.18±0.11	0.37±0.11	0.41±0.13	054± 7	B	1898-1970
9M7, 12	0.19±0.14	0.19±0.15	0.27±0.15	088±17	B	
10	-0.11±0.12	-0.10±0.11	0.15±0.12	000±21	A	1898-1972

Table 3.1 Tongariro Area strain rates ($\mu rad\ y^{-1}$), $\dot{\gamma}_1$ and $\dot{\gamma}_2$ computed for axes at 022^δ, ψ^δ is the azimuth of the principal axis of extension. One standard error shown. Zone identification, e.g. 7M3, 9, means zone 7 with points 3 and 9 excluded from the strain computation. Zone 5W includes the same re-observed points as zone 3 but with different observation data. Refer to figures 3.1 and 3.2 for location of zones and to Appendix 2 for point locations within zones.

Zone NT	$\dot{\gamma}_1$	$\dot{\gamma}_2$	$\dot{\gamma} = (\dot{\gamma}_1^2 + \dot{\gamma}_2^2)^{\frac{1}{2}}$	ψ°	Quality Grading	Period
1	-0.69±0.26	0.01±0.26	0.69±0.26	041±11	A	1886-1950
1M	-0.36±0.21	-0.24±0.21	0.44±0.21	023±14	A	
1M17,18	-0.53±0.20	-0.09±0.20	0.54±0.21	035±10	A	
2	0.75±0.66	-0.98±0.62	1.23±0.64	156±17	B	1885-1950
2M70	1.54±0.41	-0.15±0.34	1.55±0.64	133± 6	A	
2M70,71	1.43±0.51	-0.15±0.45	1.43±0.51	133±11	A	
2MM70,71	1.55±0.40	-0.26±0.34	1.57±0.40	135± 6	A	
3	0.41±0.19	-0.03±0.19	0.41±0.20	132±13	A	1883-1950
3M15,17,19	0.44±0.23	-0.10±0.21	0.45±0.23	136±13	A	
4	2.87±0.43	0.09±0.43	2.87±0.43	129± 5	A	1885-1950
4M66	3.24±0.49	0.07±0.42	3.24±0.46	129± 5	A	
4M37	3.24±0.43	-0.25±0.43	3.24±0.43	132± 5	A	
4MM37	3.21±0.43	0.16±0.43	3.21±0.43	129± 5	A	
5	2.96±0.45	0.98±0.37	3.12±0.42	121± 5	B	1883-1950
6	-0.58±0.17	-0.56±0.23	0.81±0.25	018± 8	A	1873-1950
7	0.45±0.25	-1.47±0.27	1.54±0.27	167± 6	B	1883-1950
8	-0.17±0.19	-0.34±0.15	0.38±0.20	008±16	B	1878-1950
9	-0.06±0.18	-0.33±0.22	0.33±0.22	000±18	B	1883-1950
	-0.23±0.17	-0.17±0.21	0.29±0.19	021±19	B	
10	0.47±0.34	-1.06±0.43	1.16±0.40	163±10	B	1878-1929
11	-0.35±0.19	-0.90±0.19	0.97±0.21	006± 5	A	1879-1950
12	-0.46±0.17	-0.72±0.21	0.85±0.20	011± 6	A	1873-1950
13	0.47±0.20	-0.08±0.17	0.48±0.20	135± 9	A	1883-1950
13M20	0.41±0.18	-0.10±0.16	0.42±0.18	137±11	A	
14	1.04±0.38	-0.69±0.38	1.25±0.38	147±11	A	1883-1950
15	0.64±0.20	-0.29±0.15	0.69±0.20	142± 7	A	1883-1950
16	0.12±0.11	-0.10±0.11	0.15±0.11	150±21	A	1950-1974

Table 3.2 North Taupo area strain rates (μrad y^{-1}) $\dot{\gamma}_1$ and $\dot{\gamma}_2$ computed for axes at 040° ψ° is the azimuth of the principal axis of extension. One standard error shown. Note: zone 11 is 6+10, 12 is the subset of 11 east of the Kaingaroa Fault, 13 is 3+8+9, 14 is 5+7, 15 is a northeastern subset of 13. Refer to figure 3.2 for locations of zones and to Appendix 2 for locations of points within zones.

Zone	$\dot{\gamma}_1$	$\dot{\gamma}_2$	$\dot{\gamma} = (\dot{\gamma}_1^2 + \dot{\gamma}_2^2)^{\frac{1}{2}}$	ψ^o	Quality Grading	Period
BP1	-0.03±0.05	0.03±0.05	0.04±0.05	-	A	1929-1976
BP1M7	0.05±0.05	0.02±0.05	0.05±0.05	-	A	
BP1M55	-0.01±0.04	0.01±0.04	0.01±0.04	-	A	
BP1M10	0.01±0.05	0.08±0.04	0.08±0.05	92±15	A	
BP2	0.18±0.06	0.10±0.06	0.20±0.06	120± 8	A	1925-1976
BP2M7	0.22±0.07	0.08±0.06	0.23±0.07	125± 7	B	
BP2M10	0.11±0.08	0.09±0.07	0.15±0.08	115±15	B	
BP2M16	0.18±0.06	0.08±0.06	0.20±0.06	123± 9	B	
BP3	-0.03±0.05	0.05±0.04	0.06±0.05	73±23	B	1925-1976
BP3P19) 20)	0.13±0.05	-0.03±0.05	0.13±0.05	141±11	B	
BP4	0.19±0.05	-0.05±0.05	0.20±0.05	142± 7	A	1925-1976
BP4M22	0.20±0.05	-0.04±0.05	0.20±0.05	141± 7	A	
BP4C	0.07±0.06	-0.16±0.06	0.17±0.06	167±10	B	

Table 3.3 Bay of Plenty strain rates (μrad y^{-1}). $\dot{\gamma}_1$ and $\dot{\gamma}_2$ computed for axes at 045, ψ^o is the azimuth of the principal axis of extension. One standard error shown. Zone identification as in table 3.1 except that BP3P19, 20 means zone BP3 plus points 19 and 20. BP4C is a central subset of BP4. Refer to figure 3.1 for locations of zones and to Appendix 2 for locations of points within zones.

Zone	RMS error for separate adjustments (sec) Old Survey	New Survey	Strain	Maximum Residuals in Strain Adjustments (secs) Old Survey	New Survey	No. of Re-observed Points
1	0.60	0.85	0.85	13	3	10
2	4.50	0.68	5.34	20	1	8
3	2.83	1.22	3.84	11	4	6
4	2.39	0.72	4.29	11	4	12
5	3.90	0.78	3.71	12	2	6
6	2.33	0.72	3.63	9	6	8
7	3.90	0.62	2.81	6	2	11
7M3,9	-		3.65	-		6
7M4,7	-		4.08	-		8
8	2.68	0.35	3.34	10	3	5
9	1.88	1.48	3.11	8	6	10
9M7,12	-		2.83	8	5	8
10	2.81	0.39	2.99	8	2	9

Table 3.4 Tongariro area: Adjustment statistics.

Zone NT	RMS error for separate adjustments (sec) Old Survey	New Survey	Strain	Maximum Residuals in Strain Adjustments (secs) Old Survey	New Survey	No. of Re-observed Points
1	5.78	0.64	7.43	15.7	8.9	14
2	4.54	0.58	6.81	19.2	13.3	11
3	3.30	0.72	5.16	15.2	11.1	11
4	4.33	0.76	7.01	13.5	14.3	8
5	4.13	0.97	6.39	12.1	18.1	6
6	3.92	0.68	4.74	14.2	4.5	8
7	6.02	1.05	7.63	18.2	4.3	7
8	1.91	0.89	2.50	6.4	4.4	5
9	2.15	0.47	2.45	7.6	4.3	5
10	2.0	0.33	5.14	11.3	1.4	5
11	-	-	5.01	14.4	4.9	10
12	-	-	4.93	11.1	2.2	7
13	3.14	0.85	5.18	14.5	13.9	13
14	-	-	8.52	21.8	14.8	8
15	3.42	0.70	4.95	14.2	6.6	7
16	1.09	-	1.16	3.1	0.9	8

Table 3.5 North Taupo Area: Adjustment statistics.

Zone	RMS error for separate adjustments (sec)			Maximum Residuals in Strain Adjustments (secs)		No. of Re-observed Points
	Old Survey	New Survey	Strain	Old Survey	New Survey	
BP1			0.66	1.23	2.87	8
BP1M7			0.62	0.99	2.14	7
BP1M55	0.23	0.58		1.08	1.61	7
BP1M10				0.92	2.87	7
BP2	0.66		0.95	2.61	1.08	6
BP2M7			1.11	2.40	1.17	5
BP2M10			1.09	2.04	1.24	5
BP2M16			1.09	2.56	1.19	5
BP3			1.03	2.98	1.13	5
BP3P19 20	0.47	0.39	1.05	2.90	1.13	7
BP4			0.85	1.35	2.95	8
BP4M22			0.72	1.23	2.47	7
BP4C			0.58	0.89	2.06	5

Table 3.6 Bay of Plenty Area: Adjustment statistics.

Zone NTF	$\dot{\gamma}_1$	$\dot{\gamma}_2$	$\dot{\gamma} = (\dot{\gamma}_1^2 + \dot{\gamma}_2^2)^{\frac{1}{2}}$	ψ	No. of Re-observed Angles
1	-0.56±0.36	-0.25±0.37	0.62±0.40	28±16	6
2	-0.68±0.97	-0.29±0.89	0.73±0.88	28±38	4
3	-1.56±1.06	-0.60±1.21	1.68±1.24	29±17	6
4	3.03±0.60	+0.97±0.76	3.18±0.73	121± 6	11
5	-0.44±0.41	-0.61±0.48	0.76±0.47	13±16	5
6	-0.05±0.34	-0.84±0.24	0.85±0.23	176±11	5
7	-1.14±0.73	0.71±0.32	1.35±0.72	56± 7	4

Table 3.7: North Taupo Area strain rates in μrad y^{-1} computed by Frank's method. $\dot{\gamma}_1$ and $\dot{\gamma}_2$ computed for axes at 040°, ψ is the azimuth of the principal axis of extension. One standard error shown. Refer to figure 3.6 for locations.

Zone	$\dot{\gamma}_1$	$\dot{\gamma}_2$	$\dot{\gamma} = (\dot{\gamma}_1^2 + \dot{\gamma}_2^2)^{\frac{1}{2}}$	ψ	No. of Re-observed Angles
BP1	+0.02±0.07	+0.04±0.07	0.04±0.07	101±45	9
BP2	+0.04±0.13	+0.02±0.10	0.04±0.13	126±63	9
BP3	+0.05±0.05	-0.01±0.04	0.05±0.05	128±24	12
BP4	+0.18±0.09	+0.03±0.08	0.18±0.08	130±13	17

Table 3.8: Bay of Plenty Area strain rates in μrad y^{-1} computed by Frank's method. $\dot{\gamma}_1$ and $\dot{\gamma}_2$ computed for axes at 045°, ψ is the azimuth of the principal axis of extension, one standard error shown.

CHAPTER 4 CRUSTAL SPREADING IN THE TAUPO VOLCANIC ZONE

4.1 Horizontal Strain in the Taupo Volcanic Zone 1880-1975

It was mentioned in Chapter 1 that the TVZ has a belt of faults along its centre and that the faults are thought to be normal. Therefore the TVZ is inferred to be spreading and as the width of the zone is fairly uniform it is expected that the spreading rate will be fairly constant along its length.

The inferred uniform spreading agrees with the results of resurvey analyses given in Chapter 3. For all zones in the TVZ, except those immediately north of Lake Taupo for the period 1880-1950, the shear strain rate is about 0.15 μrad y^{-1} and the azimuth of the principal axis of extension is approximately normal to the zone (figure 4.1). Immediately north of Lake Taupo strain rates for the period 1880-1950 are twenty times higher, being up to 3.2 μrad y^{-1} and with highly irregular directions of principal strain (figure 4.2). By contrast for the period 1950-1974 the strain rate and direction north of Lake Taupo are normal. The anomalous strain rate pattern is the pattern to be expected from an earthquake with normal faulting as will be seen from figure 2.8a. And, as the anomalous region coincides with that of the 1922 Taupo Earthquakes which are known to have been accompanied by normal faulting, the high strain rates are attributed to the earthquakes.

Secular strain rates in the TVZ: Disregarding for the present the anomalous zones, there are five zones within the TVZ for which strain rates have been estimated (zones BP2, NT16, T02, T03 in figure 4.1). The results abstracted from tables 3.1, 3.2 and 3.3, are given in table 4.1. The results from zone BP2 are the best estimates of strain rates obtained in the Taupo Volcanic Zone, they are significant at the 95% level. And although zone BP2 has only six re-observed points, the estimates are very stable varying by less

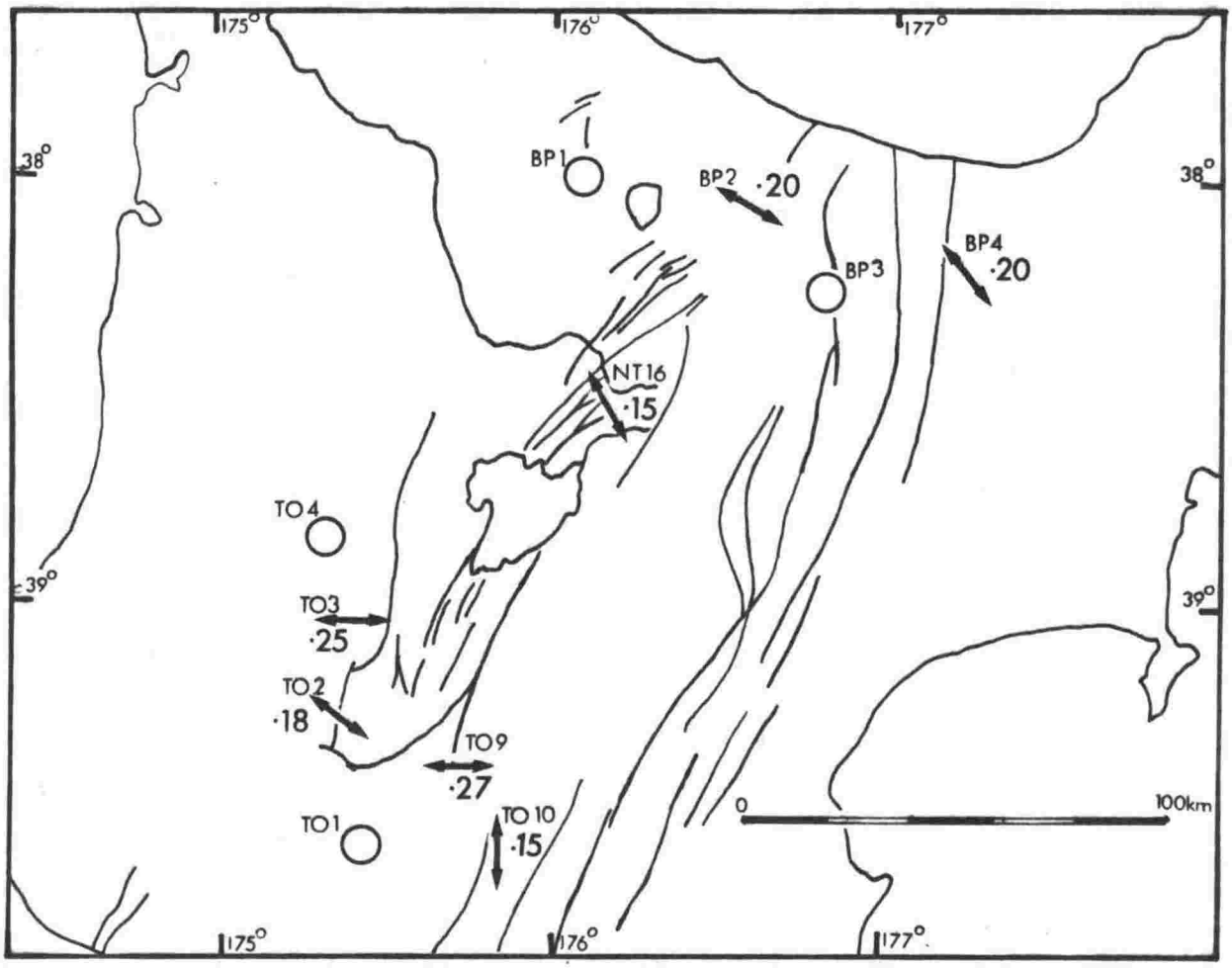

Figure 4.1 Horizontal shear strain rates in the central North Island. Arrows indicate the direction of the principal axis of extension, small numbers are zone designations, large numbers indicate strain rate in μrad y^{-1}, circles indicate zero strain rate. TO zones are for the period c.1880 to 1970, NT16 is for 1950 to 1974 and BP zones for 1925 to 1976. All strain rates in this figure are regarded as estimates of the secular strain rate.

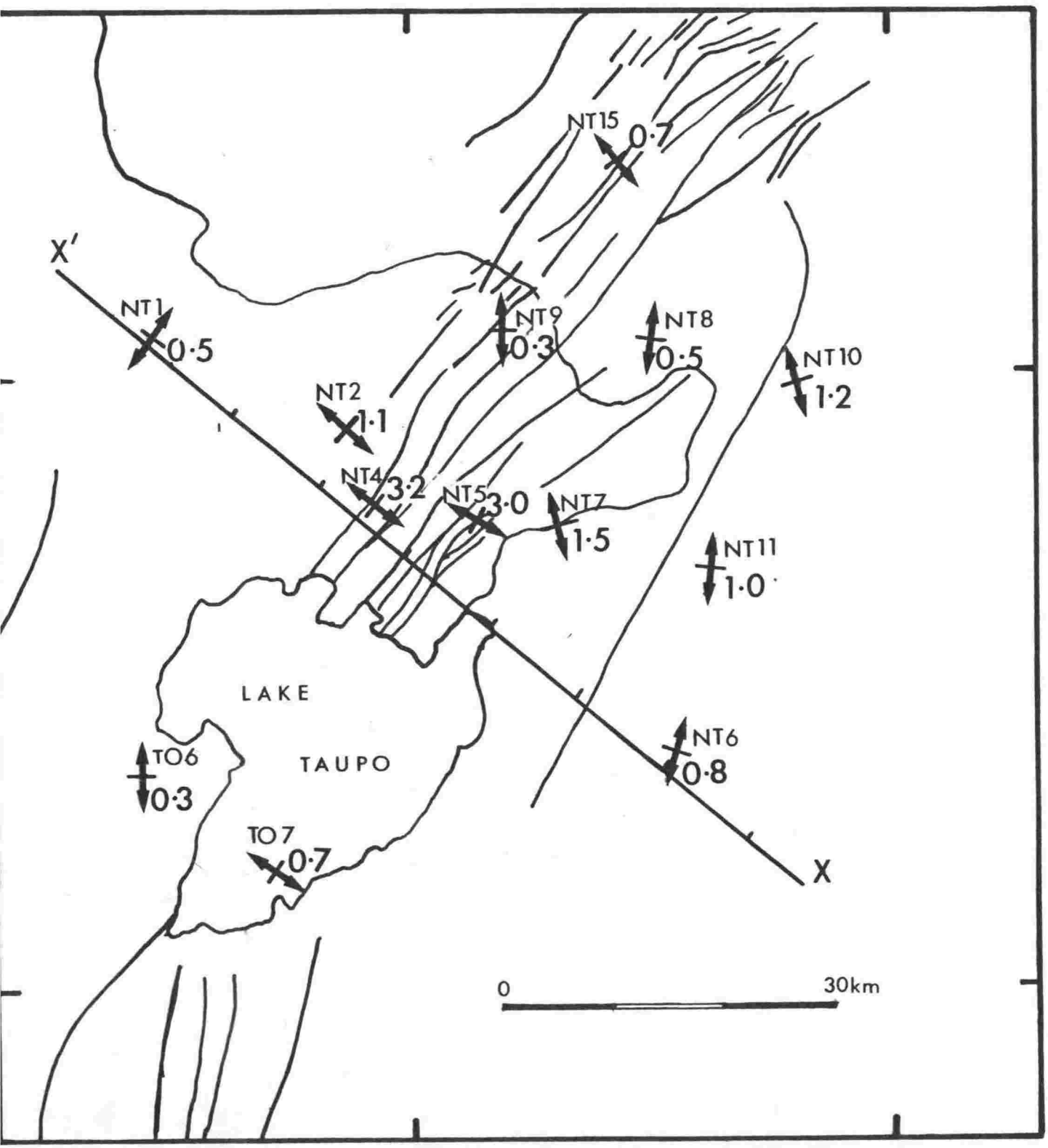

Figure 4.2 Horizontal shear strain rates in the vicinity of Lake Taupo for the period c.1880 to c.1950. Small numbers are zone designations, large numbers indicate strain rate in μrad y^{-1}, arrows indicate the direction of the principal axis of extension.

Zone	Years	Strike degrees	$\dot{\gamma}_1$ μrad y^{-1}	$\dot{\gamma}_2$ μrad y^{-1}	$\dot{\gamma}$ μrad y^{-1}	ψ degrees
BP2	1929-1976	045	0.18±0.06	+0.10±0.06	0.20±0.06	120 ± 8
NT16	1950-1974	040	0.12±0.11	-0.10±0.11	0.15±0.11	150 ±21
TO3, 5	1888-1972	022	0.22±0.18	+0.17±0.21	0.28±0.18	093 ±15
TO2	1911-1972	022	0.16±0.21	-0.09±0.21	0.18±0.21	127 ±40
TO9	1898-1970	022	0.19±0.14	+0.19±0.15	0.27±0.15	088 ±12
		Mean	0.17	0.05	0.22	116
	Standard deviation		0.04	0.15	0.06	26

Table 4.1 Secular strain rates in the Taupo Volcanic Zone, abstracted from tables 3.1, 3.2 and 3.3.

Zone NT	$\dot{\gamma}_1$ (μrad y^{-1})	Period (years)	γ_1 (μrad)	Secular Strain at 0.17 μrad y^{-1}	γ_1 Earthquake Strain (μrad)	Position on Profile XX' (km)
1	-0.53±0.21	64	- 33.92	10.90	- 45±13	0
2	+1.54±0.41	65	+100.00	11.00	+ 89±31	18.7
4	+3.24±0.19	65	+210.60	11.00	+200±12	25.5
5	+2.96±0.42	67	+198.32	11.40	+187±28	32.5
14	+1.04±0.38	67	+ 69.68	11.40	+ 58±25	36.5
7	+0.43±0.24	67	+ 28.81	11.40	+ 17±16	38.5
11	-0.35±0.19	71	- 24.85	12.10	- 37±13	55.0
6	-0.58±0.	77	- 41.18	13.10	- 54±18	60.0

Table 4.2 γ_1 strain due to the 1922 Taupo Earthquakes computed from strain rates given in table 3.2.

than a standard error with the exclusion of single points (table 3.3). In zone BP2 faults strike 045; the $\dot{\gamma}_1$ component relative to this direction is +0.18±0.06 μrad y^{-1} and the $\dot{\gamma}_2$ component is +0.10±0.06 μrad y^{-1}. As already stated, if it is assumed that length and azimuth remain constant parallel to faults, positive $\dot{\gamma}_1$ indicates spreading and positive $\dot{\gamma}_2$ sinistral fault motion. Therefore in zone BP2 there is a spreading component approximately twice as large as a sinistral component.

Although most of the individual values of $\dot{\gamma}_1$ in zones other than BP2 are not significant at the 63% level, it will be seen from table 4.1 that the average value of $\dot{\gamma}_1$ for the TVZ (+0.17 μrad y^{-1}, with a standard deviation of 0.04 μrad y^{-1}) is significant. By contrast, average value of $\dot{\gamma}_2$ (+0.01 μrad y^{-1}, with a standard deviation of 0.15 μrad y^{-1}) is not significant. Thus strain estimates indicate a significant component of spreading for the whole of the TVZ but the transcurrent motion except in zone BP2 is not significant.

Strain values in the Tongariro Area will have been affected by the Hawkes Bay Earthquake. Figure 1.7 shows that strain due to the Hawkes Bay Earthquake was 10 μrad in the region immediately east of the Tongariro Area. Assuming that in the Tongariro Area, 40 km further from the epicentre, it was half as great, the strain when averaged over the 70 years between the surveys will give a rate of 0.07 μrad y^{-1}. The strike of the earthquake strain extension axis is 171°, therefore in the frame of reference used in the Tongariro Area (faults 022°) it would have contributed -0.03 μrad y^{-1} to $\dot{\gamma}_1$ and -0.06 μrad y^{-1} to $\dot{\gamma}_2$. Thus the true secular values of shear strain rate may be 10% - 30% higher than estimated, but the correction, being smaller than standard errors of estimate, has not been made. The strain rate estimate from zone NT16 is from surveys made entirely after the Hawkes Bay Earthquake and zone BP2 is sufficiently remote from the epicentre not to have been significantly affected.

As discussed in section 2.6, crustal strain may be

either secular strain or earthquake strain. With the exceptions due to the Hawkes Bay Earthquake just considered the average strain rate in the Taupo Volcanic Zone has been determined from estimates not affected by any known significant strain events and therefore it is regarded as the secular rate. For the area affected by the 1922 Taupo Earthquakes the result from zone NT16 (0.15 μrad y^{-1} at 150°) shows that the strain rate has returned to a value very similar to the inferred secular rate.

Horizontal strain associated with the 1922 Taupo Earthquakes:

The main surveys from which strain rates were determined in the North Taupo Area were made in c.1880 and in 1950, therefore they will include the effects of the 1922 earthquake strain and also the secular strain for 44 years before and 28 years after the earthquake. The γ_1 earthquake strain determined by integrating the strain rates and subtracting the secular strain assumed to be at the rate of 0.17 μrad y^{-1} obtained above is given in table 4.2 for those zones traversed by the right bisector of the earthquake fault traces (XX' in figure 4.2). It ranges from -50 μrad to +200 μrad being much larger than the secular strain which is less than 15 μrad. Therefore small percentage errors in the estimates of the secular strain are negligible with respect to the earthquake strain.

The earthquake strain pattern (figure 4.3A) is shown quantitatively in the next chapter to be that expected from a shallow earthquake on a normal fault dipping 40° southeast. A more direct estimate of the fault dip assuming rigid body movements on each side of the fault is obtained from the relative magnitude of the vertical and horizontal motions. The total widening due to the 1922 earthquakes, as indicated by the area under the positive part of 4.3A, is 3.1 m. The total vertical displacement, given in Chapter 1, is 4 m, therefore a dip of 52° is inferred. This estimate may be affected by differential compaction of the 2 km thick Quaternary volcanic pile during the earthquakes but is in reasonable

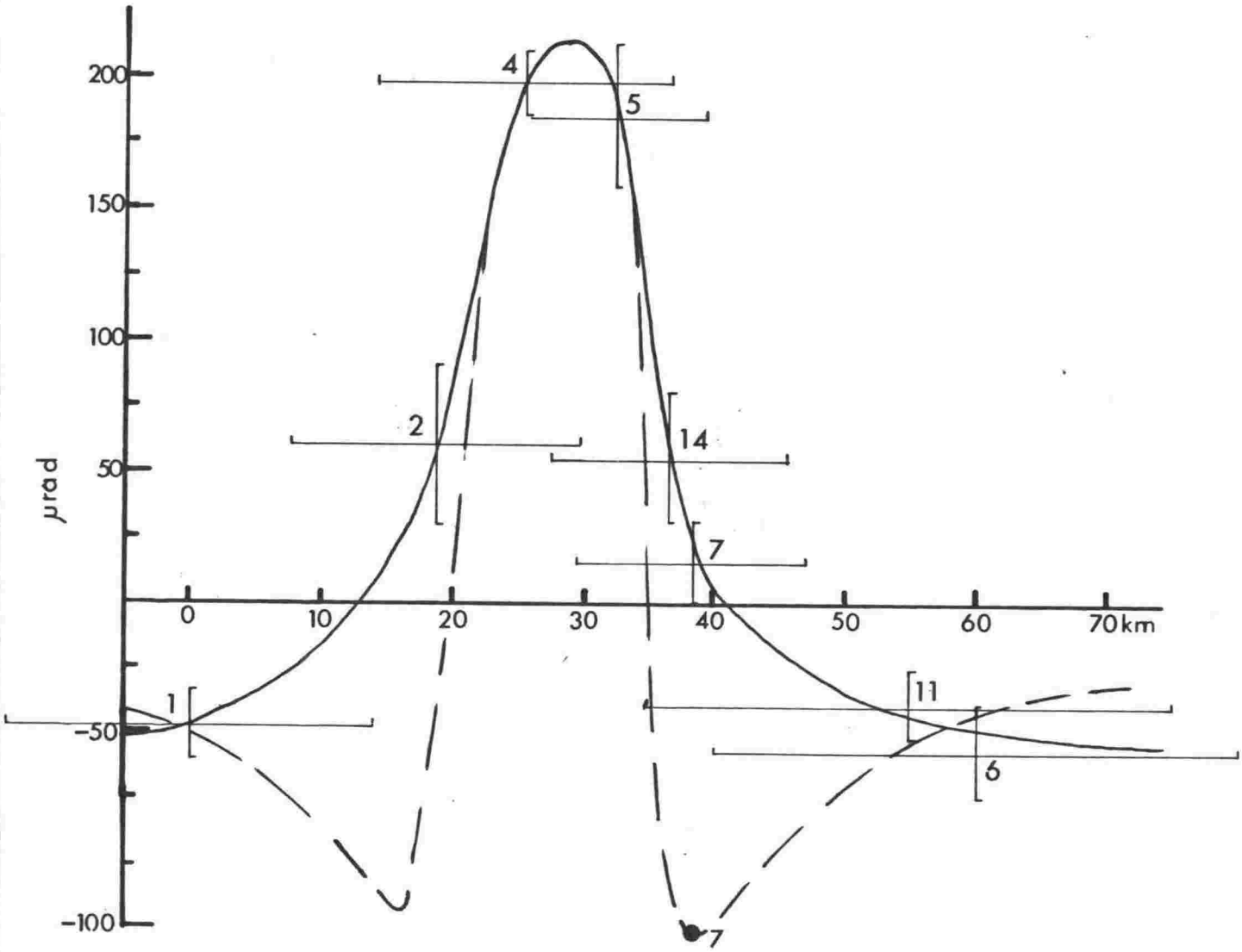

Figure 4.3A

γ_1 earthquake strain along profile line XX' as computed in table 4.2. Vertical bars indicate one standard error, horizontal bars indicate the width of the zone from which the estimate was made. The solid line is an eyefitted curve simply connecting the points. The dot indicates the total shear strain for zone 7 which, as discussed in the text, may be more appropriate because zone 7 is centred slightly north of the right bisector of earthquake faults. The dashed line is a curve similar to the theoretical curves in figure 5.4 and compatible with the measured strains including the total shear strain in zone 7.

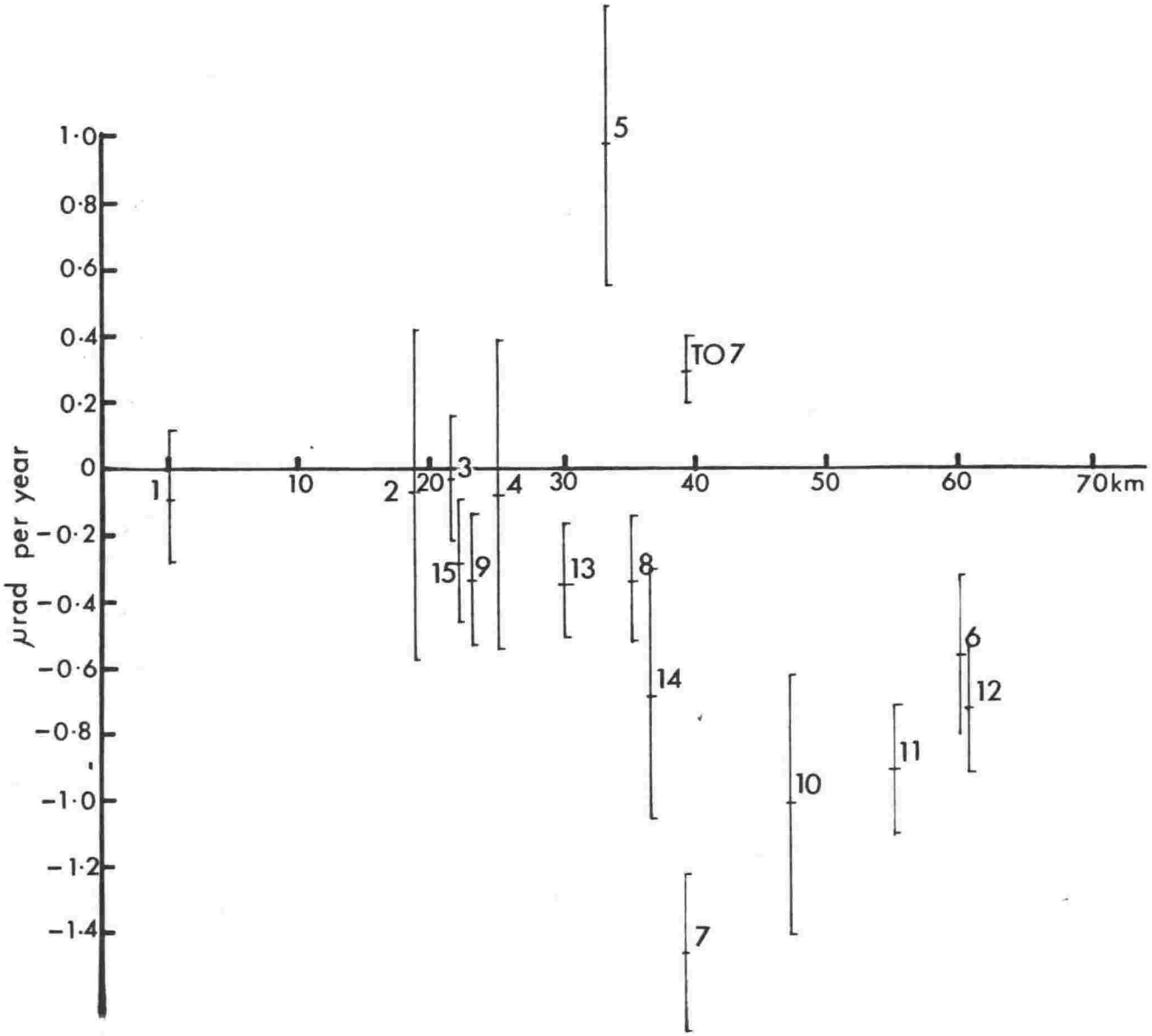

Figure 4.3B $\dot{\gamma}_2$ shear strain rate, for all zones in the North Taupo Area, from tables 3.1 and 3.2, projected on to line XX'. Vertical bars indicate one standard error.

agreement with the dip of 40° determined from the elastic model. Both estimates are considerably shallower than the dip of 70° or more found for most near surface faults by drilling.

The $\dot{\gamma}_2$ component of shear strain rate for all zones in the North Taupo Area for the period 1880 to 1950 when projected on to line XX' (figure 4.2) is shown in figure 4.3B. Almost all values are negative and therefore, if lengths parallel to faults have remained unchanged, dextral simple shear is indicated. However because of the possibility of elastic strain during the earthquakes the assumption of unchanged lengths may not be valid, and $\dot{\gamma}_2$ may represent differential longitudinal strains rather than simple shear. If the $\dot{\gamma}_2$ strain rate in zones NT5 and NT7 is interpreted as simple shear parallel to faults it would indicate that the narrow sliver of land common to both zones had translated northeast by about 1 m since 1880, but there is no surface evidence for this. If $\dot{\gamma}_2$ is interpreted in terms of longitudinal strains the positive value in zone NT5 is consistent with extension at 45° to faults and the negative value in NT7 is consistent with compression at 45° to faults. As both NT5 and NT7 are in the first quadrant of the fault-right bisector frame of reference, they would be expected to have such components of longitudinal strain and the magnitudes of the strains (70 and 98 μrad in zones NT5 and NT7 respectively) are commensurate, for the distances of the zones from the epicentre, with the extensive and compressive elastic rebound strain shown in figure 4.3A. Therefore the longitudinal strain interpretation is preferred. If the total shear values in zones NT5 and NT7 are accepted as indicating extension and elastic rebound, the dashed profile in figure 4.3A is obtained and this corresponds very closely with the theoretical profile for a fault dipping at 40° (figure 5.4).

Other zones in which $\dot{\gamma}_2$ is attributed to longitudinal strain by virtue of their position with respect to faulting are NT6, 8, 10 and 11. The remaining zones, except

T07 in which $\dot{\gamma}_2$ appears to be spurious, have an average value for $\dot{\gamma}_2$ of about -0.2 μrad y^{-1}, considerably larger than the secular rate determined above for the Taupo Volcanic Zone. The most likely cause for the high $\dot{\gamma}_2$ value is the Hawkes Bay Earthquake. As shown in figure 1.7 the earthquake caused a strain of 10 μrad at 171° in the region immediately east of the TVZ. Assuming that the earthquake strain in the North Taupo Area was half as great, then, when averaged over 70 years, it will have contributed -0.01 μrad y^{-1} to $\dot{\gamma}_1$ and -0.07 μrad y^{-1} to $\dot{\gamma}_2$ in terms of the North Taupo Area frame of reference (faults 040°). Thus slightly less than half of the -0.02 μrad y^{-1} $\dot{\gamma}_2$ strain rate in the North Taupo Area is attributable to the Hawkes Bay Earthquake and the remaining -0.01 μrad y^{-1} indicates a sinistral secular shear.

The Hawkes Bay Earthquake strain is negligible compared with the γ_1 strain computed above for the 1922 Taupo Earthquakes and if a correction were made its effect would be to lower the zero line in figure 4.3A by about 1 μrad relative to the strain curve.

4.2 Rate of Spreading in the Taupo Volcanic Zone

For strain rates computed relative to faults, if it is assumed that length changes parallel to faults are zero then the spreading rate S is given by $S = \dot{\gamma}_1 \times w$ where w is the width of the spreading region. In the Bay of Plenty area zone BP2 spans the TVZ and the zones on either side, BP1 and BP3, have a zero strain rate. The width of the spreading region, i.e. zone BP2, is 40 km and therefore for the secular $\dot{\gamma}_1$ strain rate of 0.17 μrad y^{-1} the spreading rate is 7 mm y^{-1}.

In the middle of the Taupo Volcanic Zone, zone NT16 indicates a minimum spreading width of 15 km but the strain pattern from the 1922 earthquakes strongly suggests that the spreading width is at least 40 km. At the south end of the TVZ the combined width of zones T02 and T07 indicates a minimum spreading width of 30 km. Thus the spreading width is not shown to change significantly along the length

of the TVZ and because the secular strain rate within the TVZ is uniform the spreading rate is inferred to be uniform.

Over the last 70 years, secular strain appears to have accumulated approximately homogeneously across the width of the TVZ but, in the long term, say over hundreds of years, faulting has concentrated the spreading into the Central Fault Belt. Hence the long term strain is not homogeneous across the TVZ. The 1922 earthquake swarm - where strain from a region more than 40 km across was released into a graben 9 km wide - is the latest example of such strain concentration.

The strain in the TVZ has been determined from surveys made over a period of 70 years, an extremely short period in geological terms. However, that the 1922 earthquake strain was in the same sense as secular strain indicates that the extension has been continuing for at least the return period of the earthquakes, i.e. hundreds of years. Further, because the throws during the 1922 earthquakes are only a small part of total surface fault throws and an even smaller part of basement throws (as indicated by gravity) long continued faulting and hence long continued spreading is inferred.

4.3 Total Spreading in the Taupo Volcanic Zone

If the 1.1 My age of the oldest dated rocks in the TVZ is accepted as the age of the beginning of spreading and the current spreading rate of 7 mm y^{-1} has continued throughout, the total widening is 8 km. On the other hand, if spreading is assumed to have begun when the subducting Pacific Plate first penetrated the mantle under the TVZ, i.e. about 5 My ago, the total widening is 35 km.

In either case, compared with the magnitude of late Cenozoic interplate motions in New Zealand the total widening of the Taupo Volcanic Zone is very small and is of only minor importance for the reconstruction of New Zealand.

CHAPTER 5 AN ELASTIC MODEL FOR THE 1922 TAUPO EARTHQUAKES

In this chapter a quantitative elastic dislocation model is set up for the 1922 Taupo Earthquakes. It is based on the horizontal strain profile determined in Chapter 4 and on the areal extent of surface faulting and aftershock activity discussed in Chapter 1.

Vertical displacements on several surface faults accumulated over at least the three months while the earthquakes continued, forming a 9 km-wide graben; but seismic activity was considered by Morgan et al (1923) to be confined at depth to a single earthquake fault striking parallel to surface faults. The horizontal strain was determined from surveys made 44 years before and 28 years after the earthquakes and therefore will include, in addition to the effects of the main displacement, the effects of all pre- and post-earthquake displacements other than those due to the secular strain which has been allowed for. Only the total deformation is known and this has been modelled as a single elastic dislocation on the earthquake fault.

There are several formulations for computing the displacements due to an elastic dislocation; that of Maruyama (1964) being the most general. However for the quality of data available the simpler formulae of Mansinha and Smylie (1971), which assume a constant magnitude dislocation across an inclined rectangular fault surface in an isotropic halfspace, are sufficient. The co-ordinate system used is shown in figure 5.1. There are six unknowns: the down-dip fault dimensions D_1 and D_2, the length L and dip d of the fault, and the dip-slip and strike-slip components of the slip vector. Since faulting broke the surface D_1 is considered to be zero. The region of surface faulting and aftershock activity extended for 15 km along the strike of the graben (from the shore of Lake Taupo to Oruanui) and for at least 9 km across the graben. Hence, allowing for dip, first estimates of both D_2 and L are inferred to be about 15 km. Because the largest surface fault (the Whangamata fault) is the northwesternmost and the graben

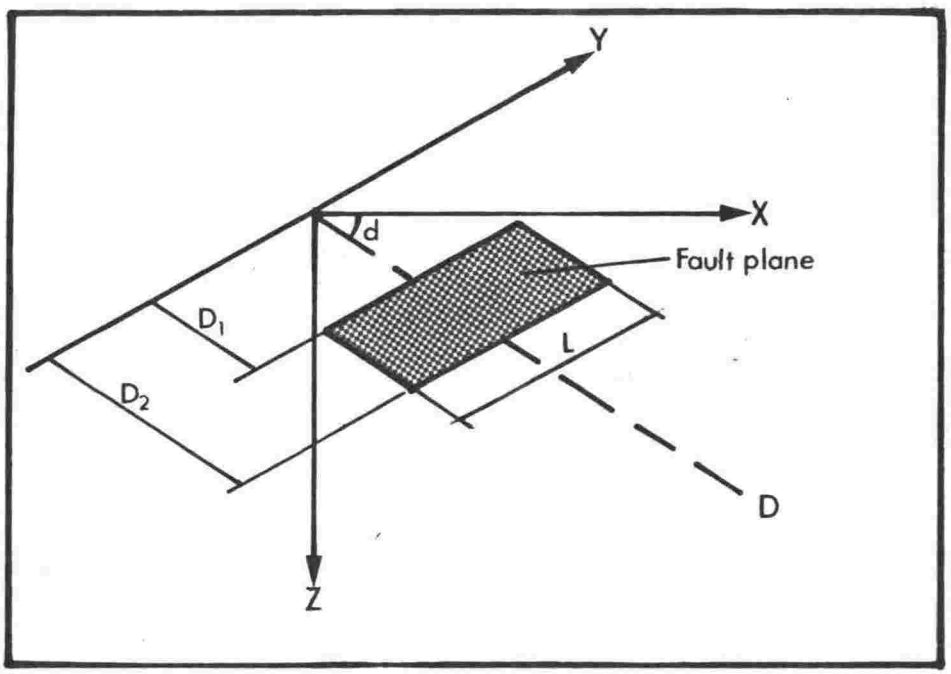

Figure 5.1 The co-ordinate system for the elastic dislocation model.

block was tilted northwest, the earthquake fault is inferred to dip southeast. It was shown above that faulting was purely normal, therefore only the dip-slip component of the slip vector is non-zero.

The γ_1 strain and the vertical displacement (u_z) along the right bisector of the fault trace were computed for a unit dislocation on a 15 km-square-fault dipping 40^o southeast, with the top edge at 0.001 km from the surface; and for a range of other faults with similar dimensions. The equations of Mansinha and Smylie give point displacements, therefore u_z was computed directly; u_z variation along the x axis is shown in figure 5.3.

The values of γ_1 determined geodetically are spatial averages for zones about 15 km across and it is necessary that theoretical γ_1 values be equivalent spatial averages. For engineering shear strain, $\gamma_1 = \frac{\partial u}{\partial x} - \frac{\partial v}{\partial y}$. For shallow normal faulting $\frac{\partial v}{\partial y}$ on the right bisector of the fault trace is small and for a 15 km-square-fault the 15 km average values were found to be approximately equal to point values (figure 5.2B). Therefore, in computing γ_1, point values for $\frac{\partial v}{\partial y}$ obtained directly from the analytical derivative of Mansinha and Smylie's formula for the displacement v were used. For shallow normal faulting $\frac{\partial u}{\partial x}$ near the fault and on the right bisector of the trace is considerably larger than $\frac{\partial v}{\partial y}$ (figure 5.2B) and is sensitive to spatial averaging. $\frac{\partial u}{\partial x}$ was obtained by computing the relative x displacement for pairs of points along the x axis and dividing by the distance between the points ('pair-length'), and thus giving an average value for $\frac{\partial u}{\partial x}$ over the distance between the points. The sensitivity of γ_1 to spatial averaging is shown in figure 5.2C where γ_1 profiles computed using pair-lengths of 10, 12.5 and 15 km are given. The average width of geodetic zones in the North Taupo area is about 15 km and therefore 15 km is the averaging width used for computing γ_1 for the model. Variation in the actual width of geodetic zones is about 5 km, and therefore as can be seen in figure 5.2C there is an uncertainty of up to ±30% in γ_1, mainly affecting the peak value.

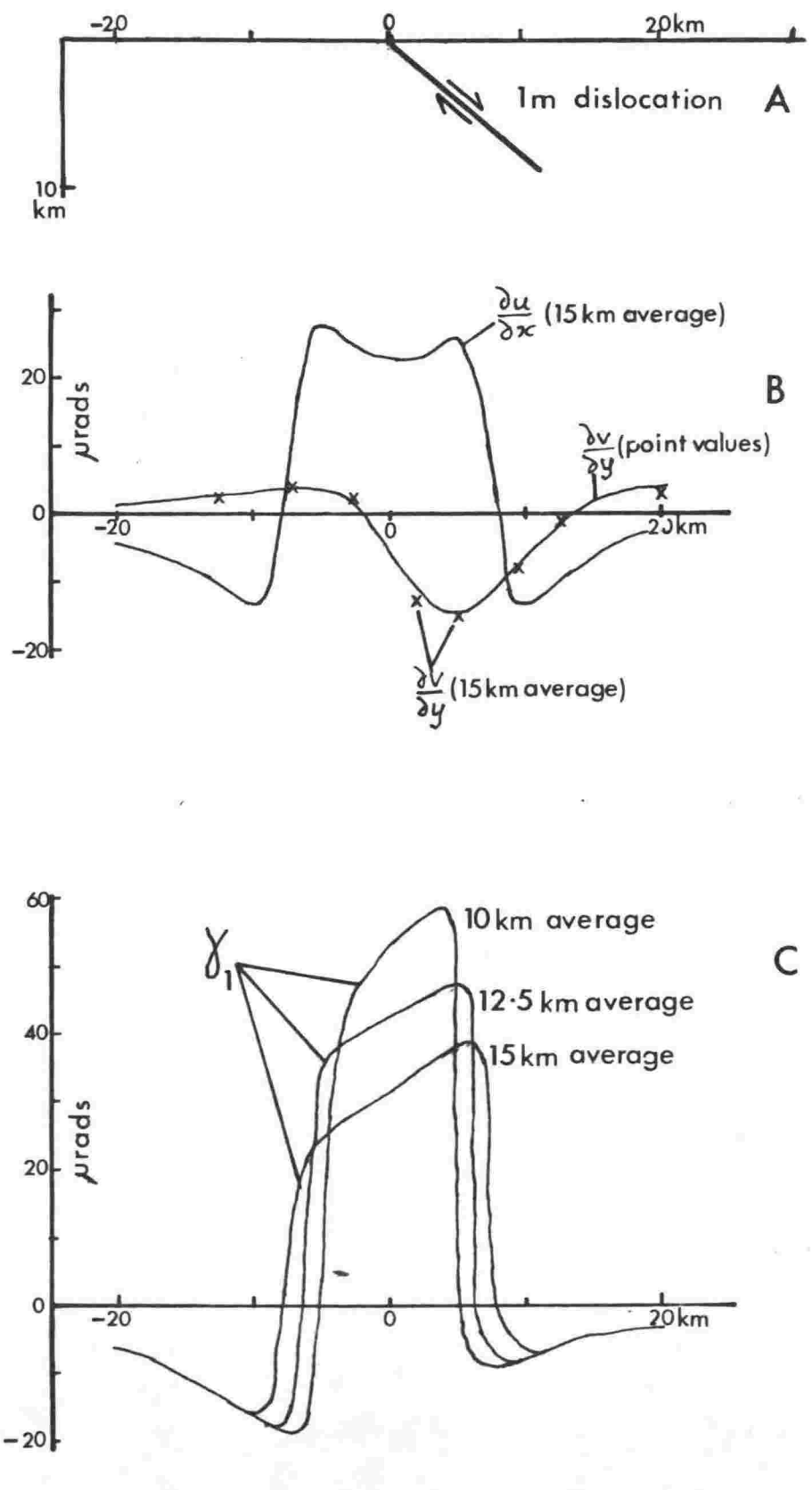

Figure 5.2 Theoretical strain on the right bisector of the fault trace for a 1 m elastic dislocation on a rectangular fault showing the effect of averaging on $\frac{\partial u}{\partial x}$, $\frac{\partial v}{\partial y}$ and γ_1.

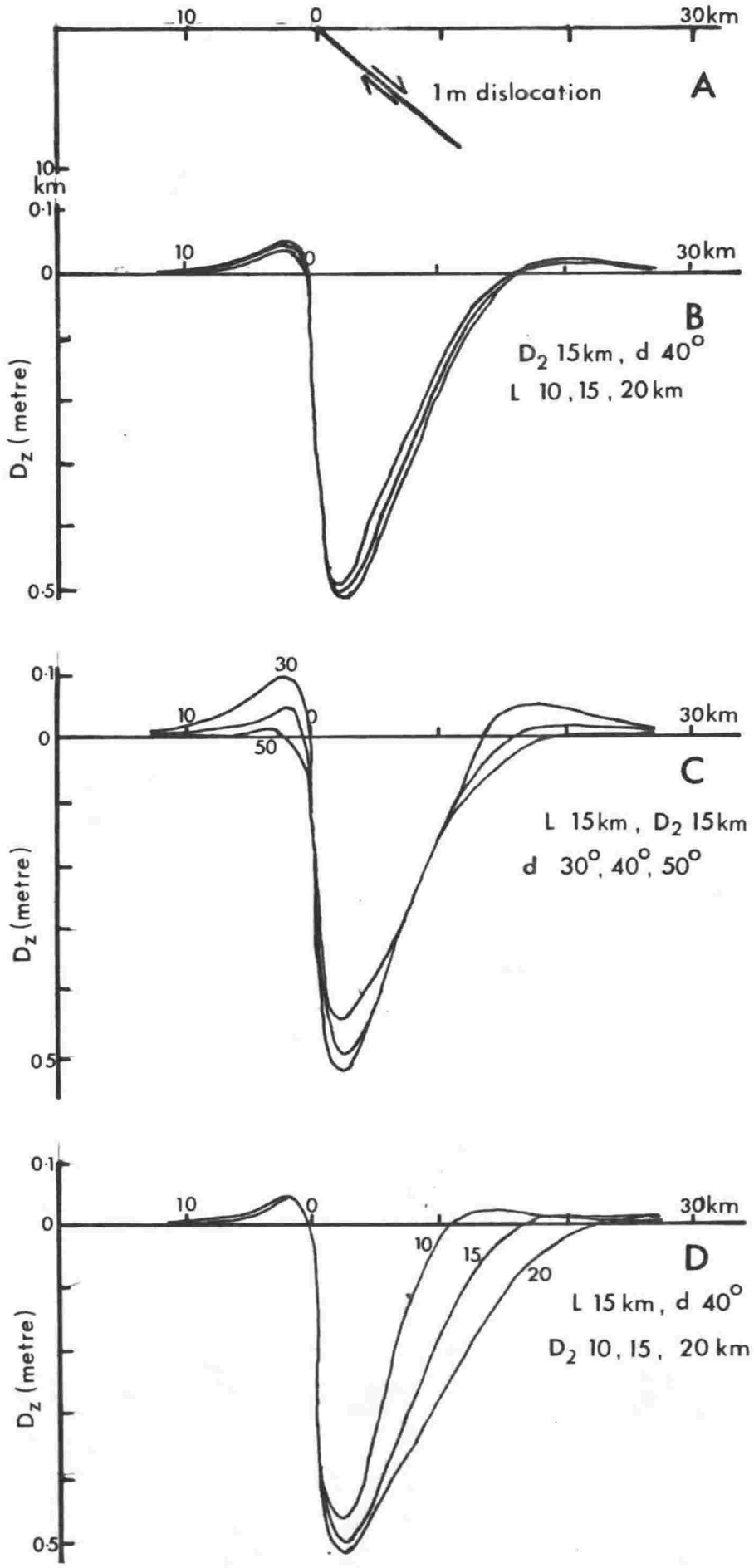

Figure 5.3 Theoretical vertical displacement on the right bisector of the fault for a unit dislocation on a rectangular fault. Dimensions D_1, D_2 and L are shown in figure 5.1. d is the fault dip. Dimension D_1 is taken as 0.001 km in all cases.

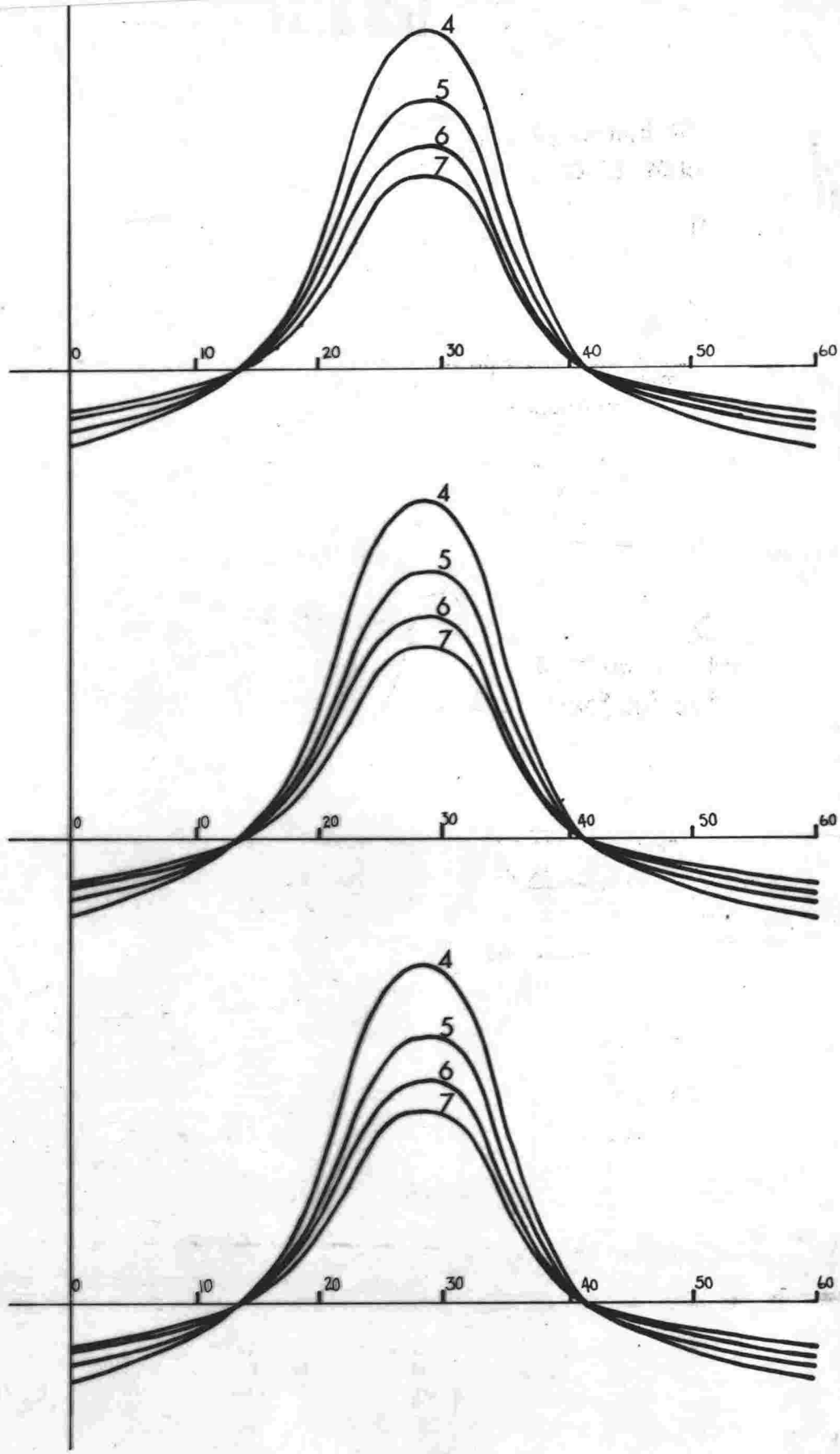
4
5
6
7
0
10
20
30
40
50
60
4
5
6
7
0
10
20
30
40
50
60
4
5
6
7
0
10
20
30
40
50
60

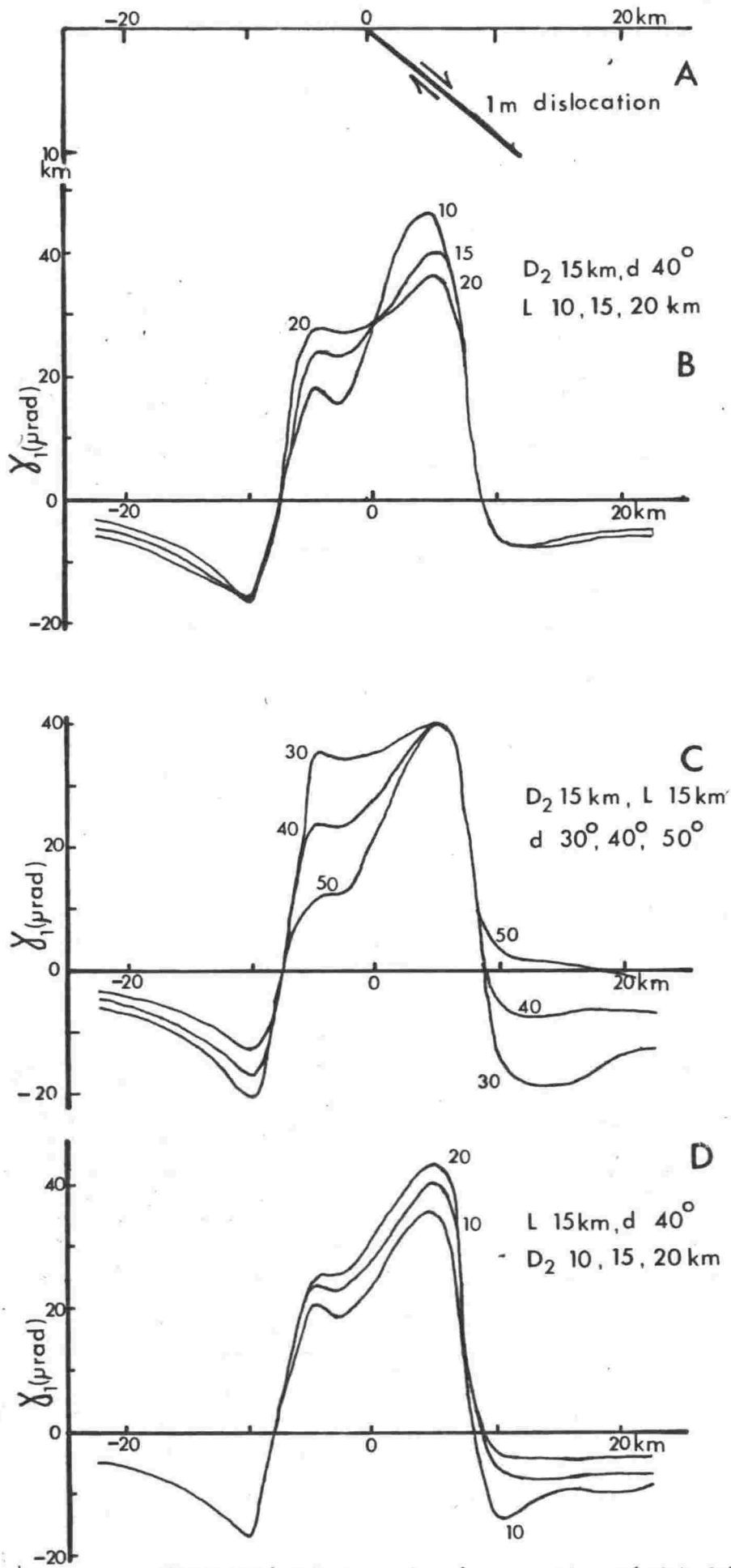

Figure 5.4 Theoretical γ_1 strain on the right bisector of the fault for a unit dislocation on a rectangular fault. Dimensions D_1, D_2 and L are shown in figure 5.1. d is the fault dip. Dimension D_1 taken as 0.001 km in all cases.

In figure 5.4 the theoretical γ_1 curves are given for ranges of D_2, L and d; they are not sensitive in the range of parameters chosen except with respect to the dip which has to be about 40° or less to give the reasonably symmetrical profile that was observed. Values of 0.001 km, 15 km and 15 km are therefore adopted for D_1, D_2 and L respectively.

Magnitude of dislocation: The measured γ_1 strain curve (figure 4.3A) replotted at scales such that the theoretical unit curves in figure 5.4 represent dislocations of 4 to 7 m is given on the overlay to figure 5.4. The best fit is obtained for a dislocation of 5.5 m. Multiplying the unit curves for u_z in figure 4.3 by 5.5 shows that the maximum subsidence indicated is about 2.8 m, somewhat less than the maximum subsidence reported relative to the level of Lake Taupo but greater than the maximum throw on the Whangamata fault. The elastic model for the earthquake thus accounts for the observed horizontal and vertical deformations. From figure 5.3D it will be seen that for a dislocation of 5.5 m the width of the region in which subsidence exceeds 1 m is only 5 km if D_2 is 10 km, while the region depressed by more than 1 m in 1922 was 9 km wide. If D_2 is 20 km, the theoretical subsidence at the outlet to Lake Taupo, 17 km from the fault trace on the down-thrown side is 0.5 m and the level of the whole of Lake Taupo would have been lowered by this amount. This did not occur. Thus it is inferred from the observed vertical displacements and from the theoretical profile in figure 5.3D that D_2 is greater than 10 km and less than 20 km.

The model assumes an isotropic halfspace homogeneously strained before the earthquake. However, it might be argued that, in a tensional environment, the geostatic pressure is the limit to the deviatoric stress that can accumulate because jointed rock bodies will not be able to withstand tension; it follows that the maximum deviatoric stress will be less near the surface than

at depth. This can be crudely modelled by assuming two layers, the upper one with zero stress and the lower one homogeneously stressed. It is shown below that the stress drop for the earthquake is about 134 bars, thus, assuming a geostatic pressure gradient of about 150 bar km^{-1}, the geostatic pressure will exceed the stress drop at a depth of just under 1 km, indicating that the superficial layer is possibly about a kilometre thick. Faults in the superficial layer are numerous and are steeper than the earthquake fault below. Figure 5.5 shows in plan and in section the inferred earthquake fault for the 1922 earthquakes.

Seismic moment and stress drop: The seismic moment, M_0, is given by $M_0 = \mu A\bar{u}$ (Aki, 1966) where μ is the rigidity usually taken to be 3×10^{11} dyne cm^{-2}, $\bar{u}$ is by convention half the dislocation across the fault, in this case therefore 2.75 m, and A is the area of the fault. For the 1922 earthquakes M_0 is 1.9×10^{26} dyne-cm. The stress drop, $\Delta\sigma$ is given by $\Delta\sigma = \frac{7}{16} \pi \frac{\bar{u}}{r} \mu$ (Keylis-Borok, 1959) where r is the equivalent radius of the fault - about 8.5 km. For the 1922 earthquakes $\Delta\sigma$ is 134 bars. Moment and stress drop are both much higher than those determined spectrally for other earthquakes in the TVZ by Gibowicz and Hatherton (1975). In their compilation of focal parameters for New Zealand crustal earthquakes, they include four earthquakes from the Taupo Volcanic Zone. The largest had a magnitude of 5.0, a moment of 7×10^{23} dyne-cm, and a dislocation of about 10 mm corresponding to a stress drop of about 1 bar. Gibowicz and Hatherton's sample is possibly from superficial faulting discussed above. The 1922 earthquakes were different, and are considered here to have fractured the entire thickness of the lithosphere under the TVZ which as discussed in Chapter 1 is probably 10 - 15 km. The stress drop of 134 bars is very high (see, e.g. Hanks, 1977) and suggests that the earthquake faulting took place in fresh rock and not along existing fault planes. This is consistent with the inferred position of the earthquake fault - underlying the entire width

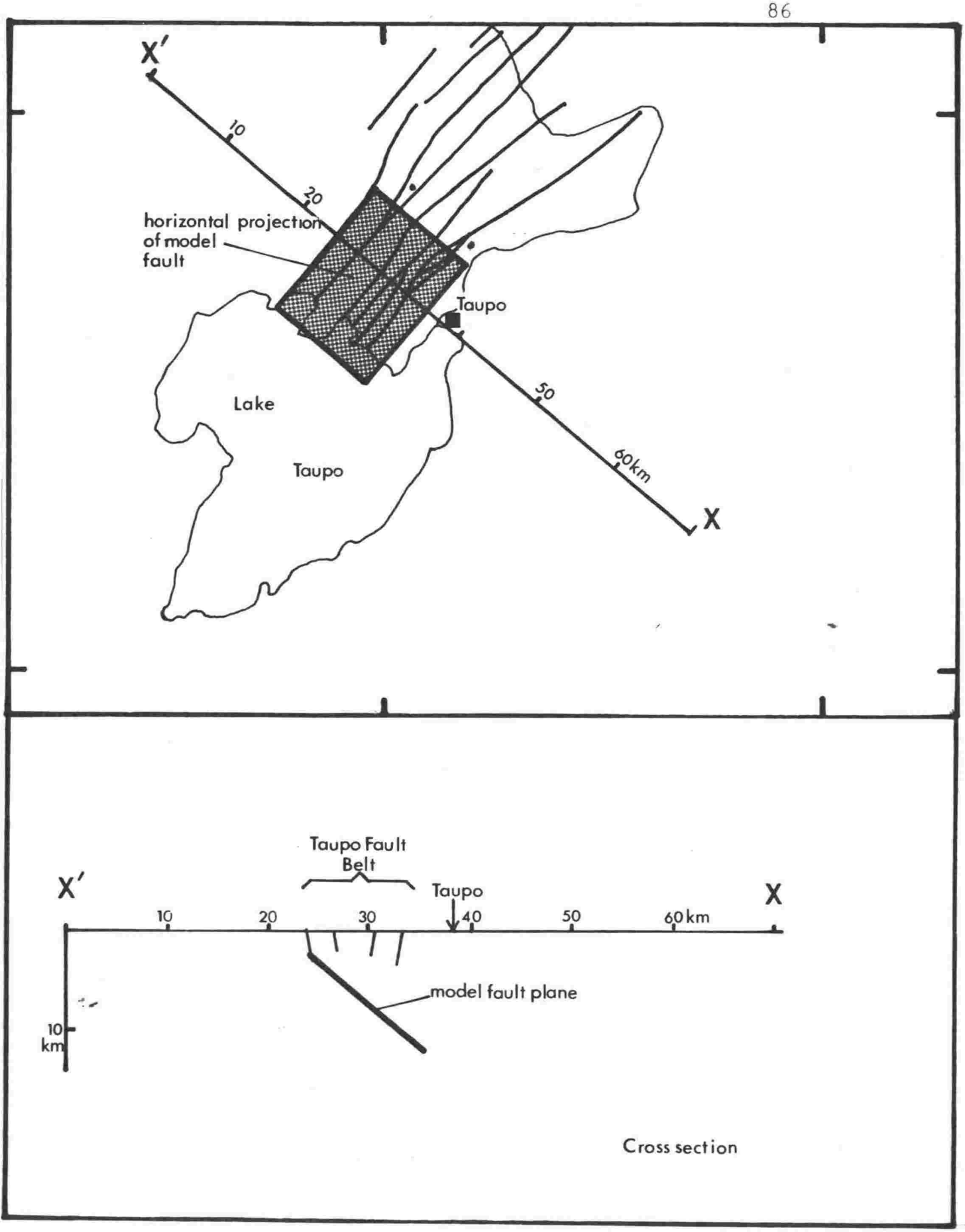

Figure 5.5 Plan and cross-section of the model fault plane.

of the Central Fault Belt, and not associated with any one superficial fault.

Strain accumulation rate and return period: An approximate return period for the 1922 events is given by the total extension of 3.1 m divided by the secular rate of widening of 7 mm y^{-1} giving 440 years.

Taking into account the frequency distribution of earthquake moments, Molnar (1979) gives the return period $T(M_0)$ for an earthquake with moment M_0 as

$$T(M_0) = \frac{{M_0}^{max}(1-\beta)}{(1-\beta)\dot{M}_0^{\Sigma}} M_0^{\beta}$$

where β is a constant approximately equal to $\frac{2}{3}$, ${M_0}^{max}$ is the maximum seismic moment to be expected in the region and $\dot{M}_0^{\Sigma}$ the rate of accumulation of seismic moment. $\dot{M}_0^{\Sigma}$ for spreading normal to the strike with faults dipping 45° is given by

$$\dot{M}_0^{\Sigma} = 2\mu A\bar{u}$$

where μ is the rigidity, A is the cross-sectional area of the elastic layer in which the strain is accumulating and $\bar{u}$ is the spreading rate.

Assuming that $\mu = 3 \times 10^{11}$ dyne cm^{-2} and that the elastic part of the crust is 10 km thick, then for a spreading rate of 7 mm y^{-1} seismic moment is accumulated at a rate of 6.3×10^{24} dyne cm y^{-1} over the 170 km length of the TVZ on land. If the moment of the Taupo Earthquakes (1.9×10^{26} dyne cm) is assumed to be ${M_0}^{max}$ the return period for such an event in the whole of the TVZ is 90 years and the return period for an earthquake with moment 10^{25} dyne cm is 13 years assuming no creep. The largest earthquakes known in the TVZ other than those in 1922 are four magnitude 5.4 shocks which will have had moments of about 10^{24}. Hence either there has been an apparent undersupply of earthquakes in the TVZ in the last 150 years or creep is accounting for up to half of the observed geodetic strain rate.

CHAPTER 6 HORIZONTAL KINEMATICS OF THE NORTH ISLAND

6.1 Data

Information regarding central North Island deformation, as determined from geodetic analyses and Quaternary fault measurements, is summarized in figure 6.1.

The region to the northwest of the Taupo Volcanic Zone is essentially the eastern edge of the rigid Indian Plate. As discussed in Chapter 1 there are very few active faults or crustal earthquakes in it and zero strain rates have been found in two zones (BP1 and T04) near its southeastern boundary.

The TVZ was shown in Chapter 4 to be spreading at 7 mm y^{-1} and without significant transcurrent motion. The spreading is thought to be back-arc spreading. To the north the spreading axis continues via a left-hand offset into the Havre Trough. To the south it is thought to extend via a right-hand offset (the 097° striking Raetihi Fault) into the Waverley Fault Zone (figure 6.1). The geodetic strain rate in zone T02 which contains the Raetihi Fault is 0.18 μrad y^{-1} with the extension axis striking 127°. In Chapter 4 this was interpreted as normal dextral motion on the 022 striking southern extension of the Hauhangaroa Fault but it may equally well be interpreted as sinistral reverse motion on the 097° striking Raetihi Fault or, as is thought to be the case, a combination of both. The adopted position for the axis is partly confirmed by geodetic results which show that the spreading axis does not continue along the strike of the TVZ through zone T01 where the strain rate is zero (figure 6.1) or to the south, through zone T010, where the strain is interpreted as east-west narrowing. Figure 1.7 shows that strain from the Hawkes Bay Earthquake is about 10 μrad in the vicinity of zone T010 with the extension axis striking 171°; when this is averaged over 70 years the rate is 0.14 μrad y^{-1} and thus accounts for most of the 0.15 μrad y^{-1} observed

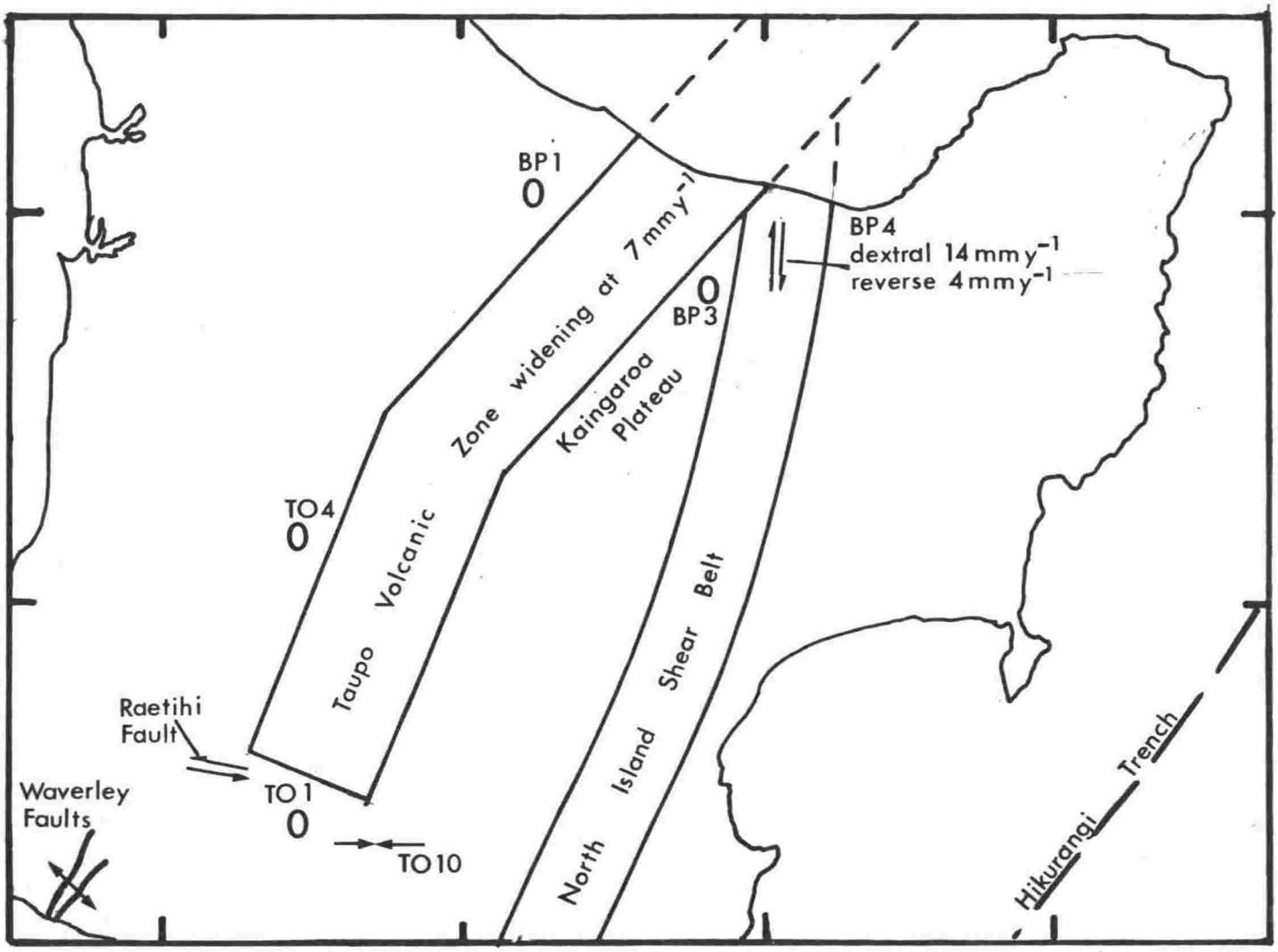

Figure 6.1 Fault data and geodetic deformation data for the central North Island.

strain rate; but the remainder still precludes extension.

Between the Taupo Volcanic Zone and the North Island Shear Belt is the Kaingaroa Plateau, a small unfaulted block from which the single available strain analysis indicates a zero strain rate.

East of the Kaingaroa Plateau, zone BP4, which spans the North Island Shear Belt, has a well-determined strain rate of 0.20 μrad y^{-1} with the extension axis striking 142°. Faults in zone BP4 strike north-south, i.e. at slightly less than 45° to the extension axis, hence the motion is interpreted as north-south dextral shear plus a minor reverse component. The zone is 75 km across and therefore, assuming zero change in azimuth and length parallel to faults, displacement rates are 14 mm y^{-1} dextral and 4 mm y^{-1} narrowing. The slip direction, 202°, is in good agreement with the postglacial slip direction of 200°, determined by Berryman from measurements on the Whakatane Fault (table 1.1).

To the east of the North Island Shear Belt in the area between zone BP2 and the east coast of the North Island, referred to here as the 'East Cape Block', there is little information. No active faults have been mapped but geodetic analyses along the east coast (Walcott, 1978b) indicate strain rates between 0.2 and 1.2 μrad y^{-1} with extension axes generally striking approximately normal to the Hikurangi Trench. Whether these represent mainly extension normal to the trench which is adjacent to the east or simple shear at 45° it is unclear. Walcott considered that the region was alternately compressed and relaxed due to stickslip subduction and that during relaxed phases, such as the present, strain is mainly extensional normal to the trench but highly inhomogeneous.

6.2 Tectonic Models

Walcott (1978a) interpreted the boundary between the Indian and Pacific macroplates as a single 100 km-wide zone of "pervasive strain". Assuming homogeneous strain in a zone with rigid parallel sides obliquely

converging at rates determined by the macroplate model of Minster et al (1974) he calculated the average strain rate to be about 0.4 μrad y^{-1} with the extension axis striking 025°. The homogeneous strain model is appropriate over much of the South Island where the majority of faults are approximately parallel and of similar nature; and where geodetic strain has been shown by Bibby (1975, 1976) to be approximately homogeneous.

The North Island situation is entirely different. Although major faults are approximately parallel they vary in nature, being normal in the Taupo Volcanic Zone, dextral reverse in the North Island Shear Belt and reverse at the Hikurangi Margin; and geodetic strain over the island as a whole has been shown not to be homogeneous. It being impossible to assume a single zone of homogeneous strain for the Indian-Pacific boundary zone in the North Island, the deformation is instead modelled as a series of rigid microplates. It should be noted that this is geometrically equivalent to a series of zones with homogeneous strain. Accordingly the fault belts are idealized as single faults. The TVZ and the Waverley Fault Zone, connected by the Raetihi Transform comprise the North Island part of the New Zealand Spreading Axis; the North Island Shear Belt becomes a single reverse dextral fault; and the Hikurangi Trench is taken as a reverse fault - being the line of subduction of the Pacific Plate. There are thus two macroplates - the Indian and the Pacific - and two microplates named here the Central and the Kermadec. In figure 6.2 the plates are numbered from left to right: 1 Indian, 2 Central, 3 Kermadec, 4 Pacific.

It happens, as will be seen in figure 6.3, that the four plates are sufficient for the description of the kinematics of the whole of the New Zealand region. Each of the plates is in contact with every other plate. There are six boundaries, and six shift poles; and four triple junctions are associated with the two microplates.

Microplate models have previously been postulated by

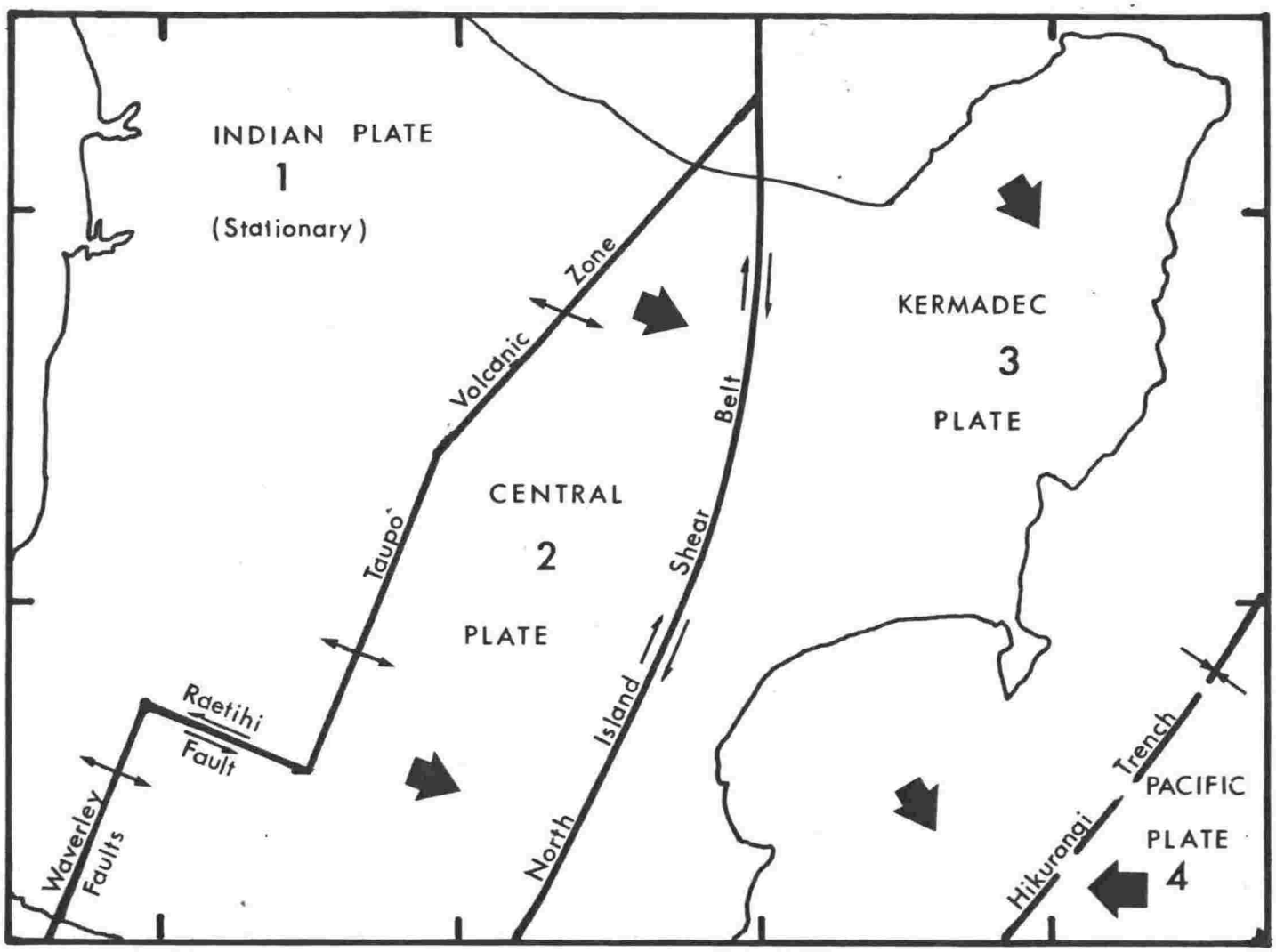

Figure 6.2 Interpretation of the horizontal tectonics of the central North Island region in terms of four rigid plates. Small arrows indicate direction of relative motion across boundaries, large arrows indicate direction of plate motion relative to the Indian Plate.

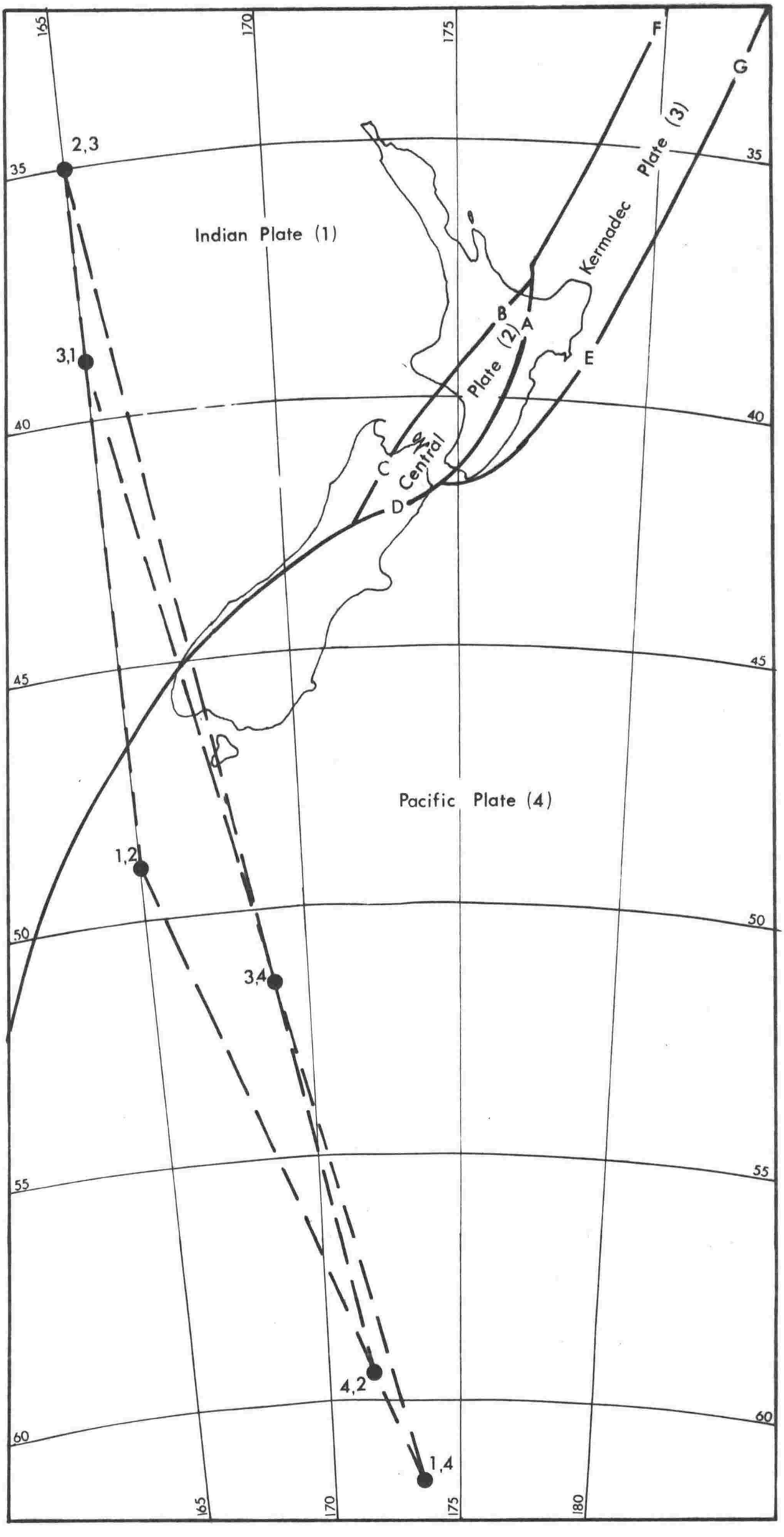

Figure 6.3 A microplate model for New Zealand. Solid lines are plate boundaries, dashed lines are those for the construction used to locate poles 3/1, 3/4, 2/4. Points A to G are discussed in the text. Conical projection, standard parallel 37°S.

Calhaem (1973), Wellman (1973) and Ballance (1976) but all include only a single microplate and therefore encounter difficulties in accounting for both the back-arc spreading and the dextral motion in the North Island.

Boundary 1/3 is the Havre Trough and boundary 3/4 is the Hikurangi Margin as defined in Chapter 1 to include both the Hikurangi and Kermadec subduction zones. Boundary 1/2 is the New Zealand Spreading Axis represented in the North Island by the Taupo Volcanic Zone and the Waverley Fault Zone. The southward continuation of boundary 1/2 crosses the South Taranaki Bight. There is some marine seismic reflection evidence for north-northeast striking lineations off the Wanganui coast consistent with a southerly extension of the Waverley Fault Zone. The further continuation may be either on a line curving round into Cook Strait following the locus of maximum crustal seismicity (figure 1.2) or on a straighter line continuing into the Waimea Depression where there is low seismicity,but geodetic strain analysis indicates a strain rate of 0.3 μrad y^{-1} with the extension axis striking 150° (H. M. Bibby, pers.comm., 1979). The Waimea line is preferred because it is parallel to the Benioff Zone, as is the rest of the boundary, and because it accounts for the strain in the Waimea Depression.

Boundaries 2/3, 2/4 and 1/4 are the North Island Shear Belt, the Marlborough Faults and the Alpine Fault respectively.

6.3 Shift Poles and Rotation Rates

The area considered - about 10°square - is small enough for the solution of the plate kinematics to be treated on a flat surface. Interplate motion is considered in terms of rotations about shift poles.

Pole 1/4 (figure 6.3) at 62S, 174E with a rotation rate of 1.27°/My is the Indian-Pacific pole of Chase (1978). Pole 1/2 is inferred to be on the strike of the New Zealand Spreading Axis because observed slip directions do not vary consistently from the normal to the axis. The spreading rate in the Taupo Volcanic Zone is 7 mm y^{-1}. If the spreading

zone in the Waimea Depression is 15 km wide the strain rate there of 0.3 μrad y^{-1} indicates a spreading rate of 4.5 mm y^{-1}. Together these values indicate a pole near 49S, 165E with a rotation rate of 0.27°/My.

Boundary 2/3 is a dextral reverse fault forming an approximately circular arc concave west thus indicating a pole to the west of the North Island. The small reverse component is probably greater to the south and therefore the position of the pole will be somewhat to the north of the centre of the arc. A pole at 35S, 165E is adopted and the spreading rate, determined from the slip rate of 14.6 mm y^{-1} in zone BP4, is 0.76°/My. The positions and rotation rates of the remaining poles can be computed from the above data according to the laws that govern rigid plate motions. As is shown in Appendix 3, any group of three plates has three associated shift poles which lie on a straight line in positions determined by their rotation rates; the rotation rates sum to zero. The position and rotation rates of all the six poles are given in table 6.1.

Boundary	Plates	Pole Position		Rotation Rate
		latitude °S	longitude °E	°/My
New Zealand Spreading Axis	1/2	49	165	-0.27
Havre Trough	3/1	39	165	+1.03
North Island Shear Belt	2/3	35	165	-0.76
Hikurangi Margin	3/4	51	168	+2.30
Marlborough Faults	4/2	59	172	+1.54
Alpine Fault	1/4	62	174	+1.27

Table 6.1 Pole positions and rotation rates for microplate model of the North Island.

6.4 Testing of the Model

The model is based on slip vectors at points A, B and C in figure 6.3 and on the assumption that certain fault and earthquake belts form microplate boundaries; it is tested by comparing the observed and predicted relative plate

velocities at some other points and by considering the interaction of boundaries at triple junctions.

At point D (figure 6.3) Bibby (1976) gives a slip vector, assuming simple shear on faults, of 46 mm y^{-1} at 247°; the slip vector inferred from the model, controlled mainly by the position and rotation rate of the pole 1/4 of Chase (1978), is 51 mm y^{-1} at 273°. At points B and E spreading and subduction rates of 7 mm y^{-1} and 60 mm y^{-1} are inferred and at points F and G, 27 mm y^{-1} and 90 mm y^{-1}. According to theoretical models such as that of Andrews and Sleep (1974) back-arc spreading rates will be up to about one-quarter of the subduction rate, so that rates predicted on boundaries 1/3 and 3/4 are of approximately the correct relative magnitudes. At 19.5°S, 176.8°E in the Lau Basin (the northern continuation of the Havre Trough) Lawver et al (1976) from their admittedly tenuous marine magnetic correlations give a spreading rate of 29 mm y^{-1} at 130°, the model predicts 50 mm y^{-1} at 134°.

Thus the model gives not unreasonable rates of motion throughout the New Zealand region; although as regards back-arc spreading, velocities are about twice as high as they should be in the Lau Basin. In addition it will be noted that there is a significant dextral component to the motion at the south end of the Havre Trough. If motion is not in fact oblique here a further boundary has to be postulated near the Bay of Plenty triple junction to divide the Kermadec Plate into a northern and a southern part.

It will be seen in the plate model that the transform between the Taupo Volcanic Zone and the Havre Trough is a north-south striking dextral transform.

The main shortcoming of the model is that the predicted extension rate across the Waverley Fault Zone is only slightly less than the 7 mm y^{-1} across the Taupo Volcanic Zone whereas from the appearance of faulting the rate is likely to be considerably less. A solution to this problem would be to bring the 1/2 pole up into the South Taranaki Bight and in consequence require a further boundary and a further

plate to account for spreading at Waimea.

Triple junctions: While a triple junction consisting of any combination of three boundaries can exist instantaneously only certain kinds are stable for finite displacements (McKenzie and Morgan, 1969), therefore the stability of triple junctions in the model is investigated. Of the four triple junctions associated with the microplates, that at the northern end of boundary 1/3 has variously been interpreted by Sclater et al (1972) and Weissel (1977) as an RRR or RFF triple junction and is not considered further here. Velocity vector diagrams for the other three junctions, all of which are stable, are given in figure 6.5. Junction 1/2/3 in the Bay of Plenty is moving northwest relative to the Central Plate at about 4 mm y^{-1}, junction 2/3/4 in Cook Strait is almost stationary with respect to the Central Plate, and junction 1/2/4 at the south end of the Waimea Depression is moving northeast relative to the Central Plate at about 30 mm y^{-1}.

6.5 Moment Accumulation and Seismicity on Boundaries

As discussed in Chapter 5, according to Molnar (1979) the rate of accumulation of seismic moment on a boundary is given by $\dot{M}_0^{\Sigma} = \mu A \bar{u}$ where μ is the rigidity (taken as 3×10^{11} dyne cm^{-2} for crustal rocks), A is the area of the boundary and $\bar{u}$ is the slip rate. Where faults are oblique to the slip direction as for instance where reverse faults dip at 45° to horizontal shortening, $\dot{M}_0^{\Sigma} = 2\mu A \bar{u}$ where A is the vertical cross-sectional area. In table 6.2 the rates are calculated for the five plate boundaries in New Zealand including the Hikurangi Trough as far north as East Cape and the Alpine Fault as far south as Milford Sound.

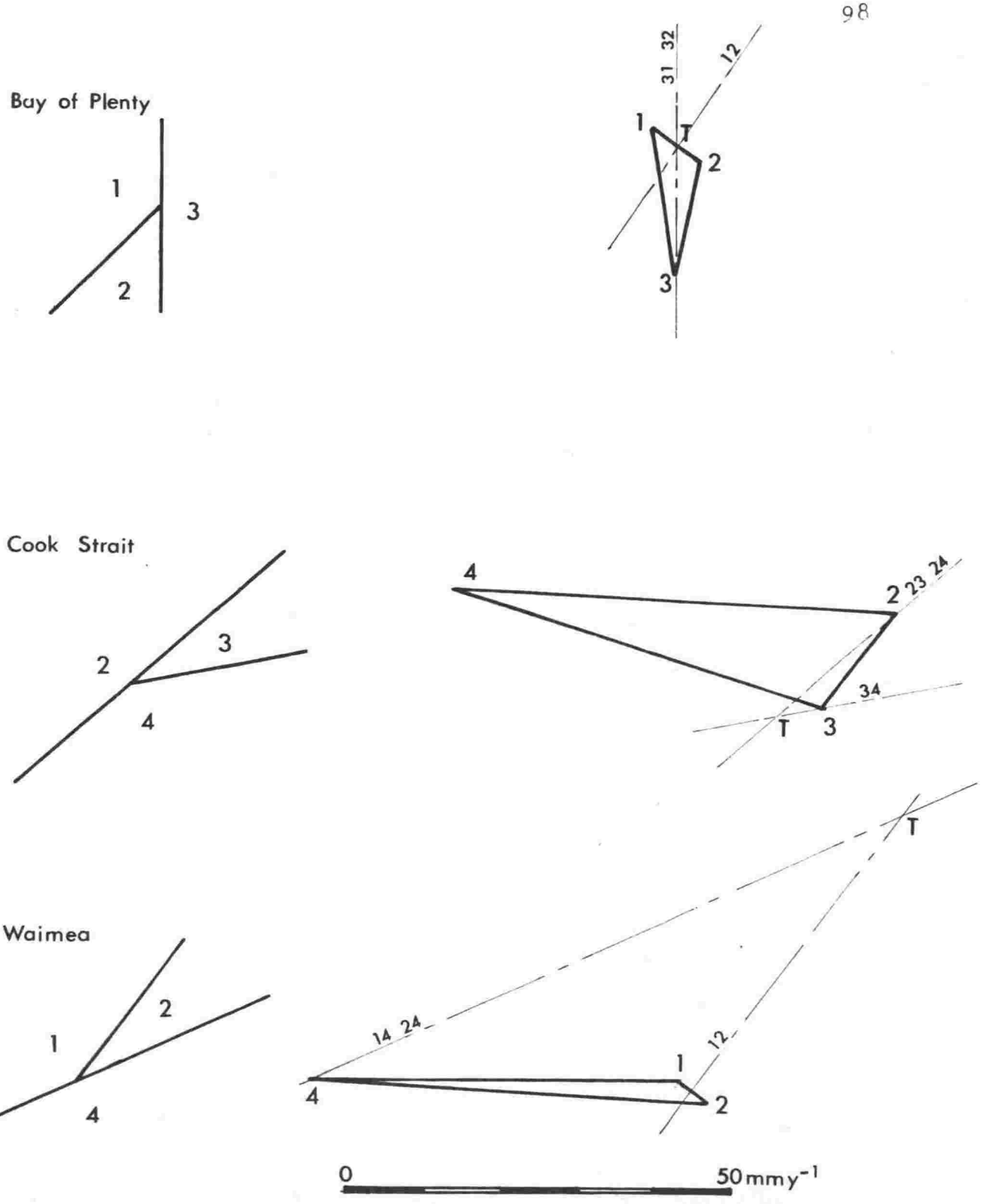

Figure 6.4 Plans and velocity vector diagrams for the three triple junctions associated with the Central Plate. Fine lines identified as 12 or 31 etc. indicate the position of boundaries in vector space, T indicates the triple junction.

Boundary	Length (km)	Depth (km)	Average Slip Rate (mm y^{-1})	$\dot{M}_0^{\Sigma}$ (dyne cm y^{-1})	$T(M_0{}^{27})$ (yr)
New Zealand Spreading Axis	600	2 x 10	5	1.8×10^{25}	359
North Island Shear Belt	500	20	15	4.5×10^{25}	143
Hikurangi Margin (to East Cape)	600	2 x 20	60	4.3×10^{26}	15
Marlborough Faults	200	20	50	6.0×10^{25}	107
AlpineFault (to Milford Sd.)	500	20	40	1.2×10^{26}	54

Table 6.2 Rates of moment accumulation on microplate boundaries in New Zealand

The values for $\dot{M}_0^{\Sigma}$ are an estimate of the maximum amount of seismic energy which may be stored in each boundary per year. If there is no creep, the long-term rate of dissipation of strain by earthquakes will equal the rate of moment accumulation. Then, as discussed in Chapter 5, the return period for an earthquake with moment M_0 in a region where the largest earthquake would have the moment $M_0{}^{max}$ is given by

$$T(M_0) = \frac{M_0{}^{max\ 1-\beta}}{(1-\beta)\dot{M}_0^{\Sigma}} M_0{}^{\beta} \qquad - 1$$

where β depends on the frequency distribution of seismic moment which can be expected to vary from region to region but which Molnar (1979) infers from the frequency distribution of magnitudes and the empirical relationship of magnitude to moment to be about 2/3. Assuming that the largest moment expected in New Zealand is 10^{28}dyne-cm, the return period for earthquakes with moment of 10^{27}dyne-cm is calculated using equation 1 for each of the plate boundaries in New Zealand and is given in table 6.2. For a shallow earthquake with moment 10^{27}dyne cm and a fault 50 km long, a surface displacement of about 3 m would be expected, which suggests that a 10^{27}dyne cm earthquake will be larger than the Inangahua Earthquake and smaller than the Murchison Earthquake.

It is unlikely that earthquakes with moment as large as 10^{27} occur at the New Zealand Spreading Axis and as

discussed in Chapter 5 smaller more frequent earthquakes would be expected and are found there, even so it was concluded that creep is occurring. In the North Island Shear Belt and Marlborough Faults large historical earthquakes probably account for the observed strain rate but at the Hikurangi Margin and on the Alpine Fault there is an undersupply of earthquakes with moment 10^{27}dyne-cm, or larger, the situation being the more anomalous at the Hikurangi Margin where it seems necessary to postulate that the majority of slip occurs aseismically.

6.6 Conclusion

While two plates are sufficient to describe the tectonics of most of the South Island at least four are required for the North Island. Three subparallel microplate boundaries are postulated which separately accommodate the back-arc spreading, dextral and convergent components of motion in the Indian-Pacific Boundary Zone in the North Island. Geodetic analyses show that the back-arc spreading rate in the Taupo Volcanic Zone is 7 mm y^{-1} and that in the North Island Shear Belt the dextral displacement rate is 14 mm y^{-1} and the narrowing rate is 4 mm y^{-1}. The plate model presented depends on the identification of fault belts with microplate boundaries. Then by accepting the Indian-Pacific pole and rotation rate determined from macroplate tectonics the four plate model can be constructed. Relative plate motions are conveniently described in terms of rotations about shift poles. Almost no redundancy has been used in the establishment of pole positions and rotation rates, but the model accounts for most deformation in New Zealand and gives reasonable relative plate velocities. With further information, it will be possible to define pole positions and rotation rates more closely. Alternatively it may prove necessary to introduce further plates.

Addendum

Healy, J. 1964. Volcanic mechanisms in the Taupo Volcanic Zone N.Z.J.Geol.Geophys., 7: 6-23

Weissel, J. K. 1977. Evolution of the Lau Basin by the growth of small plates. In: Talwani, M. & Pitman, W. C. (eds.) Island Arcs, Deep Sea Trenches and Back-Arc Basins Am.Geophys.Union

Wellman, H. W. 1964. Age of the alpine fault, New Zealand. In: Proceedings of 22nd Int.Geol.Congr., India pp.148-162

REFERENCES

Adams, R. D. & Ware, D. E. 1977. Subcrustal earthquakes beneath New Zealand: locations determined with a laterally inhomogeneous velocity model N.Z.J.Geol.Geophys., 20: 59-83

Aki, K. 1966. Generation and propagation of G waves from the Niigata earthquake of June 16, 1964; 2, Estimation of earthquake moment, released energy, and stress-strain drop from G wave spectruum Bull.Earthq.Res.Inst. Tokyo Univ., 44: 73-88

Andrews & Sleep 1974. Numerical modelling of tectonic flow behind island arcs Geophys.J.R.Astro.Soc., 38: 237-51

Arabasz & Robinson 1976. Microseismicity and geologic structure of the northern South Island, New Zealand N.Z.J.Geol.Geophys., 19: 569-601

Ballance, P. F. 1976. Evolution of the Upper Cenozoic magmatic arc and plate boundary in northern New Zealand Earth Planet. Sci.Lett., 28: 356-370

Banwell, C. J. 1964. Thermal energy from the earth's crust N.Z.J.Geol.Geophys., 7: 585-93

Bibby, H. M. 1973. The reduction of geodetic survey data for the detection of earth deformation Geophysics Division Report No.84, N.Z.D.S.I.R., Wellington

_____ 1975. Crustal strain from triangulation in Marlborough, New Zealand Tectonophysics, 29: 529-40

_____ 1976. Crustal strain across the Marlborough Faults, New Zealand N.Z.J.Geol.Geophys., 19: 407-25

_____ & Walcott, R. I. 1977. Earth deformation and triangulation in New Zealand N.Z.Surveyor, 28: 741-62

Bomford, G. 1971. Geodesy 3rd ed. London, Oxford University Press

Bosman, E. R. & Kubik, K. 1971. The computation of geodetic networds with simultaneous estimation of weights of measured quantities Bull.Geodesique, 102: 441-9

Browne, P. R. L. 1978. Petrological logs of drill holes, Kawerau geotheral field Geological Survey Report No.84 N.Z.D.S.I.R., Wellington

Bullen, K. E. 1938. An analysis of the Hawkes Bay earthquakes during February 1931 N.Z.J.Sci.Tech., 19: 497-519

Calhaem, I. M. 1973. Heatflow Measurements under some Lakes in the North Island, New Zealand Ph.D thesis, Victoria University of Wellington, New Zealand

Chase, C. G. 1978. Plate kinematics: the Americas, East Africa, and the rest of the world Earth Planet.Sci.Lett., 37: 355-68

Cole, J. W. 1970. Structure and eruptive history of the Tarawera Volcanic Complex N.Z.J.Geol.Geophys., 13: 879-903

_____ 1973. High-alumina basalts of the Taupo Volcanic Zone, New Zealand Lithos, 6: 53-64

_____ & Hunt, T. M. 1968. Basalt dikes in the Tarawera Volcanic Complex, New Zealand N.Z.J.Geol.Geophys., 11: 1203-6

Cotton, C. A. 1951. Fault valleys and shutter ridges at Wellington N.Z.Geogr., 7 (1): 62-8

Eiby, G. A. 1968. An annotated list of New Zealand earthquakes N.Z.J.Geol.Geophys., 11: 630-47

_____ 1977. The junction of the main New Zealand and Kermadec seismic regions International Symposium on Geodynamics in the Southwest Pacific, Noumea, Sept.1976, Editions Technip, Paris 1977, pp.167-78

Evison, F. F., Robinson, R. & Arabasz, W. J. 1976. Microearthquakes, geothermal activity, and structure, central North Island, New Zealand N.Z.J.Geol.Geophys., 19: 625-37

Fleming, C. A. 1953. The geology of the Wanganui Subdivision N.Z.Geol.Survey Bull., n.s. 52, 362 pp.

Frank, F. C. 1966. Deduction of earth strains from survey data Bull.Seis.Soc.of Am., 56: 35-42

Gibowicz, S. J. 1973. Variation of frequency-magnitude relationships during Taupo earthquake swarm of 1964-65 N.Z.J.Geol.Geophys., 16: 18-51

_____ & Hatherton, T. 1975. Source properties of shallow earthquakes in New Zealand and their tectonic associations Geophys.J.R.Astro.Soc., 43: 589-605

Grange, L. I. 1932. Taupo earthquakes, 1922 N.Z.J.Sci.Tech., 14: 139-41

Grindley, G. W. 1960. Geological map of New Zealand 1:250000 Sheet 8 Taupo 1st Ed. N.Z.D.S.I.R., Wellington

_____ 1965. The geology structure and exploitation of the Wairakei Geothermal Field, Taupo, New Zealand N.Z.Geol.Survey Bull., n.s. 75

Grindley, G. W. 1970. Subsurface structures and relation to steam production in the Broadlands Geothermal Field, New Zealand U.N.Symposium on the Development and Utilization of Geothermal Resources, Pisa, 1970 Vol.2, Part 1: 248-61

Hamilton, R. M. & Gale, A. W. 1968. Seismicity and structure of North Island, New Zealand J.Geophys.Res., 73: 3859-76

Hanks, T. C. 1977. Earthquake stress drops, ambient tectonic stresses and stresses that drive plate motions Pageoph., 115: 441-58

Hatherton, T. 1969. The geophysical significance of calc-alkaline andesites in New Zealand N.Z.J.Geol.Geophys., 12: 436-59

_____ & Syms, M. 1975. Junction of Kermadec and Hikurangi Gravity Anomalies (Note) N.Z.J.Geol.Geophys., 18: 753-6

Healy, J. 1962. Structure and volcanism in Taupo Volcanic Zone, New Zealand Am.Geophysical Union Geophysical Monograph, 6: 151-7

_____, Schofield, J. C. & Thompson, B. N. 1964. Geological map of New Zealand 1:250000 Sheet 5 Rotorua 1st Ed. N.Z.D.S.I.R., Wellington

Henderson, J. 1933. The geological aspects of the Hawkes Bay earthquakes N.Z.J.Sci.Tech., 16: 38-75

Hochstein, M. P. 1976. Estimation of geothermal resources In: Nathan, S. (ed.) Excursion Guide 55A & 56C 25th International Geological Congress

Jaeger, J. C. & Cook, N. G. W. 1971. Fundamentals of Rock Mechanics London, Chapman & Hall, 515 pp.

Karig, D. E. 1970a. Kermadec Arc-New Zealand Tectonic Confluence N.Z.J.Geol.Geophys., 13: 21-9

_____ 1970b. Ridges and basins of the Tonga-Kermadec Island Arc System J.Geophys.Res., 75: 239-54

_____ 1971. Origin and development of marginal basins in the western Pacific J.Geophys.Res., 76: 2542-61

Katz, H. R. 1974. Margins of the Southwest Pacific In: Burk, C. A. & Drake, C. L. (eds.) The Geology of Continental Margins N.Y., Springer-Verlag, 549-65

Keylis-Borok, V. I. 1959. An estimation of the displacement in an earthquake and of source dimensions Ann.Geofis. (Rome), 12: 205-14

Lawrence, P. 1967. New Zealand Region; Bathymetry 1:6,000,000 N.Z.Oceanogr.Inst.Chart, Miscellaneous Series 15

Lawver, L. A., Hawkins, J. W. & Sclater, J. G. 1976. Magnetic anomalies and crustal dilation in the Lau Basin Earth Planet.Sci.Lett., 33: 27-35

Lensen, G. J. 1968. Analysis of progressive fault displacement during down cutting at the Branch River Terraces, South Island, New Zealand Geol.Soc.Am.Bull., 79: 545-56

_____ 1975. Earth-deformation studies in New Zealand Tectonophysics, 29: 541-51

_____ & Vella, P. 1971. The Waiohine River faulted terrace sequence Roy.Soc.of N.Z.Bull., 9: 117-9

Malahoff, A. 1968. Origin of magnetic anomalies over the central volcanic region of New Zealand Am.Geophys.Union Geophys.Monograph, 12: 218-40

Mansinha, L. & Smylie, D. E. 1971. The displacement fields of inclined faults Bull.Seis.Soc.Am., 61: 1433-40

Maruyama, T. 1964. Statical elastic dislocations in an infinite and semi-infinite medium Bull.of the Earthquake Res.Inst. Tokyo, 42: 289-368

McKenzie, D. P. & Morgan, W. J. 1969. Evolution of triple junctions Nature, 224: 125-34

Midha, R. K. 1979. Geoelectromagnetic Induction Studies in the North Island Volcanic Region, New Zealand Ph.D thesis, Victoria University of Wellington, New Zealand

Minster, J. B., Jordan, T. H., Molnar, P. & Haines, E. 1974. Numerical modelling of instantaneous plate tectonics Geophys.J.R.Astro.Soc., 36: 541-76

Modriniak, N. & Studt, F. E. 1959. Geological structure and volcanism of the Taupo-Tarawera district N.Z.J.Geol.Geophys., 2: 654-84

Molnar, P. 1979. Earthquake recurrence intervals and plate tectonics Bull.Seis.Soc.of Am., 69: 115-33

Morgan, P. G. 1923. Taupo earthquakes N.Z.Geol.Survey 17th Annual Report, 10-1

_____, Marsden, E. & Adams, C. E. 1922. Unpublished letter to Minister of Internal Affairs, copy held by Geological Survey, N.Z.D.S.I.R., Wellington

Murphy, R. P. 1977. The Volcanic Geology of the Matahana Basin M.Sc. thesis, Victoria University of Wellington, New Zealand

Nairn, I. E. 1976. Late Quaternary faulting in the Taupo Volcanic Zone. In: Nathan, S. (ed.) 25th Int.Geol.Congress Excursion Guide No.55A

Ongley, M. 1943. The surface trace of the 1855 earthquake Trans.Roy.Soc.N.Z., 73: 84-9

Prescott, W. H. 1976. An extension of Frank's method for obtaining crustal shear strains from survey data Bull.Seis.Soc.of Am., 66: 1847-53

Ramsay, J. G. 1967. Folding and Fracturing of Rocks N.Y., McGraw-Hill, 568 pp.

Reilly, W. I., Whiteford, C. M. & Doone, A. 1977. Gravity Map of New Zealand 1:1,000,000 Isostatic Anomalies N.Z.D.S.I.R., Wellington

Reyners, M. E. 1978. A Microearthquake Study of the Plate Boundary, North Island, New Zealand Ph.D thesis, Victoria University of Wellington, New Zealand

Roberts, N. L. 1967. Magnetic survey of Bay of Plenty Geophysics Div.Report No.40, N.Z.D.S.I.R., Wellington

Stern, T. 1979. (in press) N.Z.J.Geol.Geophys.

Sykes, L. R. 1966. The seismicity and deep structure of island arcs J.Geophys.Res., 71: 2981

Tapponier, P. & Francheteau, J. 1978. Necking of the lithosphere and the mechanics of slowly accreting plate boundaries J.Geophys.Res., 83 No.B8: 3955-70

Toksöz, M. N. & Hsui, A. T. 1978. Numerical studies of back-arc convection and the formation of marginal basins Tectonophysics, 50: 177-96

van der Linden, W. J. M. 1967. Structural relationships in the Tasman Sea and South West Pacific Ocean N.Z.J.Geol.Geophys., 10: 1280-301

Walcott, R. I. 1978a. Present tectonics and Late Cenozoic evolution of New Zealand Geophys.J.R.Astro.Soc., 52: 137-64

_____ 1978b. Geodetic strains and large earthquakes in the arcial tectonic belt of North Island, New Zealand J.Geophys.Res., 83 No.B9: 4419-29

Ward, R. H. 1922a. Unpublished letter to E. Marsden, copy held by N.Z.Geol.Survey, Wellington

_____ 1922b. A note on the significance of the recent subsidence of the shore of Lake Taupo N.Z.J.Sci.Tech., 5: 280-1

Wellman, H. W. 1953. Data for the study of recent and late Pleistocene faulting in the South Island of New Zealand N.Z.J.Sci.Tech., B34: 270-88

_____ 1969. Tilted marine beach ridges at Cape Tukakirae, New Zealand Tuatara, 17: 82-93

_____ 1973. New Zealand fault zones and sea-floor spreading. In: Coleman, P. J. (ed.) The Western Pacific: Island Arcs, Marginal Seas, Geochemistry University of Western Australia Press

Whiteford, C. M. 1976. Magnetic anomaly map of the central volcanic region Geophysics Division, Report No.101 N.Z.D.S.I.R., Wellington

Whitten, C. A. & Claire, C. N. 1960. Analysis of geodetic measurements along the San Andreas Fault Bull.of Seis.Soc.of Am., 50: 404-15

APPENDIX 1 DATA SOURCES

All geodetic data used in the thesis are held by the Department of Lands and Survey. Indexed summaries of all 1st and 2nd order observations made since 1910 are stored at Head Office, Wellington; and are therefore easily obtainable. Pre-1910 data are not summarized and field books containing them are stored at District Offices. Data from the following old field books have been used.

	Field book number	Surveyor	Year	Instrument	Number of sets
a)	stored at Hamilton District Office				
	724	W. Cussen	1886	6" transit	8
	637	L. Cussen	1883	10" Everest	12
	37	S. Percy-Smith	1873	10" Everest	12
b)	stored at Wellington District Office				
	1180	A. D. Wilson	1886	6" transit	8
	1155	J. A. Thorpe	1886	5" Everest	12
	973	J. A. Thorpe	1887	5" Everest	12
	2130	H. J. Lowe	1898	10" Everest	12
	2164	H. J. Lowe	1899	10" Everest	12
	2108	H. J. Lowe	1897	10" Everest	8
	2069	H. J. Lowe	1898	5" & 8" transits	8

APPENDIX 2 ADJUSTMENT FIGURES

The figures of the survey nets used to obtain the strain estimates given in tables 3.1, 3.2 and 3.3 are given in the following pages. The rays represent observations of direction; distance observations are included in many post-1960 surveys but are not identified. Station numbers are given for re-observed stations only and are the numbers assigned for the computer analysis, not Department of Lands and Survey designations. The scale is 1:500,000 for the Tongariro and North Taupo Areas and 1:707,000 for the Bay of Plenty Area.

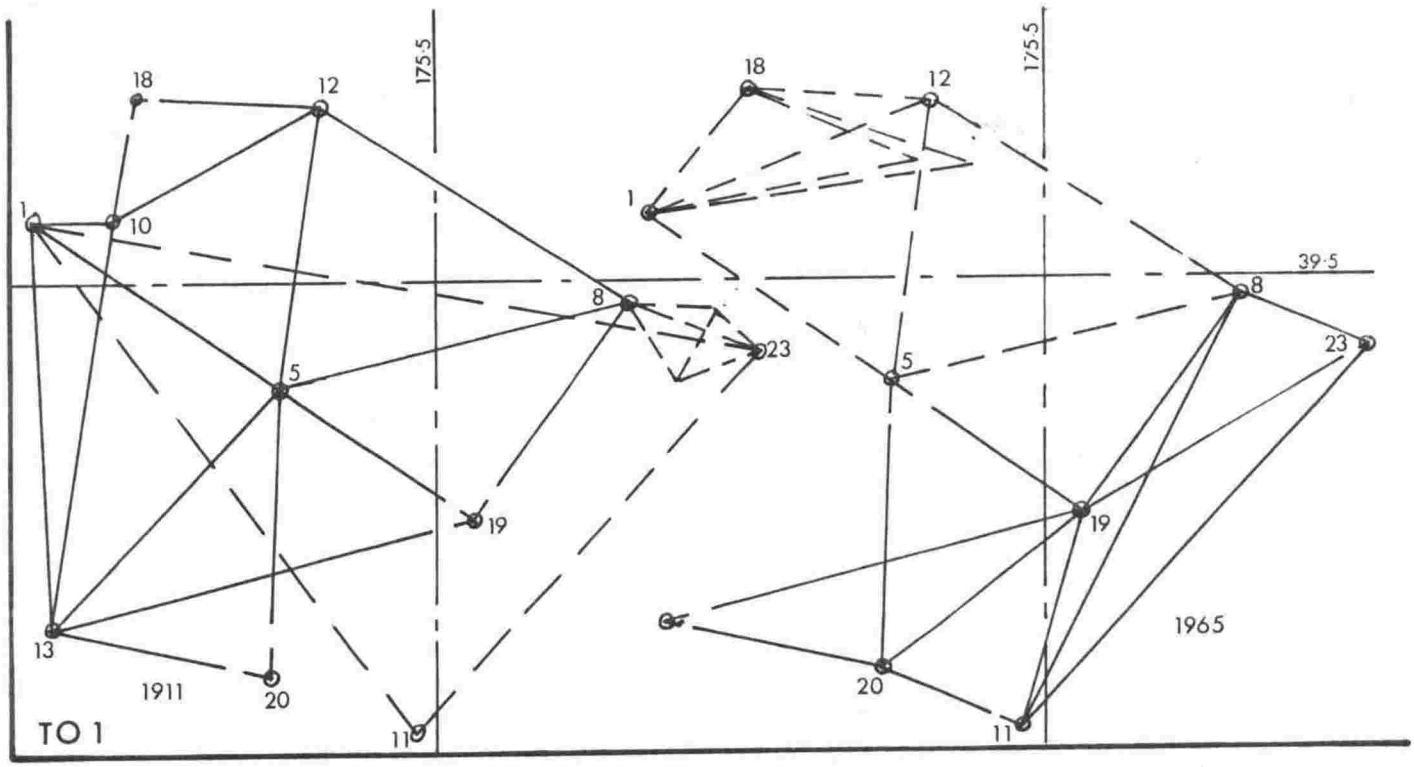
175·5
18
12
1
10
8
23
5
19
13
1911
20
11
TO 1
175·5
18
12
1
39·5
8
23
5
19
1965
20
11

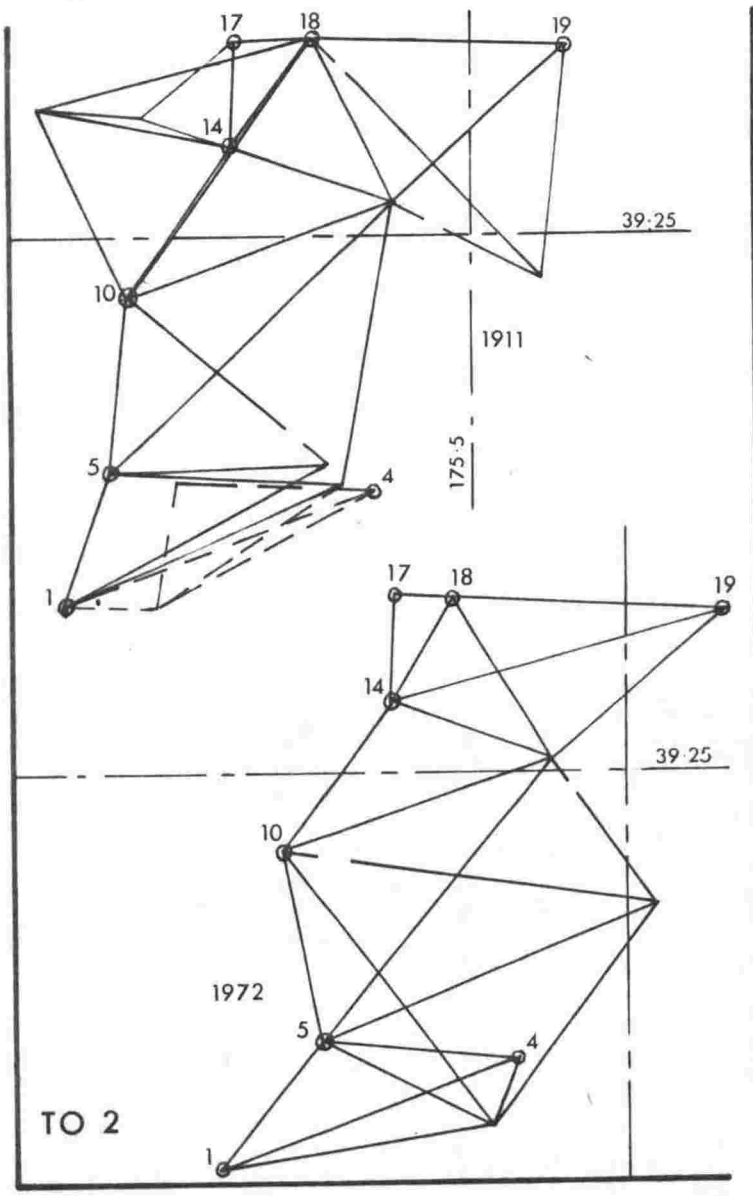
17
18
19
14
39·25
10
1911
175·5
5
4
1
17
18
19
14
39·25
10
1972
5
4
1
TO 2

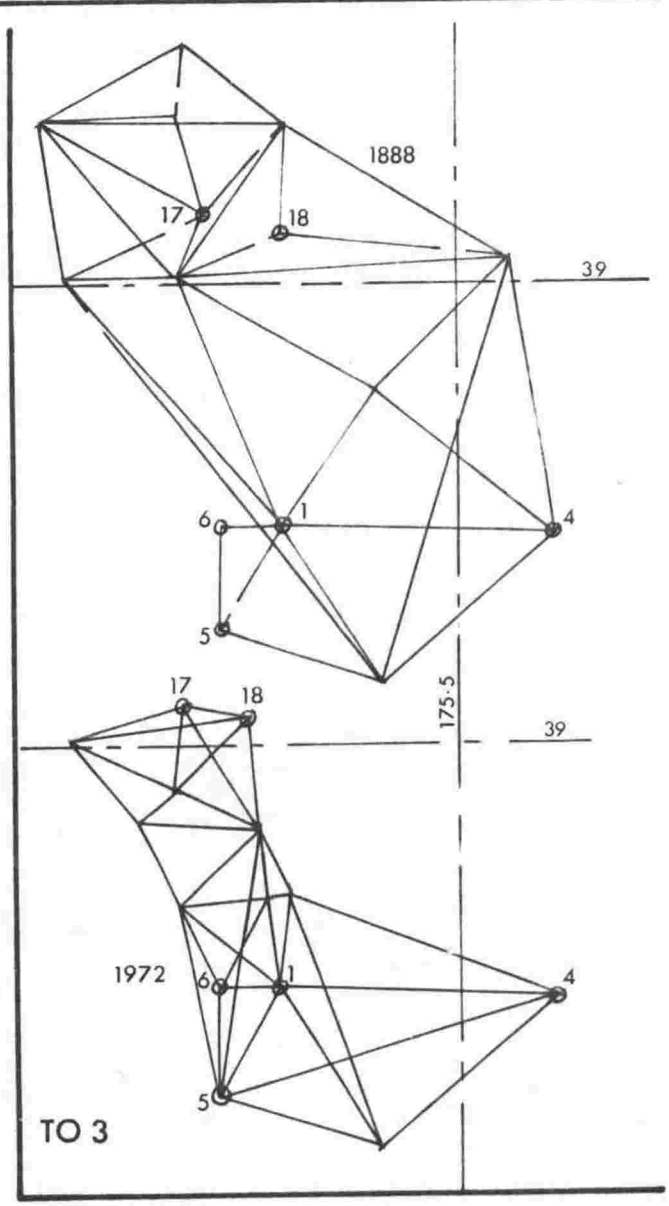
1888
17
18
39
6
1
4
5
17
18
175·5
39
1972
6
1
4
5
TO 3

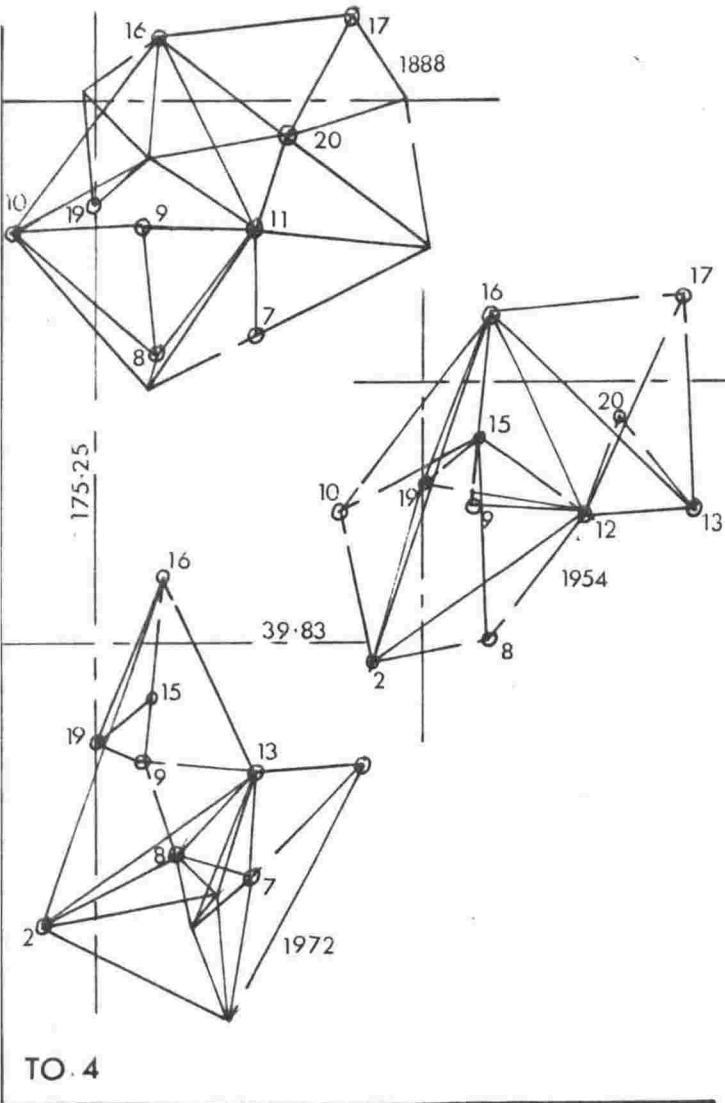

TO 4

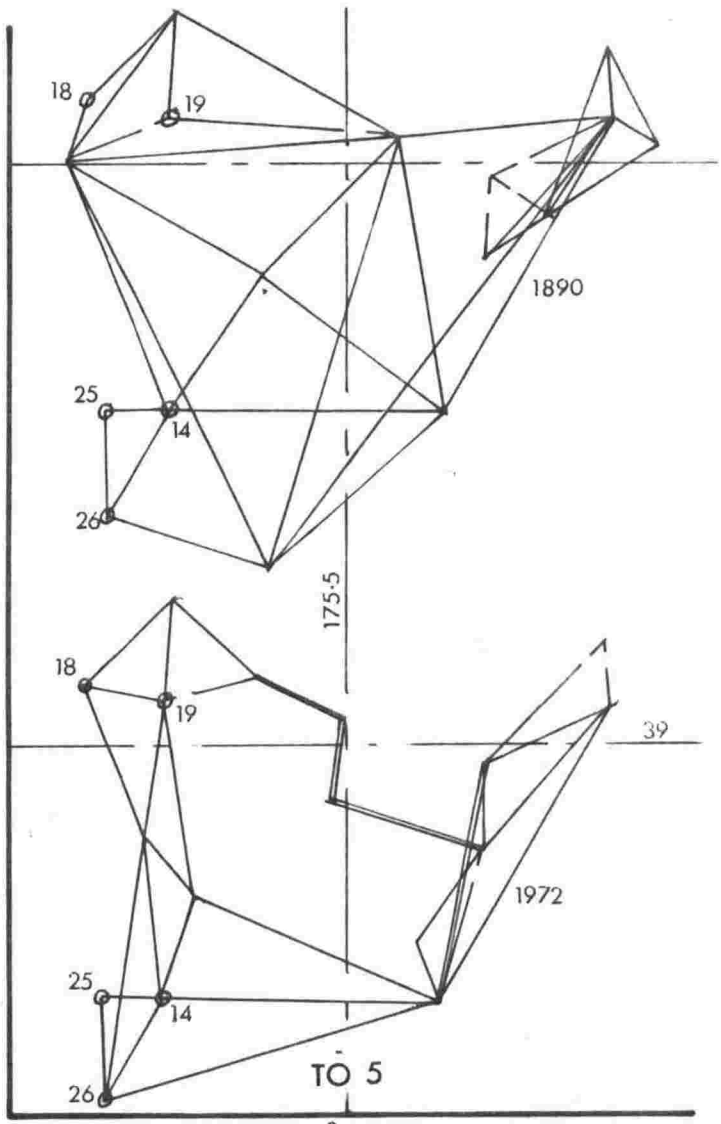

TO 5

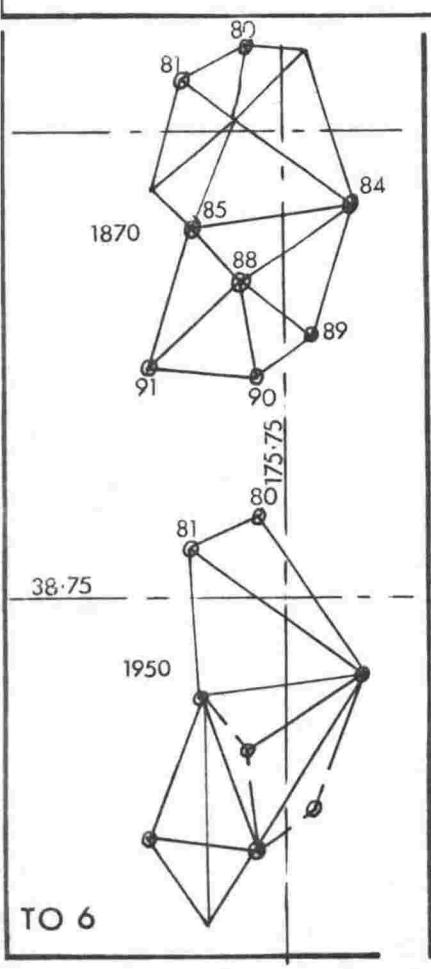

TO 6

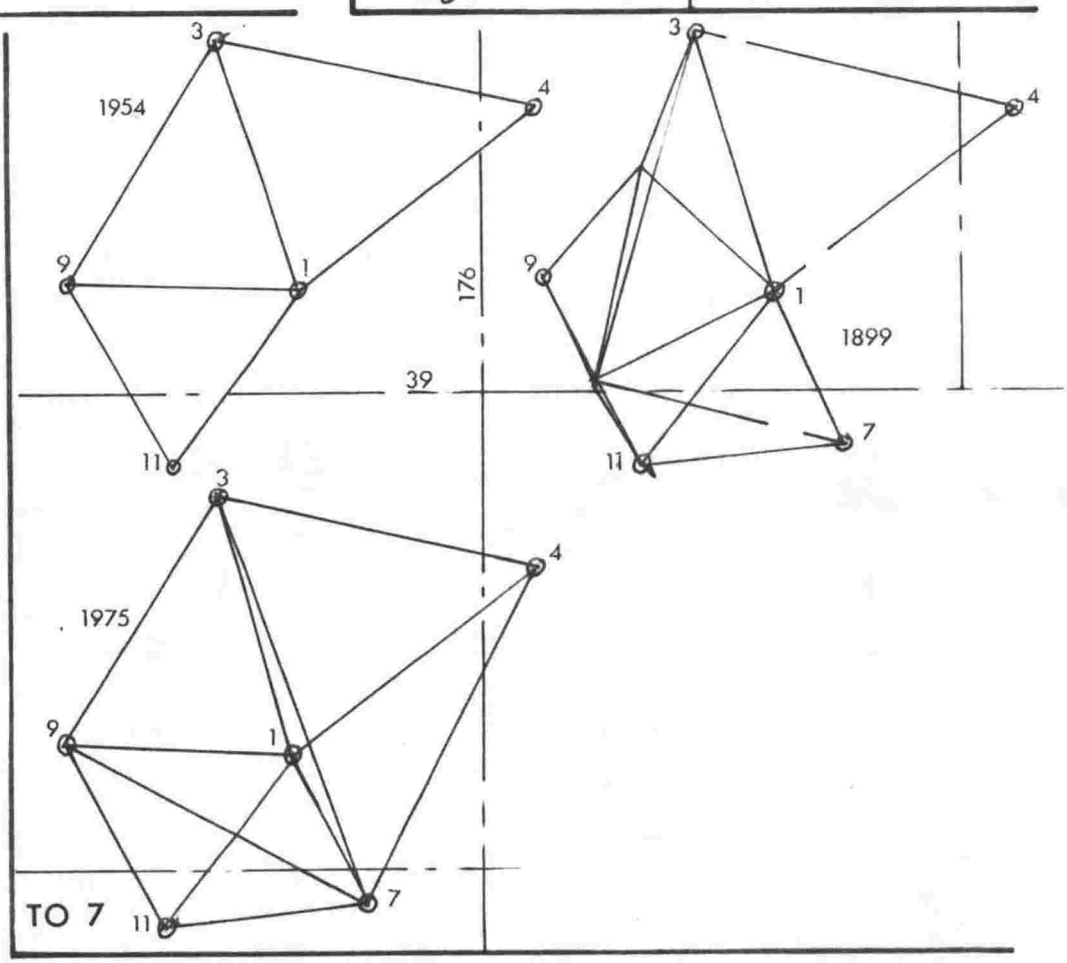

TO 7

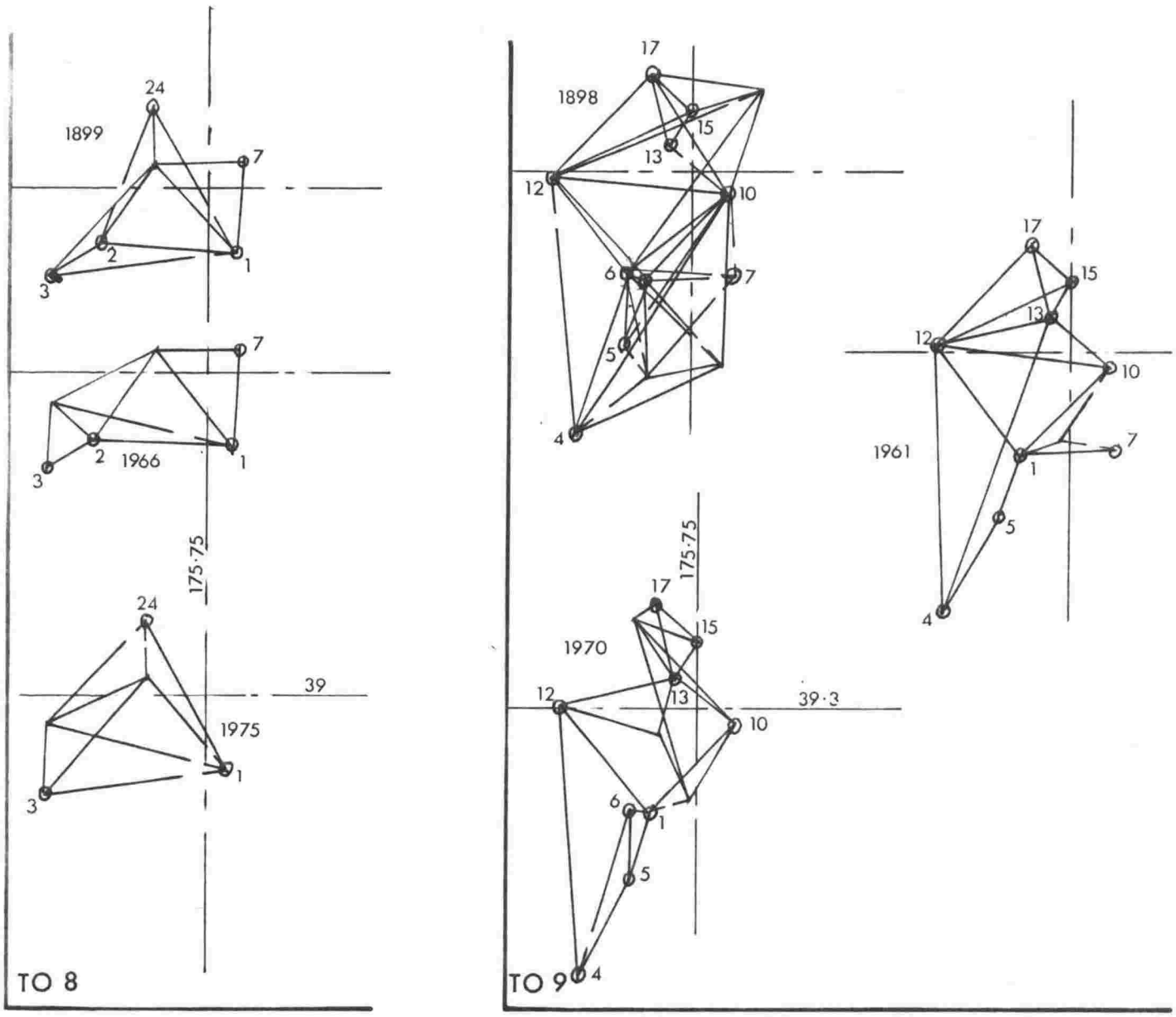
1899
1966
1975
175·75
39
TO 8
1898
1961
1970
175·75
39·3
TO 9

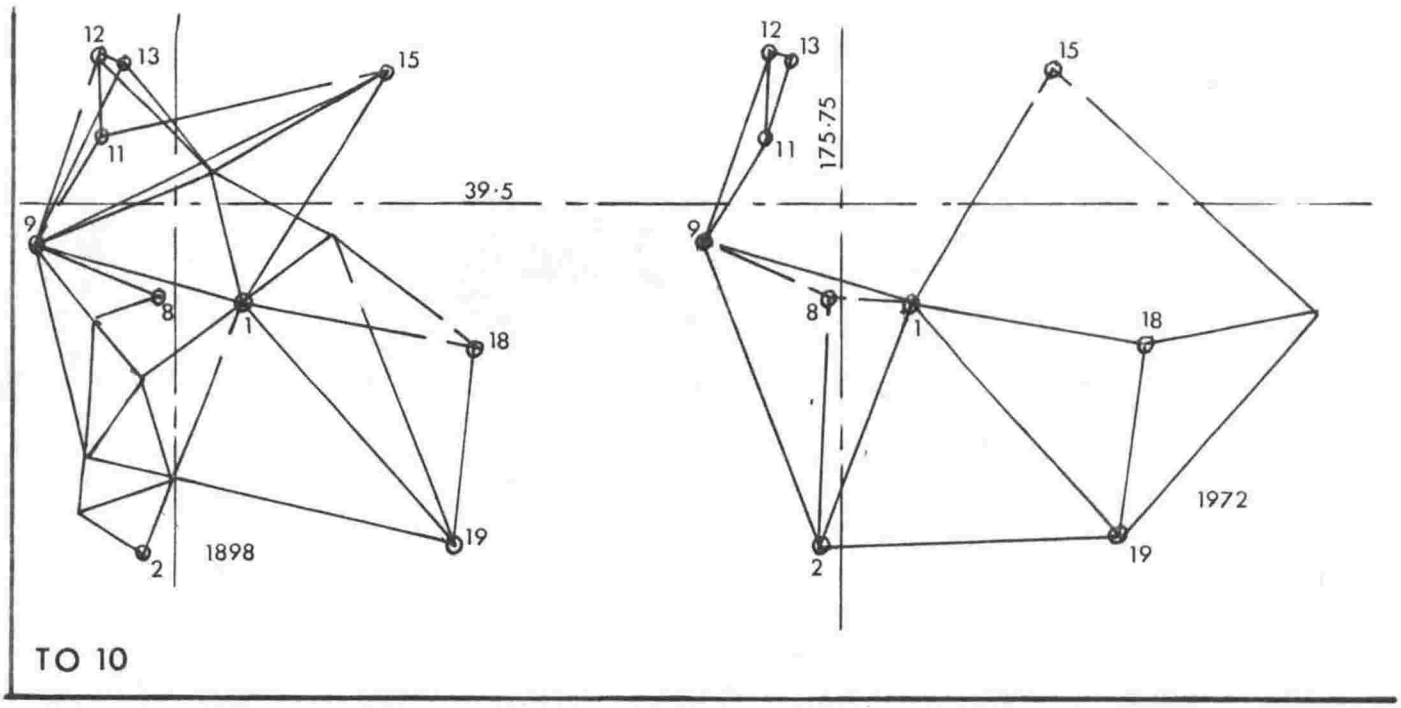
1898
39·5
TO 10
175·75
1972

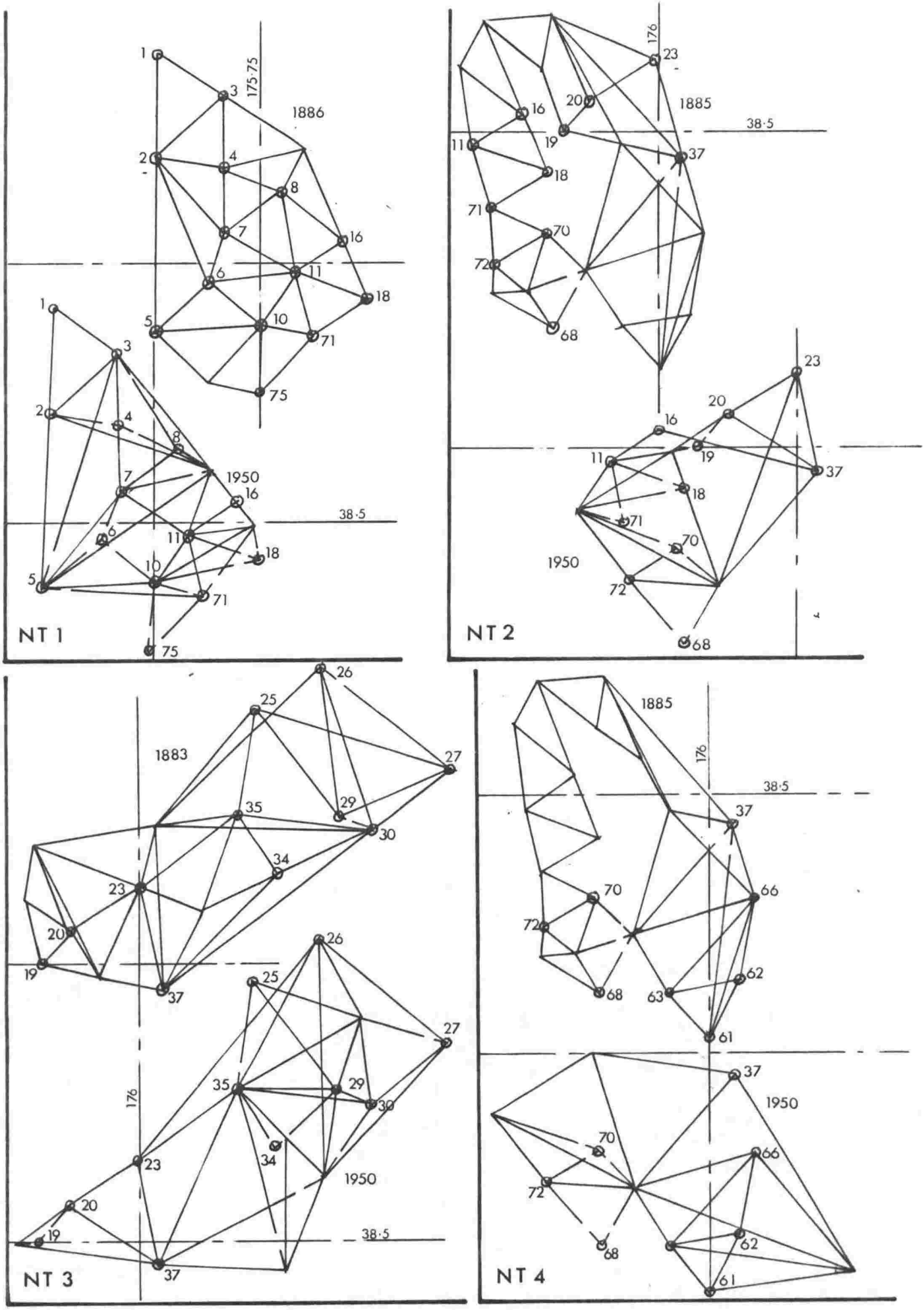
1
2
3
4
5
6
7
8
10
11
16
18
71
75
175·75
1886
1950
38·5
NT 1
20
23
37
68
72
70
66
62
63
61
176
1885
NT 2
25
26
27
29
30
34
35
NT 3
NT 4

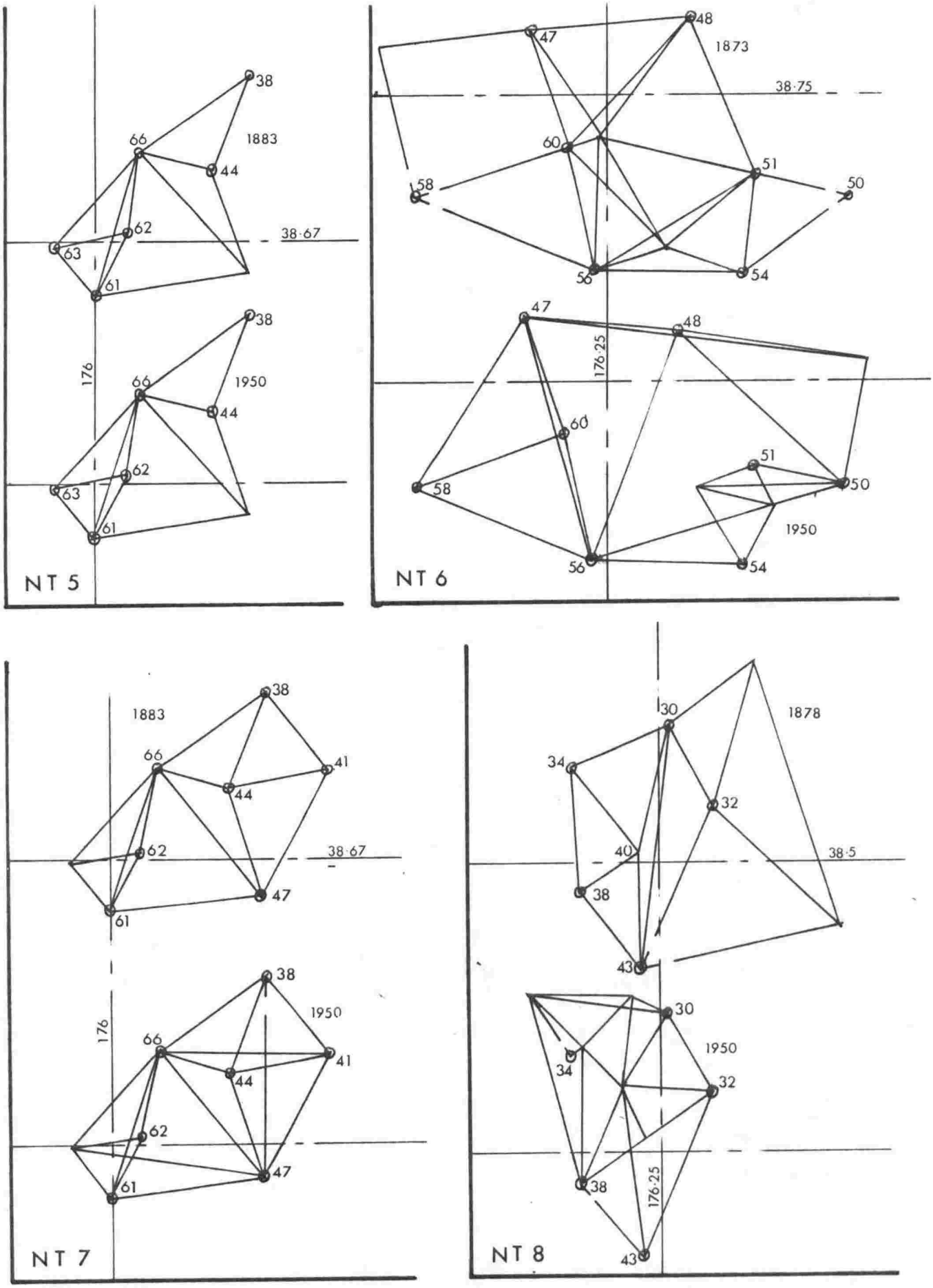

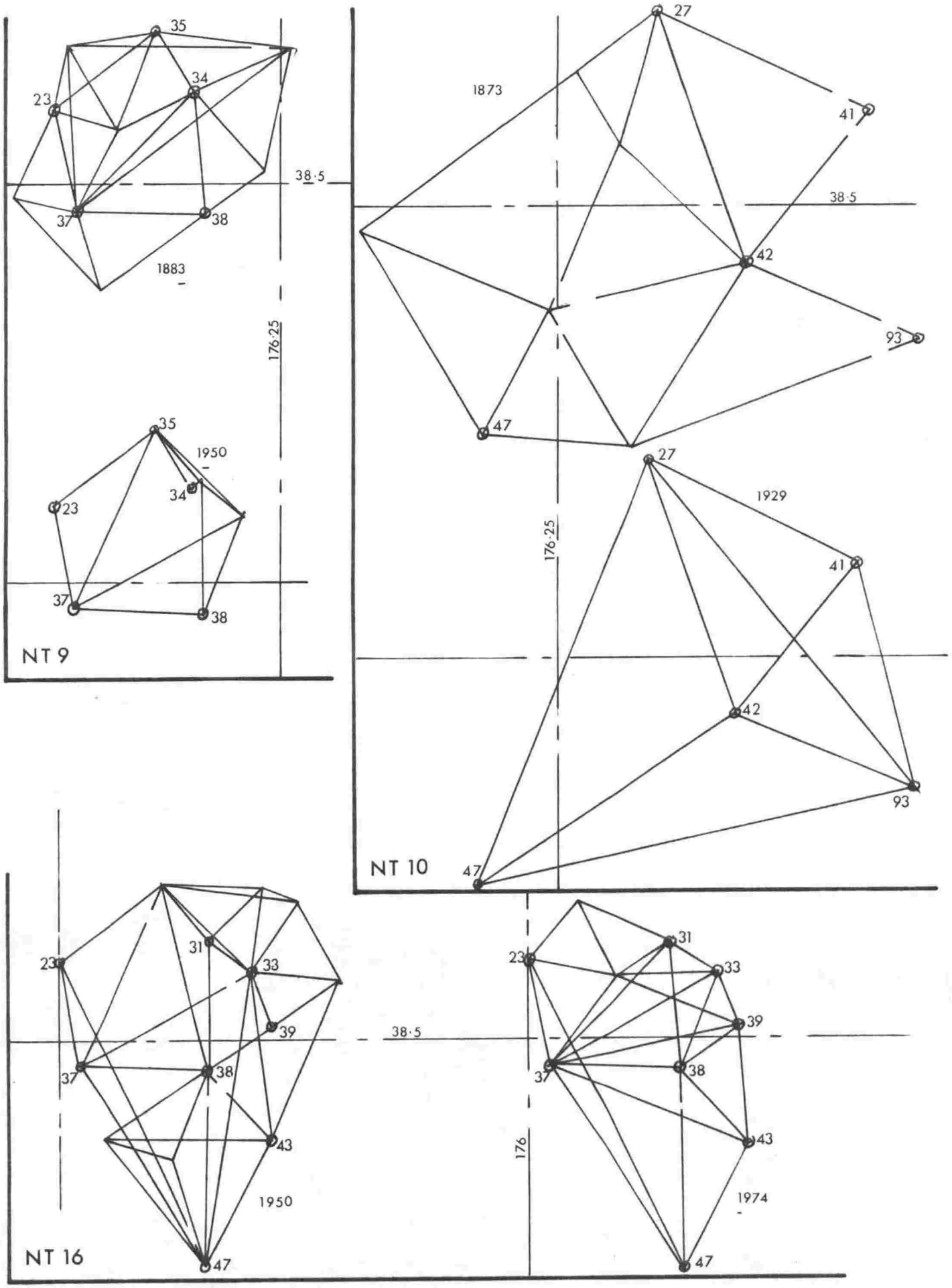
35
34
23
37
38
1883
38·5
176·25
35
1950
34
23
37
38
NT 9
27
1873
41
38·5
42
93
47
27
1929
41
176·25
42
93
47
NT 10
31
23
33
39
37
38
43
1950
47
NT 16
31
23
33
39
37
38
43
176
1974
47

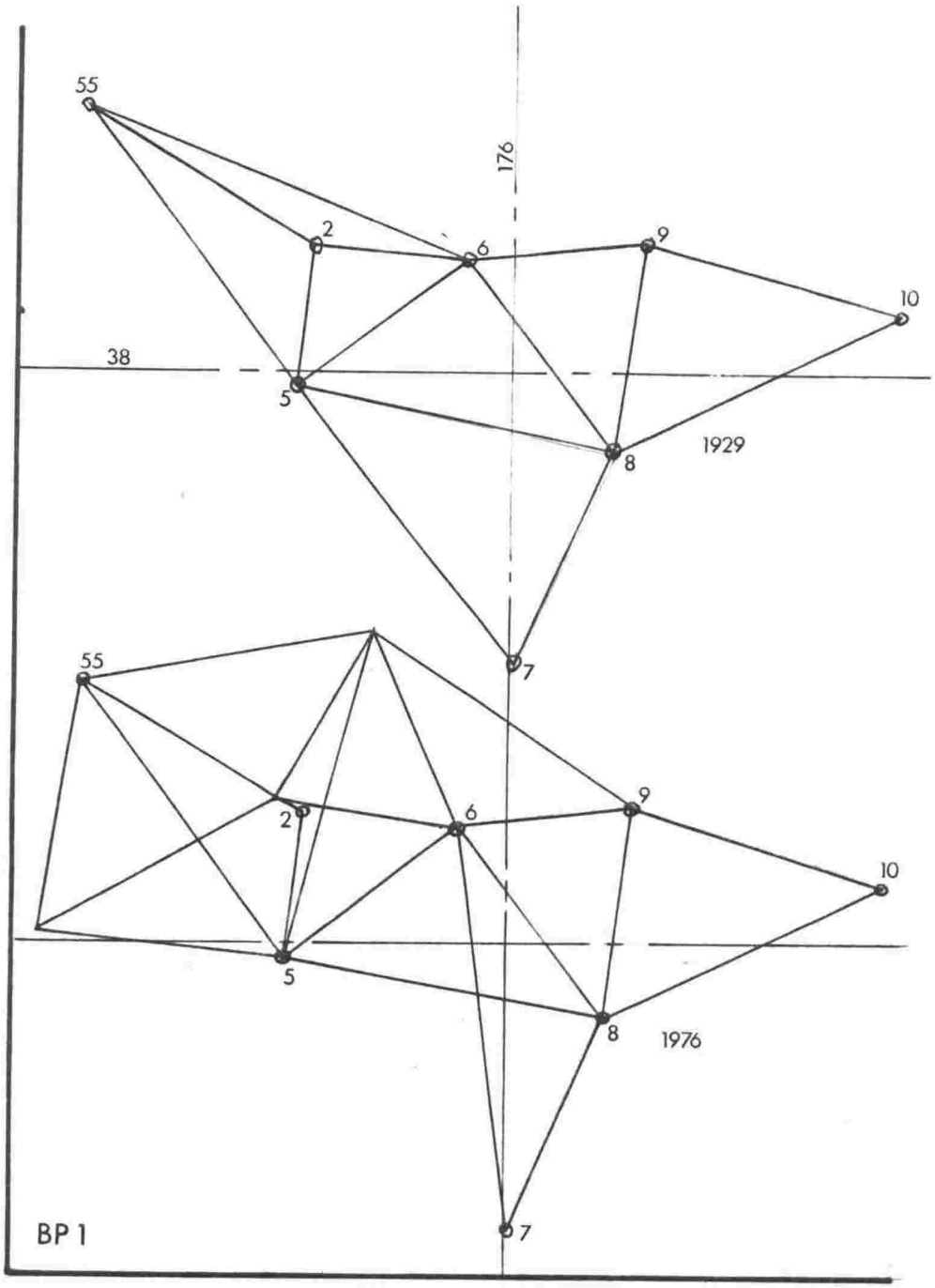
55
176
2
6
9
10
38
5
8
1929
7
55
2
6
9
10
5
8
1976
7
BP 1

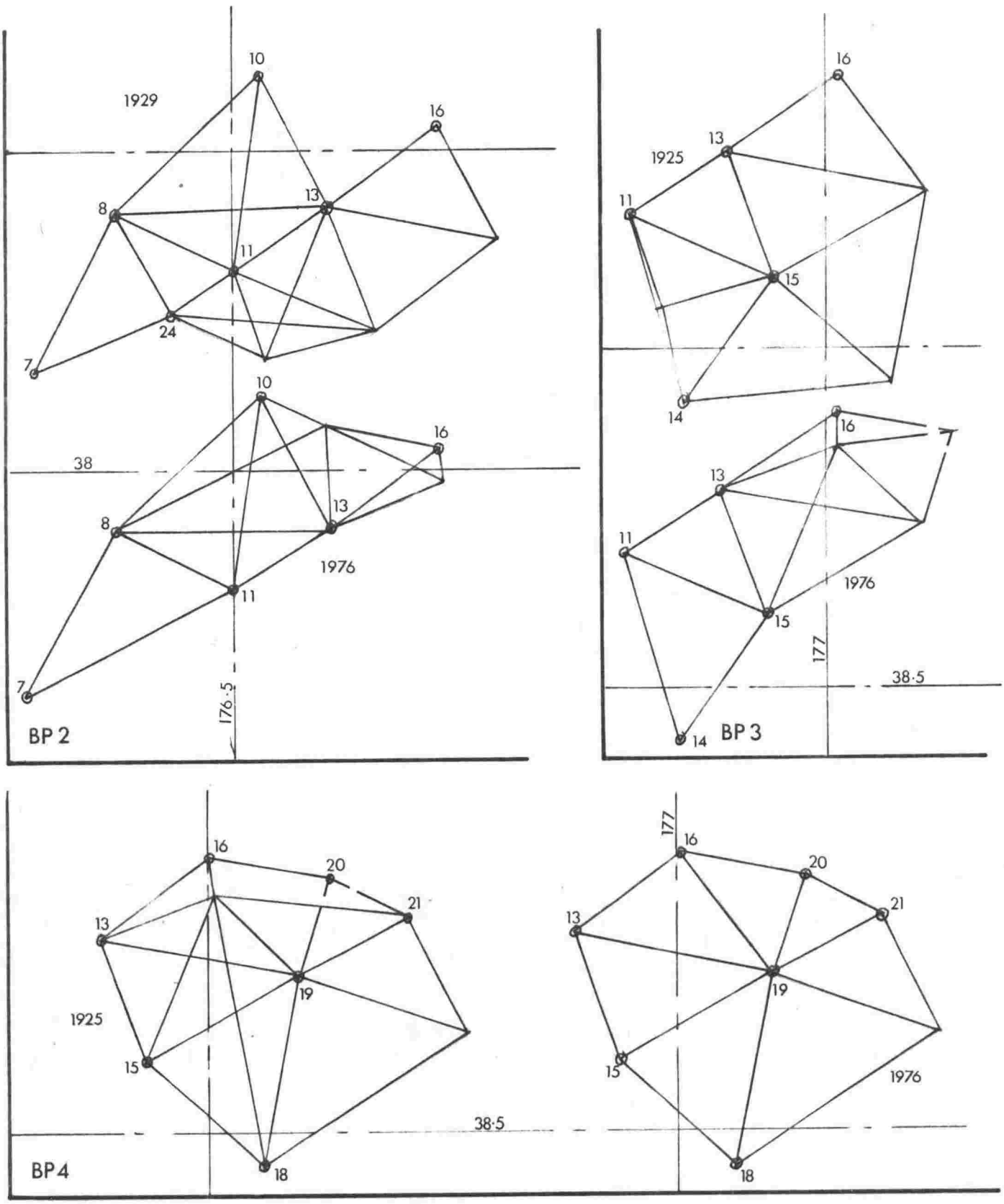
1929
10
16
8
13
11
24
7
38
1976
176·5
BP 2
1925
16
13
11
15
14
177
38·5
BP 3
20
21
19
18
BP4

APPENDIX 3 THREE-PLATE KINEMATICS

Eulers Theorem states that the general displacement of a rigid body with one fixed point is a rotation about an axis through that point (Goldstein, 1950, p.18). For plates constrained to move on a sphere the centre of the sphere may be considered fixed; hence any displacement of a plate relative to the sphere is a rotation about a central axis of the sphere and the relative displacement of any two plates on a sphere is likewise a rotation about a central axis of the sphere. A central axis has two antipodal poles the more distant of which, from the plates, is neglected.

For three plates (a, b, c) there are three plate pairs and therefore three poles to consider (A, B, C in figure A.1). Any three poles on a sphere form a spherical triangle. Choose plate b as the stationary frame and let the plates be displaced relative to one another about the poles. The positions of poles A and C will be unchanged by the displacement since they are in the stationary plate. Pole B will be displaced but its distances from A and C must be the same before and after displacement. Hence B can only occupy positions symmetrically disposed to line AC and the three poles before and after displacement form a pair of spherical triangles reflected in AC. In figure A.1, B and B' denote the positions of pole B before and after displacement.

Denote the rotation of plate b relative to plate a by ω_{ab} where ω_{ab} is positive if b moves anticlockwise relative to a. From figure A.1 $\omega_{ab}/2$ = angle BCA, $\omega_{bc}/2$ = angle BAC, and $\pi - \omega_{ac}/2$ = angle CBA.

Applying the Sine Rule we have:

$$\frac{\mathrm{Sin}(\omega_{bc}/2)}{\theta a} = \frac{\mathrm{Sin}(\omega_{ac}/2)}{\theta b} = \frac{\mathrm{Sin}(\omega_{ab}/2)}{\theta c}$$

where θa, θb and θc are the angles subtended at the centre of the sphere by lines a, b and c respectively. For small regions assume plane triangles, then

$$\frac{\mathrm{Sin}(\omega_{bc}/2)}{a} = \frac{\mathrm{Sin}(\omega_{ac}/2)}{b} = \frac{\mathrm{Sin}(\omega_{ab}/2)}{c}$$

For small rotations $\mathrm{Sin}(\omega_{bc}/2) \rightarrow \omega_{bc}/2$ etc., hence

$$\frac{\omega_{bc}}{a} \simeq \frac{\omega_{ac}}{b} \simeq \frac{\omega_{ab}}{c}$$

and as rotations tend to zero B and B' approach one another until, in the limit, for instantaneous poles, A B and C form a straight line. Then b = a + c and

$$\frac{\omega_{bc}}{a} = \frac{\omega_{ac}}{a+c} = \frac{\omega_{ab}}{c}$$

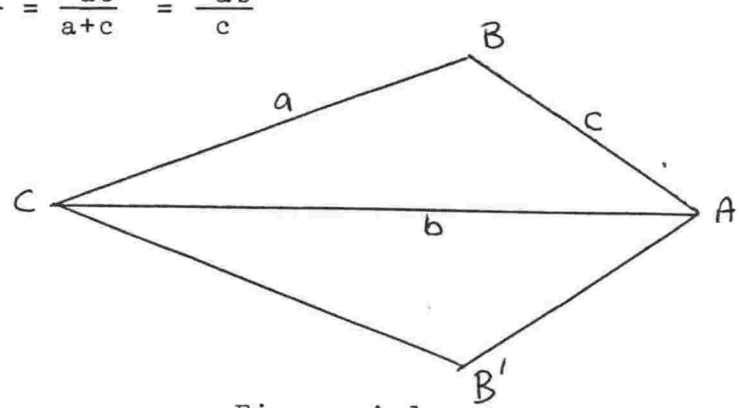

Figure A.1

Infinitesimal rotations behave as vectors (Goldstein, 1950, p.127), hence the infinitesimal rotation of plate a relative to plate c is the sum of the infinitesimal rotations of plate a relative to plate b and plate b relative to plate c, i.e. $\underset{\sim}{\omega}_{ac} = \underset{\sim}{\omega}_{ab} + \underset{\sim}{\omega}_{bc}$.

Reference

Goldstein, H. 1950 Classical Mechanics Addison-Wesley 399 pp.